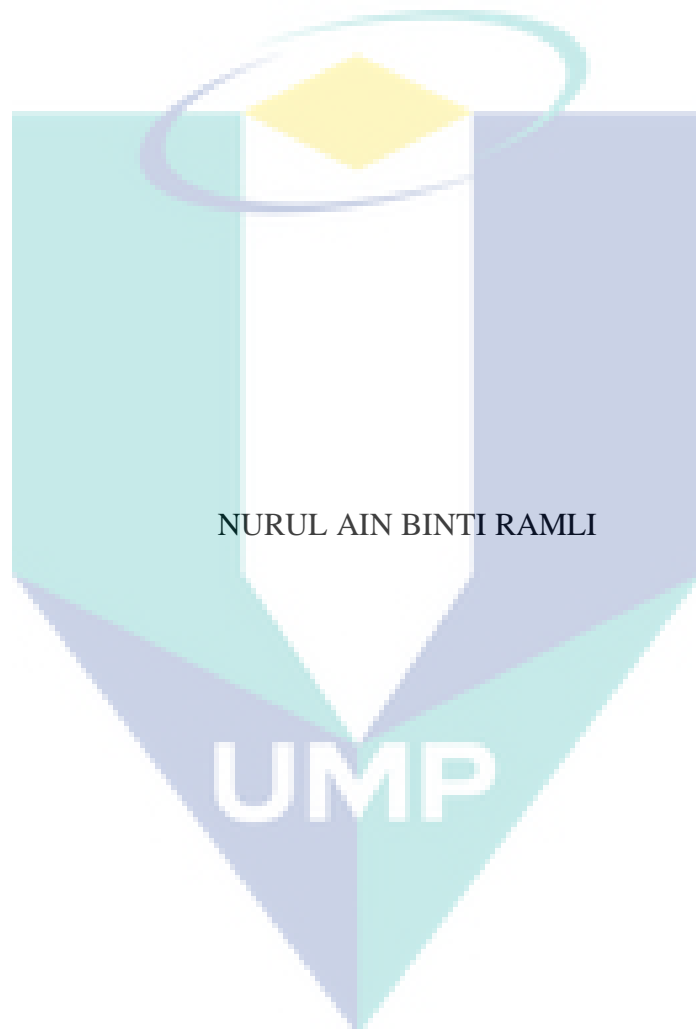SYNTHESIS AND CHARACTERIZATION OF Ni AND Pd NANOPARTICLES IN
NATURAL RUBBER LATEX AND THEIR CATALYTIC ACTIVITY FOR
HYDROGENATION OF LATEX

NURUL AIN BINTI RAMLI

MASTER OF SCIENCE (INDUSTRIAL CHEMISTRY)
UNIVERSITI MALAYSIA PAHANG

SYNTHESIS AND CHARACTERIZATION OF Ni AND Pd NANOPARTICLES IN
NATURAL RUBBER LATEX AND THEIR CATALYTIC ACTIVITY FOR
HYDROGENATION OF LATEX

NURUL AIN BINTI RAMLI

Thesis submitted in fulfillment of the requirements
for the award of the degree of
Master of Science (Industrial Chemistry)

Faculty of Industrial Science and Technology
UNIVERSITI MALAYSIA PAHANG

JANUARY 2013
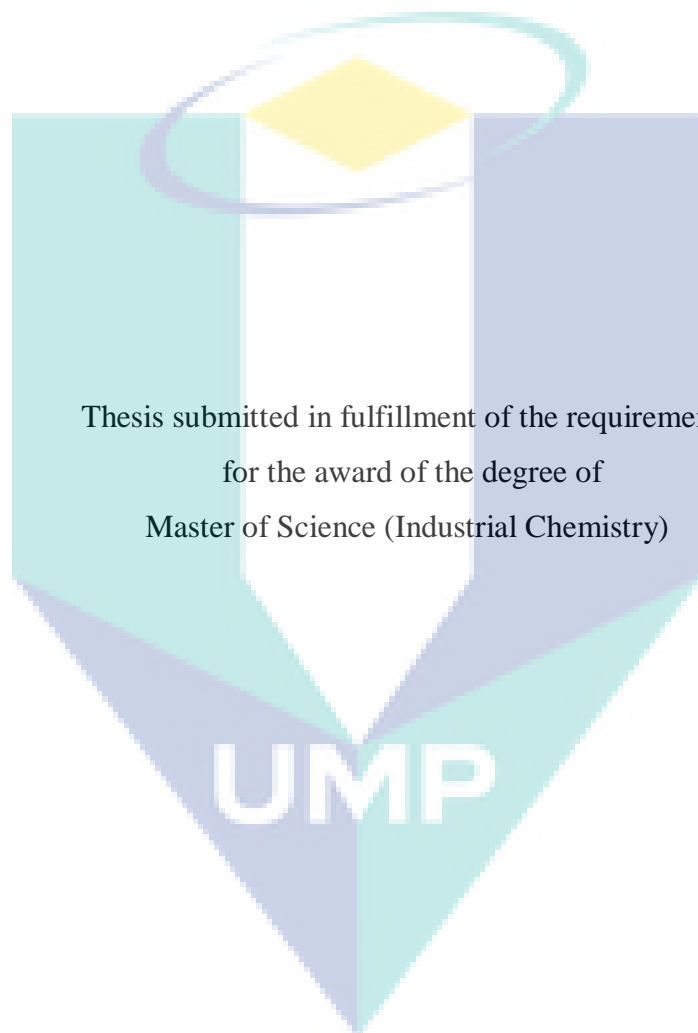
Thesis submitted in fulfillment of the requirements

for the award of the degree of

Master of Science (Industrial Chemistry)

## SUPERVISOR'S DECLARATION

We hereby declare that we have checked this thesis and in our opinion, this thesis is adequate in terms of scope and quality for the award of the degree of Master of Science (Industrial Chemistry).

Signature:
Name of Supervisor:
Position:
Date:

Signature:
Name of Co-Supervisor:
Position:
Date:

**STUDENT'S DECLARATION**

I hereby declared that the work in this thesis is my own except for quotations and summaries that have been duly acknowledged. The thesis has not been accepted for any degree and is not concurrently submitted for the award of other degree.

Signature:
Name:
ID Number:
Date:

*Dedicated to:*

My Lovely Parents, My Siblings and In Law

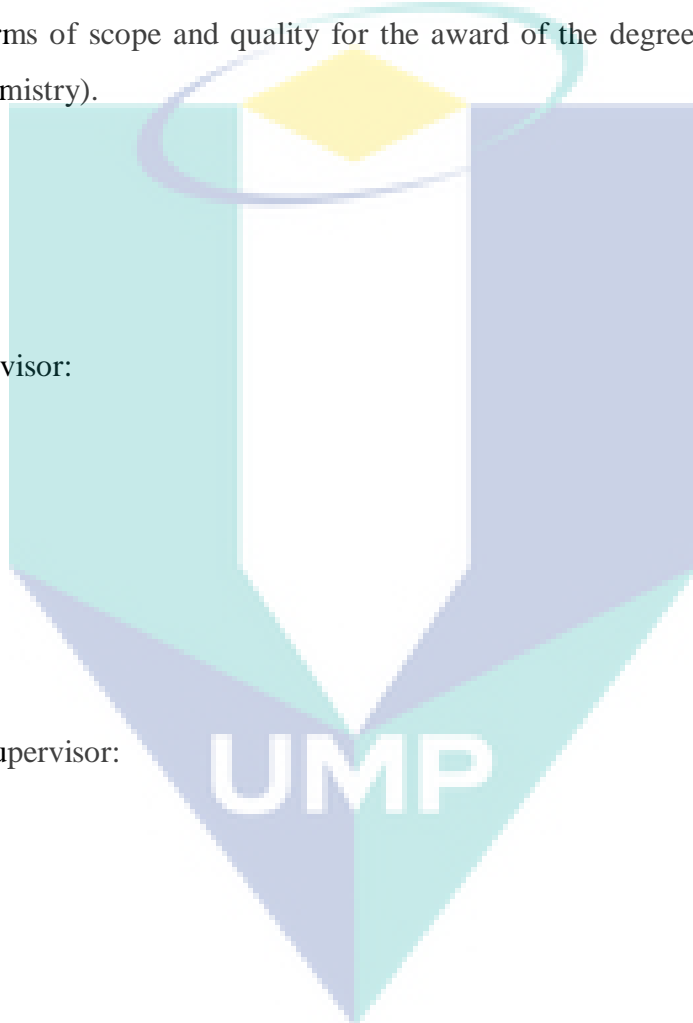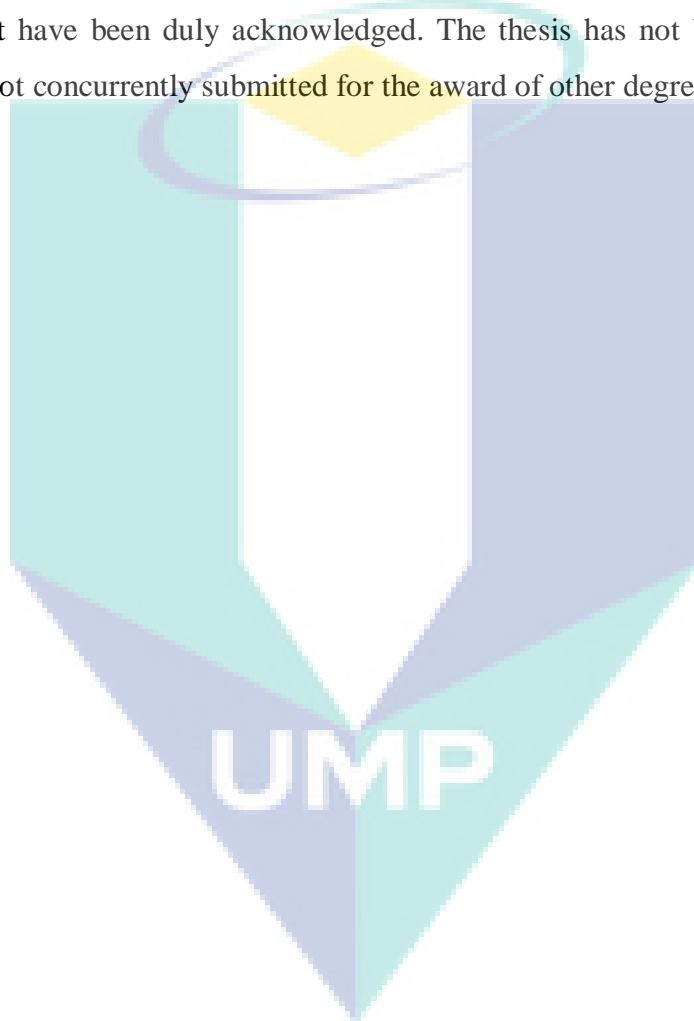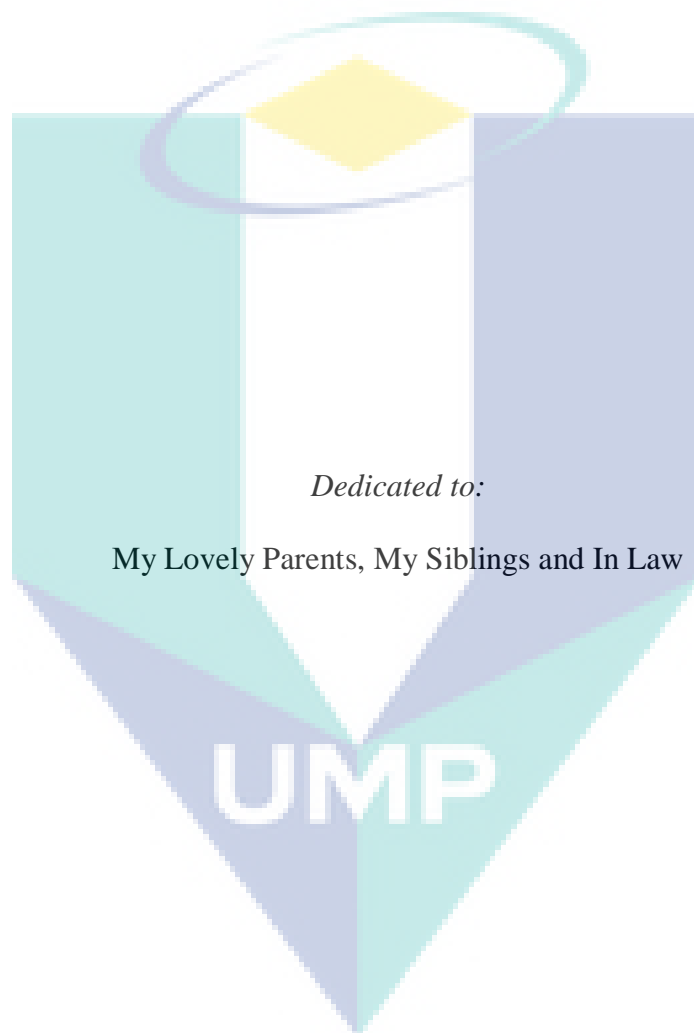# ACKNOWLEDGEMENT

*Assalamualaikum Wrth. Wbth.*

Alhamdulillah, all praises to Allah for the strengths and His blessing in enabling me to complete this thesis. The completion of this thesis would not have been possible without the guidance and help of several individuals who in one way or another contributed and extended their valuable assistance in the preparation and completion of this study.

Special appreciation goes to my supervisor, Prof. Dr. Mohd. Ridzuan Nordin, for his guidance. His constructive comments and suggestions throughout the experimental and thesis writing stages have contributed to the success of this research. My appreciation is also due to my co-supervisor and ex-supervisor, Siti Maznah Kabeb and Prof. Dr. Liew Kong Yong, for their support and guidance.

I would like to express my appreciation to the Dean, Faculty of Industrial Science and Technology, Prof. Dr. Mashitah Mohd. Yusoff and also to the Deputy Dean (Research), Dr. Mohd. Hasbi Abd. Rahim for supporting towards my postgraduate candidature. I would also like to record my appreciation to the Ministry of Education and University Malaysia Pahang (UMP) for providing the financial means and laboratory facilities. My acknowledgement also goes to all the technicians and office staffs of Faculty of Industrial Science and Technology (UMP), Central Laboratory (UMP), Microscopy Unit (Universiti Putra Malaysia & Universiti Islam Antrabangsa) for their cooperation and assistance.

Sincere thanks to all my friends especially Hazrul, Shuhada, Salimah, Azwa, Zuriah, Asma, Syee, Aini, Haizal, Nugroho, Faridah, Siti, Li Hua and others for their kindness and moral support during my study. Thanks for the friendship and memories.

Finally yet importantly, my deepest gratitude goes to my beloved parents; Mr. Ramli Ibrahim and Mrs. Norihan Kamarudin and also to my lovely siblings, sister in-law and Adib for their endless love, care, prayers and encouragement. To those who indirectly contributed in this research, your kindness means a lot to me. Thank you very much.

# ABSTRACT

Natural rubber latex (NRL) is widely used as raw materials for rubber based products. The use of natural rubber based polymer is constrained by its degradation in the environment due to the presence of carbon-carbon double bonds in their polymer backbone. Modifications of NRL via catalytic hydrogenation overcome this limitation. This research investigated the synthesis of Ni and Pd nanoparticles (NPs) in latex and determined the catalytic performances of both nanoparticles for the hydrogenation of latex. The effects of synthesis method, pH, sonication time and concentration of latex and metal ions precursor towards the formation of metal nanoparticles (Me-NPs) were studied. Transmission electron microscopy (TEM) was employed to study the morphology and particle size distribution of the NPs. The interactions between NPs with latex were studied using Fourier transform infrared (FTIR) spectroscopy. The catalytic hydrogenations of NRL by as-prepared NPs were studied under different reaction conditions in order to investigate the effect of these variables towards the extent of hydrogenation. These include the effect of catalyst amount, nanoparticles size and solvent types. The structure, morphology and degree of hydrogenation of the hydrogenated NRL were determined by FTIR, scanning electron microscopy (SEM), field emission scanning electron microscopy (FESEM) and $^1$H nuclear magnetic resonance (NMR) spectroscopy respectively. Latex was found to be able to stabilize Ni and Pd NPs. Preparation involving the combination of ultrasonication and microwave irradiation upon the addition of $NaBH_4$ into latex and metal ion mixture resulted in the most well dispersed NPs. The particle size of the NPs decreases as pH, sonication time, and stabilizer concentration increases. However, the particle size increases with the increase of metal ions precursor's concentration. It was found that 10 ml of 0.003 M metal ions precursor concentration with 30 ml of stabilizer at pH 11.50 exposed to 15 minutes of sonication is an optimum condition to synthesize Ni-NRL and Pd-NRL. Under this preparation condition, the mean size of Ni-NRL was 10.8±0.3 nm while that for Pd-NRL was 30.6±2.9 nm. Hydrogenation of NRL using as-prepared NPs showed that the degree of hydrogenation increases with catalyst amount. The extent of hydrogenation is dependent on the particles sizes of the Ni-NRL but weakly dependent on and Pd-NRL NPs. Under similar reaction condition, Pd-NRL caused higher conversion than that of Ni-NRL. Monochlorobenzene was observed to be a suitable solvent for the hydrogenation reaction. Aqueous phase catalytic hydrogenations of NRL by the Ni-NRL and Pd-NRL were also investigated and found to cause 30% conversion compared to 70% for that in monochlorobenzene. Quadrupling the amount of nanocatalyst used to $2.4 \times 10^{-5}$ mole led to 90% conversion of latex. Hence in this research it was found that not only the nanoparticles of Ni and Pd could be formed and stabilized in natural rubber latex but they could catalyze the hydrogenation reaction of the latex. It was also found that the nanoparticles could also facilitate the hydrogenation reaction in aqueous medium at moderate condition indicating the possibility of green catalysis for hydrogenation of latex.

# ABSTRAK

Lateks getah asli digunakan secara meluas sebagai bahan mentah bagi produk berasaskan getah. Tahap rintangan yang rendah terhadap tindak balas dalam persekitaran disebabkan oleh kehadiran ikatan ganda dua dalam molekul polimer getah asli membataskan penggunaannya. Pengubahsuaian getah asli melalui kaedah hidrogenan menggunakan mangkin dipercayai dapat mengatasi masalah ini. Dalam kajian ini sintesis nanopartikel Ni dan Pd menggunakan lateks getah asli sebagai penstabil telah dijalankan dan keupayaan kedua-dua nanopartikel ini sebagai mangkin untuk tindak balas hidrogenan lateks telah ditentukan. Kesan kaedah sintesis, pH, tempoh masa ultrasonikasi serta kepekatan getah dan ion logam prekursor terhadap sintesis nanopartikel logam telah dikaji. TEM telah digunakan untuk mengkaji morfologi dan distribusi saiz zarah nanopartikel. Interaksi antara nanopartikel dan getah telah dikaji menggunakan FTIR spektroskopi. Beberapa pembolehubah telah dimanipulasi bagi mengkaji kadar tindak balas hidrogenan lateks getah asli. Ini termasuk kesan kepekatan mangkin, saiz nanopartikel dan jenis pelarut. Struktur, morfologi dan darjah hidrogenan getah yang telah dimodifikasi masing-masing telah ditentukan menggunakan FTIR, SEM, FESEM dan $^1$H NMR spektroskopi. Getah asli telah didapati mampu menstabilkan nanopartikel Ni dan Pd. Gabungan proses ultrasonikasi dan sinaran gelombang mikro apabila $NaBH_4$ dicampurkan ke dalam campuran susu getah dan ion logam menghasilkan taburan nanopartikel yang paling baik. Saiz zarah nanopartikel berkurangan dengan pH, julat masa ultrasonikasi, dan kepekatan penstabil. Walau bagaimanapun, saiz zarah meningkat dengan peningkatan kepekatan prekursor ion logam. Kajian mendapati bahawa campuran 10 ml larutan logam prekursor ion berkepekatan 0.003 M dengan 30 ml penstabil pada pH 11.50 dan didedahkan dengan 15 minit ultrasonikasi adalah satu keadaan yang optimum untuk mensintesis nanopartikel Ni dan Pd. Di bawah keadaan penyediaan ini purata saiz nanopartikel Ni adalah $10.8 \pm 0.3$ nm, manakala bagi Pd adalah $30.6 \pm 2.9$ nm. Hidrogenan lateks getah asli menggunakan nanopartikel yang telah disintesis menunjukkan peningkatan hidrogenan selaras dengan jumlah mangkin. Saiz zarah nanopartikel Ni mempengaruhi kadar hidrogenan lateks getah asli, walaubagaimanapun nanopartikel Pd adalah sebaliknya. Dalam keadaan tindak balas yang sama, nanopartikel Pd menunjukkan kesan yang lebih baik bagi tindak balas hidrogenan. Penghidrogenan lateks getah asli dalam fasa akueus menggunakan nanopartikel Ni dan Pd juga dijalankan dan kajian mendapati bahawa sebanyak 30% kadar tindak balas telah berlaku berbanding dengan 70% dalam pelarut monoklorobenzena. Sebanyak 90% darjah hidrogenan telah dicapai menggunakan empat kali ganda kuantiti nanokatalis iaitu $2.4 \times 10^{-5}$ mol. Kajian mendapati bahawa lateks getah asli bukan sahaja mampu membentuk dan menstabilkan nanopartikel Ni dan Pd, malah mampu berfungsi sebagai mangkin bagi tindak balas hidrogenan lateks. Selain itu, nanopartikel ini juga didapati mampu merangsang tindak balas hidrogenan dalam medium akueus dan ini berpotensi memperkenalkan kesan pemangkinan hijau untuk hidrogenasi lateks.

# TABLE OF CONTENTS

# LIST OF TABLES

# LIST OF FIGURES

# LIST OF SYMBOLS

| | |
|---|---|
| $^{o}$C | Celsius |
| F | Fahrenheit |
| *di* | Individual particle diameter |
| *d* | Average particle size |
| *μ* | Unit micro |
| σ | Standard deviation |
| M | Molar |
| nm | nanometer |
| mg | milligram |

# LIST OF ABBREVIATIONS

| | |
|---|---|
| ATR | Autothermal reforming |
| $CDCl_3$ | Deuterated chloroform |
| CPIP | *Cis*-1,4-polyisoprene |
| DMF | Dimethylformamide |
| DPNR | Deproteinized natural rubber |
| DRC | Dry rubber content |
| DSC | Differential scanning calorimetry |
| FTIR | Fourier transforms infrared |
| HPO | Cumene hydroperoxide |
| Me-NPS | Metal nanoparticles |
| MMA | Methyl methacrylate |
| MMA-g-NR | Methyl methacrylate grafted natural rubber |
| $NaBH_4$ | Sodium borohydride |
| NBR | Nitrile butadiene rubber |
| Ni-HNRL | Hydrogenated natural rubber catalyzed by nickel nanoparticles |
| Ni-NRL | Nickel nanoparticles stabilized by natural rubber latex |
| NMR | Nuclear magnetic resonance |
| NPs | Nanoparticles |
| NR | Natural rubber |

| | |
|---|---|
| NRL | Natural rubber latex |
| Pd-HNRL | Hydrogenated natural rubber catalyzed by palladium nanoparticles |
| Pd-NRL | Palladium nanoparticles stabilized by natural rubber latex |
| PVP | Polyvinylpyrrolidone |
| SDS | Sodium dodecylsulfate |
| SEM | Scanning electron microscopy |
| ST | Styrene |
| ST-g-NR | Styrene grafted natural rubber |
| TEM | Transmission electron microscopy |
| TEPA | Tetraethylenepentamine |
| TGA | Thermogravimetric analyzer |
| TMS | Tetramethylsilane |
| UNCTAD | United Nations Conference on Trade and Development |

# CHAPTER 1

## INTRODUCTION

## 1.1     BACKGROUND OF NATURAL RUBBER (NR)

Natural rubber, chemically known as *cis*-1-4 polyisoprene with an empirical formula of $(C_5H_8)_n$ is obtained from the sap ("latex") of several rubber-yielding plants such as *Hevea Brasiliensis* and *Parthenia argentatum*. Latex is a polydispersed colloidal system of rubber particles in an aqueous phase. Natural rubber latex (NRL) is harvested from rubber tree by cutting grooves in and excising the bark at an angle from the tree. Latex flows down along the cut segment of the tree into a small collection cup. The latex is collected from the cups and processed into commercial rubber latex (Perrella and Gaspari, 2002).

The latex from *Hevea brasiliensis*, the commercial source of natural rubber, is composed of about 36% of rubber fraction, 5% of non-rubbers components such as protein, lipid and sugar, with water accounting for the remaining 59%. The rubber particles are generally spherical, although medium-sized and larger particles in latex from certain mature trees may be pear shaped. A complex film containing proteins and lipids encapsulate natural rubber particles, and the lipids and proteins layers made up the inner and outer layers of rubber particle, respectively (Sansatsadeekul et al., 2011). The non-rubber compounds play an important role in stabilizing the latex particles and in contributing to the outstanding properties of natural rubber (Nawamawat et al., 2011).

Ammonium hydroxide is added to the latex to ensure the latex remains liquid and allow for the manufacture of product by dipping technology. Ammoniation partially hydrolyzes the proteins and alters their native conformation by causing breakdown and/or aggregation of the protein (Beezhold et al., 2002). In addition, the alkaline conditions of ammoniated latex can denature some proteins and may even partially hydrolyze others to smaller polypeptides (Perrella and Gaspari, 2002).

### 1.1.1. Protein in Natural Rubber Latex (NRL)

NRL proteins are organic substances that contain carbon, hydrogen, nitrogen, oxygen, and sulfur. They are naturally occurring polymers that may contain hundreds of individual amino acid residues linked together by peptide bonds. The smaller degraded natural rubber proteins of 10 amino acids or less are typically called peptides. NRL undergoes several changes during ammonia addition and storage. Typically, some of the proteins are partially degraded by the alkaline conditions imparted by the ammonia. The change in the composition of proteins in NRL can affect the physical properties of the latex such as elasticity and tensile strength (Morris et al., 1995 and Siti Maznah et al., 2008). Some of the proteins lose their secondary structure and are partially hydrolyzed to small peptides (Truscott et al., 1995). Freshly prepared centrifuged NRL typically ages over a 4-week maturation period before used for dipping purposes. There are hundreds of different proteins in the latex of the rubber tree. Several of these proteins have been well characterized and their amino acid sequences determined (Perrella and Gaspari, 2002).

The total protein content of fresh latex is approximately 1–1.5%, of which about 20% of it is adsorbed on the rubber particles and a similar portion is associated with the bottom fraction (non-rubber phase) while the remainder is dissolved in the serum phase. The major component of the adsorbed proteins is most likely to be α -globulin that has a molecular weight of approximately 200 kDa and is insoluble in pure water. Herein, the second major protein in latex has a molecular weight of 5 kDa and is a water-soluble protein generally present in the bottom fraction of latex. Those proteins adsorbed on NR particle are composed of many types of amino acids, including neutral amino acid, acidic

amino acid and basic amino acid. The amino acid composition of each protein is also distinct leading to different isoelectric points. Proteins from latex can be separated and identified based on its electrophoresis mobility. The proteins adsorbed on the rubber particles have not been studied in much detail due to the difficulties in removing them unchanged from the particle surface. However, proteins from fresh latex particles have isoelectric points ranging from pH 4.0 to 4.6, depending on the rubber clones. This indicates that more than one kind of proteins are adsorbed on the rubber particle and that the relative proportion of the adsorbed proteins on the rubber particle is a characteristic of the clone (Sansatsadeekul et al., 2011).

### 1.1.2 Lipids in Natural Rubber Latex (NRL)

Lipids associated with NR are comprised mainly of neutral lipids and phospholipids (Hasma and Subramaniam, 1986). The principle phospholipids of the rubber particles are α-lecithin. Other lipids are sterol esters, fats, which are a subgroup of lipids called triglycerides, and waxes (Tangpakdee, 1998). The presence of the phosphatidylcholine and small amounts of phosphatidylethanolamine associated with the rubber particles has also been reported (Dupont et al, 1976). Recently, NR was described to contain phospholipid molecules at the α-terminal of the rubber chain associated with mono- and diphosphate groups at the chain-end. Moreover, it also appears that the phosphate groups of phospholipids caused the branching formation in deproteinized natural rubber (DPNR) (Tarachiwin et al, 2005).

The surface surrounding the rubber particles contains both positive and negative charges and has been investigated by using the electrophoresis mobility technique. The negative charges are attributed to ionization of adsorbed carboxylic group on phospholipid molecules and the positive charges are generated from certain amino groups of the adsorbed proteins. The isoelectric point of *Hevea* latex is reported to be within the pH range of 3.0–5.0, corresponding to the characteristics of adsorbed proteins (Ho et al, 1976). Above the isoelectric point, the negative charge of the adsorbed long-chain fatty acid and the hydrolysis products of phospholipids (Southorn and E. Yip, 1968) stabilize NR

particles. Figure 1.1 illustrates two possible models for the structure of the rubber latex particle surface. Structure A shows the current model of NR latex particle surrounded by a double-layer of proteins and phospholipids whereas a proposed new model consisting of a mixed layer of proteins and phospholipids around the latex particle is shown as structure B. Phospholipids in NR latex have been identified as mainly L, α-phosphatidylcholine and phosphatidylethanolamine (Hasma and Subramaniam, 1986). Figure 1.2 illustrates the chemical structures of the phospholipids.
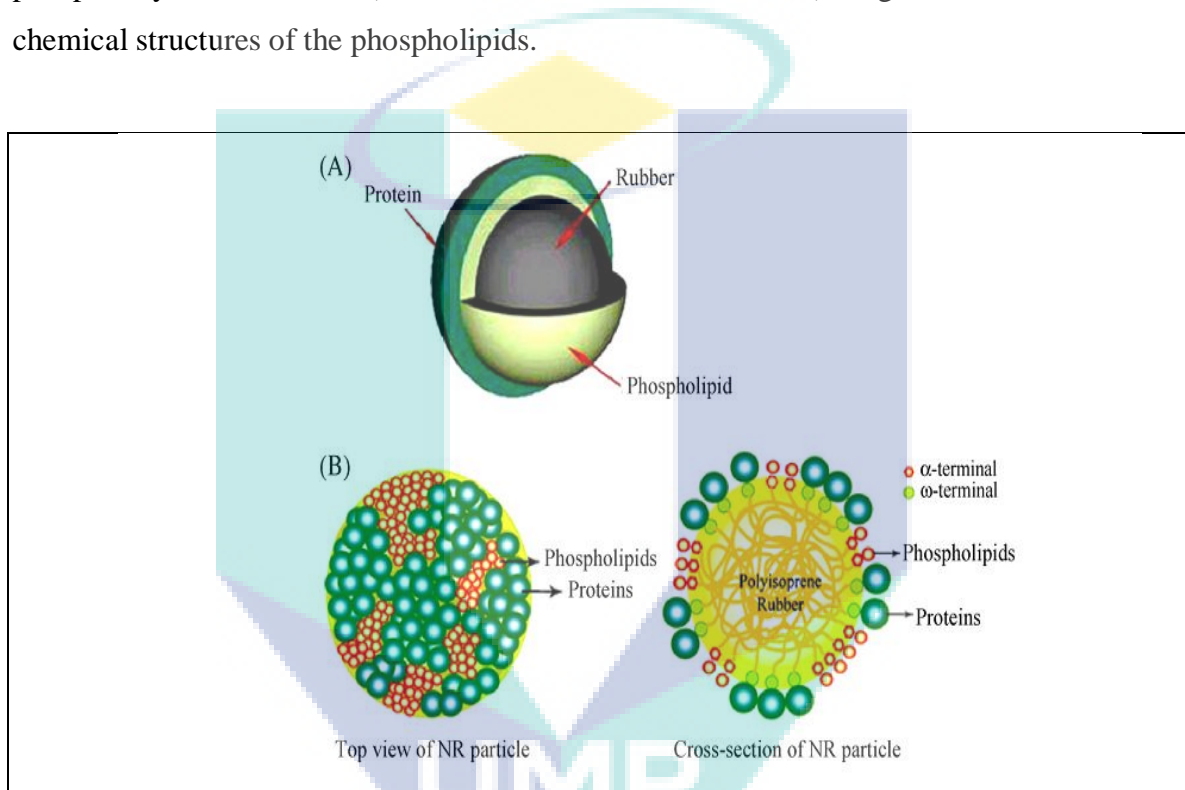


**Figure 1.1**: Models for the structure of the rubber latex particle surface

**Source**: Nawamawat et al. (2011)
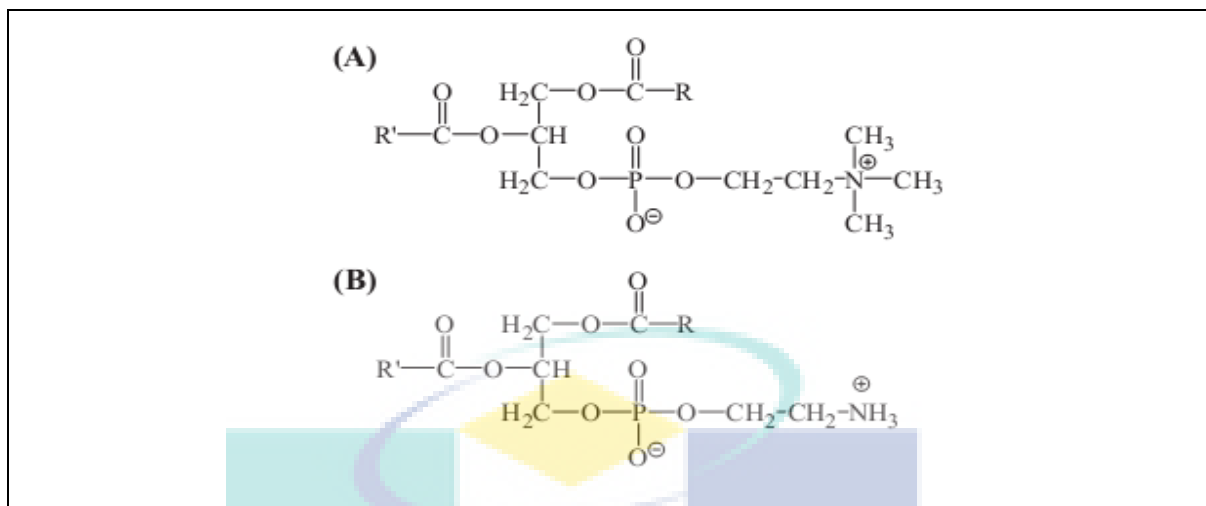
**Figure 1.2**: The chemical structures of (A) L, $\alpha_c$-phosphatidyl choline and (B) phosphatidyl ethanolamine where R and R' are long-chain alkyl groups

**Source**: Nawamawat et al. (2011)

### 1.1.3 Properties of Natural Rubber

Crude rubber is a tough and an elastic solid. It becomes soft and sticky as the temperature rises. Its specific gravity is 0.915. The glass transition of natural rubber is -70$^o$ Celsius and its melting point is 25$^o$ Celsius. The most important property of natural rubber is its elasticity. When stretched, it expands and attains its original state, when released. This is due to its coil-like structure. The molecules straighten out when stretched and when released, they coil up again. Therefore applying a stress can easily deform rubber. Note that when this stress is removed, it regains its original shape. Raw NR has elasticity over a narrow range of temperature from 10 to 60 $^o$C. The maximum tensile strength and elongation at 21$^o$C is 4000 psi and 750 % respectively. It hardness range is 30 – 100 Shore A. Because of this, articles made of raw NR do not work well in hot weather. Rubber's elasticity, toughness, impermeability, adhesiveness, and electrical resistance make it useful as adhesive, coating composition, fiber, molding compound, and electrical insulator.

NR also exhibits excellent physical resistance such as excellent resilience, high impact strength and excellent cut growth resistance. In environmental term, it has excellent water resistance, good low temperature flexibility, and good oxidation resistance. It has poor ozone resistance, poor sunlight resistance and very little flame retardance.

Rubber is water repellent and resistant to alkalis and weak acids. It is insoluble in water, alcohols, acetone, dilute acids and alkalis. However, rubber is soluble in a number of hydrocarbons, including benzene, toluene, gasoline and lubricating oils. Table 1.1 summarizes the properties of natural rubber.

**Table 1.1:** Properties of Natural Rubber

| Categories | Properties | Value/Description for NR |
|---|---|---|
| | i. Glass Transition Temperature ($^{o}$C) | -70 |
| | ii. Melting Temperature ($^{o}$C) | 25 |
| 1. Physical Behavior | iii. Hardness range (Shore A) | 30-100 |
| | iv. Maximum tensile strength (at 70 F, psi) | 4000 |
| | v. Maximum elongation (at 70 F, %) | 750 |

| | | |
|---|---|---|
| | i. Physical Resistance | Excellent resilience<br>Excellent tear strength<br>Excellent abrasion resistance<br>Excellent impact strength<br>Excellent cut growth resistance<br>Good compression set |
| 2. Advantages | ii. Environmental Resistance | Excellent water resistance<br>Good-excellent low temperature flexibility<br>Fair-good oxidation resistance |
| | iii. Chemical Resistance | Good resistance to alcohols and oxygenated solvents<br>Fair-good resistance to acids |
| 3. Limits | i. Environmental resistance | Poor ozone resistance<br>Poor sunlight resistance<br>Very little flame retardance |
| | ii. Chemical resistance | Poor oil and gasoline resistance<br>Poor resistance to (aliphatic and aromatic) hydrocarbon solvents |

**Source:** United Nations Conference on Trade and Development (UNCTAD) (2007)

### 1.1.4   Rubber and its usage

Because of its elasticity, resilience, and toughness, NR is the basic constituent of many products used in the transportation, industrial, consumer, hygienic and medical sectors.

In transportation sector, NR is mainly converted into tires for truck, bus and other automobile. Besides that, the non-tire rubber items include industrial products such as transmission and elevator belts, hoses, tubes, industrial lining, and bridge bearings. For consumer products, it is used in football balls and other recreational and sports goods, erasers, footwear and other apparel. On the other hand, it also used as seismic materials. For instance, over 500 and 2,500 buildings are respectively fitted with seismic rubber bearings in China and Japan (UNCTAD, 2007)

For NR latex, the application is mainly in medical and health sector notably for condoms, catheters and surgical gloves because it is waterproof. NR latex is possibly the best protection against pathogens such as Human Immunodeficiency Virus (HIV). Latex products include, inter alia, condoms, gloves, threads, adhesives, and moulded foams. However, the recent awareness that the natural protein stabilizer can cause allergic reactions has limited its use. Because of this consideration, natural rubber latex products have been replaced to some degree by synthetic rubber products, especially in unsupported examination gloves (Dzikowicz, 2003).

According to the Annual Rubber Statistics in Malaysia (2010), domestic consumption of NR in 2009 was 468,706 tonnes, an increase of 18,460 tonnes (+4.1%) compared to 2007. This rise was mainly due to the increase of consumption in the rubber gloves industry. The three main industries that contributed to total domestic consumption in 2009 were rubber gloves (67.6%), rubber threads (12.4%) and tyres and tubes (7.9%). Figure 1.3 compares the consumption of these three industries for 2007 and 2009.
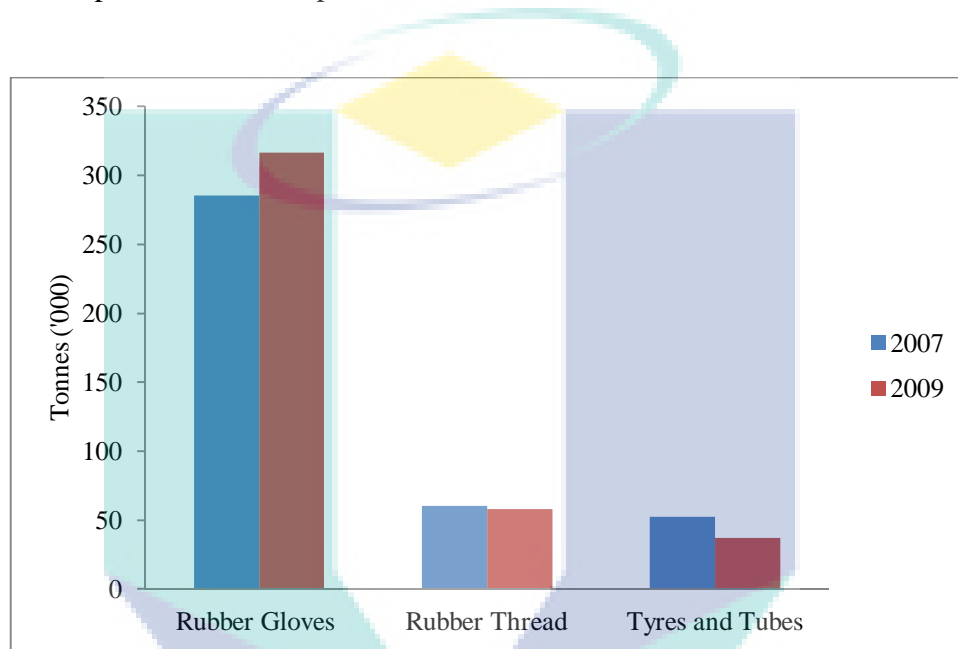


**Figure 1.3:** Domestic consumption of natural rubber by industry, 2000-2009

**Source**: Department of Statistics, Malaysia (2010)

## 1.2    INTRODUCTION TO NANOCATALYSIS

The field of nanocatalysis both in homogeneous and heterogeneous catalysis has attracted a lot of attention and builds great expectation in the academic, investing, governments, and industrial communities. Nanocatalyst has large surface-to-volume ratio compared to bulk materials which make it highly efficient for use as catalysts. Nanocatalysis research is meant to produce 100% selectivity, extremely high activity, low energy consumption processes, and long lifetime catalyst.

The advantages of nanocatalyst are derived from its particle size and other characteristics. By applying the nanoscale catalyst, the selectivity and activity of catalysts will increase. Replacement of precious metal catalysts by nanoscale catalysts and use of base metals will improve the chemical reactivity and reduce process costs.

Nanocatalysis is extensively explored in several sectors such as biomass, oil, gas, fossil fuels and fuel cells because of their potential benefits. It includes the production of biodiesel from waste cooking oil, hydrogen production by steam reforming of ethanol over nanostructured indium oxide catalysts and in situ hydrogen production by reaction of ammonia and nanocatalysts (Nagaraju Rao, 2010).

## 1.3    SYNTHESIS OF METAL NANOPARTICLES (Me-NPs)

The method for the synthesis of nanoparticles (NPs) is typically grouped into two categories: "top-down" and "bottom-up". The first category involves division of a massive solid into smaller portions through milling or attrition, chemical methods, and volatilization of a solid followed by condensation of the volatilized components. The second category, "bottom-up" methods of nanoparticles fabrication involves condensation of atoms or molecular entities in a gas phase or in solution. The latter approach is far more popular in the synthesis of NPs (Gopalakrishnan, 1995).

The wet-chemical procedure is widely used for synthesis of Me-NPs. A typical procedure involves growing nanoparticles in a liquid medium containing various reactants, in particular reducing agents such as sodium borohydride, potassium bitartrate, methoxypolyethylene glycol and hydrazine. To prevent the agglomeration of Me-NPs, a stabilizing agent such as sodium dodecyl benzyl sulfate and polyvinylpyrrolidone is also added to the reaction mixture. Generally, the chemical methods are low-cost for high volume; however, their drawbacks include contamination from precursor chemicals, use of toxic solvents, and generation of hazardous by-products. Hence, there is an increasing need to develop high-yield, low cost, nontoxic, and environmentally benign procedures for the synthesis of Me-NPs (Thakkar et al, 2009).

## 1.4 MODIFICATIONS OF RUBBER

Chemical modifications of polymers especially NR to produce final product with desirable physical and chemical properties has been an attractive research field. The modifications include epoxidation, chlorination, vulcanization, grafting, hydrogenation, and other chemical process (Kongparakul et al., 2008). Several reports have recently appeared on the subject of grafting vinyl monomers onto NR (Thiraphattaphun et al., 2001; Prasassarakich et al., 2001; Arayapranee et al., 2002a, b, 2003; Suriyachi et al., 2004; Kochthongrasamee et al., 2006). Methyl methacrylate (MMA) and styrene (ST) are believed to be the most suitable monomers for these types of modification with the use of cumene hydroperoxide (HPO) and tetraethylenepentamine (TEPA) as redox initiator system (Arayapranee et al., 2003; Kochthongrasamee et al., 2006). Result showed that the mechanical properties of the blends such as tensile strength, hardness and modulus elasticity are improved upon the addition of graft copolymer. However, thermo-oxidative degradation occurred because of the oxidation of the unsaturated double bond within NR.

Hydrogenation method would be an effective way to overcome the degradation problem. It will reduce the extent of unsaturated carbon-carbon double bonds in the polymers backbone such as grafted NR (Kongparakul et al., 2008a, b, 2009; Mahittikul et al., 2009) and NR or *cis*-1,4-polyisoprene (CPIP) (Mahittikul et al., 2009). Hydrogenation of NR can be achieved by both catalytic and non-catalytic. Although non-catalytic hydrogenation method does not require specialized hydrogenation equipment, literatures indicated that catalytic hydrogenation which extensively involved the use of complex metals and non solvent-free system has been more widely applied for diene polymers (Hinchiranan et al., 2008).

## 1.5    GREEN CHEMISTRY

Green chemistry is the utilization of a set of principles that reduces or eliminates the use or generation of hazardous substances in the design, manufacture, and application of chemical products (Anastas and Warner, 1998).

The developments of green chemistry can potentially provide benefits for chemical synthesis in terms of resource efficiency, energy efficiency, product selectivity, operational simplicity, and health and environmental safety. These benefits can be achieved by developing new chemical processes to replace unacceptable methods, apply innovative catalyst technology to establish industrial processes and develop environmentally acceptable routes to the products. Besides that, it requires a new design for environmentally friendly materials that are based on renewable resources (Clark, 2001).

Thus, green chemistry is the guiding principle towards the environmentally benign products and processes. This concept is embodied in the 12 Principles of Green Chemistry that includes waste prevention instead of remediation, atom efficiency, innocuous solvents and auxiliaries, energy efficient by design, preferably renewable raw materials, catalytic rather than stoichiometric reagents, and inherently safer processes (Arends et al., 2007).

## 1.6    PROBLEM STATEMENT

Applications of noble metal catalyst gain much attention in recent decades. Different morphologies of the nanoparticles can influence the catalytic and other properties of the system differently (Heilmann et al., 1994a, b, 1995; Akamatsu et al., 2000). Thus, the study of the morphology control of nanoparticles with desirable shape and size is essential to enhance their catalytic performance (Yu et al., 2006).

One of the attractive researches using nanocatalyst is catalytic hydrogenation of unsaturated hydrocarbons. However, until now, detailed understanding of the catalytic hydrogenation of NRL using nanocatalyst system is yet to be published. The use of complex catalyst system, high energy requirement and use of organic solvents were extensively applied to hydrogenate the NRL (Kongparakul et al., 2008a, b, 2009; Mahittikul et al., 2009). The application of catalytic hydrogenation of NRL using synthesized metallic nanoparticles in aqueous solvent could be considered a green catalytic process, due to the possible reduction on environmental impact by the modified methods.

## 1.7    OBJECTIVES AND SCOPES OF RESEARCH

The first objective of this research is to study the formation and dispersion of nickel (Ni) and palladium (Pd) nanoparticles in natural rubber latex. A microwave and ultrasonic irradiation methods are selected to prepare the catalyst and in-comparison with the conventional heating method. The purpose is to elucidate the use of microwave and ultrasonic irradiation in synthesizing Me-NPs with small particles size and highly dispersed catalyst. Characterization of the mono-metallic Ni and Pd will be done using transmission electron microscopy (TEM) and Fourier transform infrared spectroscopy (FTIR). The factors influencing the morphology and distribution of particles will be explored to optimize the reaction conditions.

The second objective is to investigate the catalytic performance of the prepared NPs towards the hydrogenation of NRL at various reaction conditions using conventional stirring. The catalytic reaction is determined using Nuclear magnetic resonance (NMR) spectroscopy of the partially hydrogenated NRL. The performances of Ni and Pd nanocatalyst under different reaction conditions will be determined and compared.

The third objective is to investigate the hydrogenation of NRL in aqueous medium using the prepared NPs. The potential of green catalysis approach with different reaction conditions will be explored.

Finally, the hydrogenated product will be characterized to elucidate the interaction between the catalyst and natural rubber particles and to determine the changes in the thermal properties of NRL. This involves the use of FTIR, scanning electron microscopy (SEM), field emission scanning electron microscopy (FESEM) and thermogravimetric analyzer (TGA).

This research is limited to the following scope of work:

i.    The study use NRL from Gambang Estate in Kuantan, Pahang as sample.
ii.   The preparation of Me-NPs involve the use of sodium borohydride (NaBH$_4$) as reducing agent
iii.  The catalytic study uses batch reactor of laboratory scale.

## 1.8     THESIS STRUCTURE

Chapter one provides the general information and background of the research, while chapter two provides the literature reviews.

Chapter three discussed experimental techniques used in this work. This chapter gives detail information on how nickel and palladium nanoparticles were prepared and how the whole experiments are carried out. This chapter also provides the information about chemical reagents and characterization procedures used.

In chapter four, results from present work are presented and discussed. The preparation of metal nanoparticles and their catalytic performance for hydrogenation of natural rubber latex are presented here. The effect of solvent types, catalyst loading and nanoparticles sizes towards the hydrogenation process were also discussed.

Conclusion from this work and recommendations for future work are presented in chapter five.

# CHAPTER 2

# LITERATURE REVIEW

## 2.1 INTRODUCTION

The purpose of this chapter is to provide a review of past research efforts related to synthesis of Me-NPs. A review of other relevant research areas such as catalytic hydrogenation of NRL and other hydrocarbons and the effect of reaction conditions are also done. The review is organized chronologically to offer insight to how past research efforts have laid the groundwork for subsequent studies, including the present research effort. The review is detailed so that the present research effort can be properly tailored and to justify the scope and direction of the present research effort.

## 2.2 SYNTHESIS OF METAL NANOPARTICLES

Developments in the field of nanotechnology especially Me-NPs are meant to benefit from the NPs unique properties. These properties originate from the size, shape and surface effects that enhance the material performance for various applications such as in electronics, optics, and catalysis (Chen et al., 2008). Wet chemical reduction was found to be a versatile and economic preparation routes to obtain well defined mono and bi-metallic particles (Chen et al., 1999 and Devarajan et al., 2005). Synthesis of Me-NPs can be achieved through the control of the nucleation and growth by varying the synthesis parameters such as preparation method, reducing agents, stabilizer, pH, concentration of precursor and reaction temperature.

### 2.2.1 Preparation method of metal nanoparticles

Up to now, various preparation methods have been employed to prepare Me-NPs with different size and shape from a suitable metal precursor through microwave irradiation, conventional heating and sonochemical method. A review on synthesizing Me-NPs using all these methods will be done in detail in the next subchapter.

*Microwave irradiation versus conventional heating*

Conventional heating usually involves the use of a furnace or oil bath that heats the walls of the reactors by convection or conduction. The core of the sample takes much longer to achieve the target temperature. On the other hand, microwave penetrates inside the material and heat is generated through direct microwave and material interaction (Saxene and Usha Chandra, 2010).

Microwave chemistry has received great attention especially in food industry, preparative chemistry and material science since 1986 (Zhu et al., 2009). Microwave frequencies are in the range of 300 MHz to 300 GHz that correspond to the wavelength of 1 m to 1 mm. The most commonly used frequency is 2.45 GHz. Compared to conventional heating, microwave heating has great advantages of homogeneous nucleation, shorter crystallization time, and can heat a substance uniformly through a glass or plastic reaction container (Kijima et al., 2011). Moreover, it causes higher reaction rate, higher chemical yield, lower energy usage and different reaction selectivity over conventional methods (Saxene and Usha Chandra, 2010 and Komarneni et al., 1994).

Microwave irradiation produces efficient internal heating (in core volumetric heating) by direct coupling of microwave energy with the molecules (solvents, reagents, catalysts) that are present in the reaction mixture as shown in Figure 2.1b. Microwave irradiation, therefore, raises the temperature of the whole volume simultaneously (bulk heating) whereas in the conventionally heated vessel, the reaction mixture in contact with the vessel wall is heated first as shown in Figure. 2.1a.
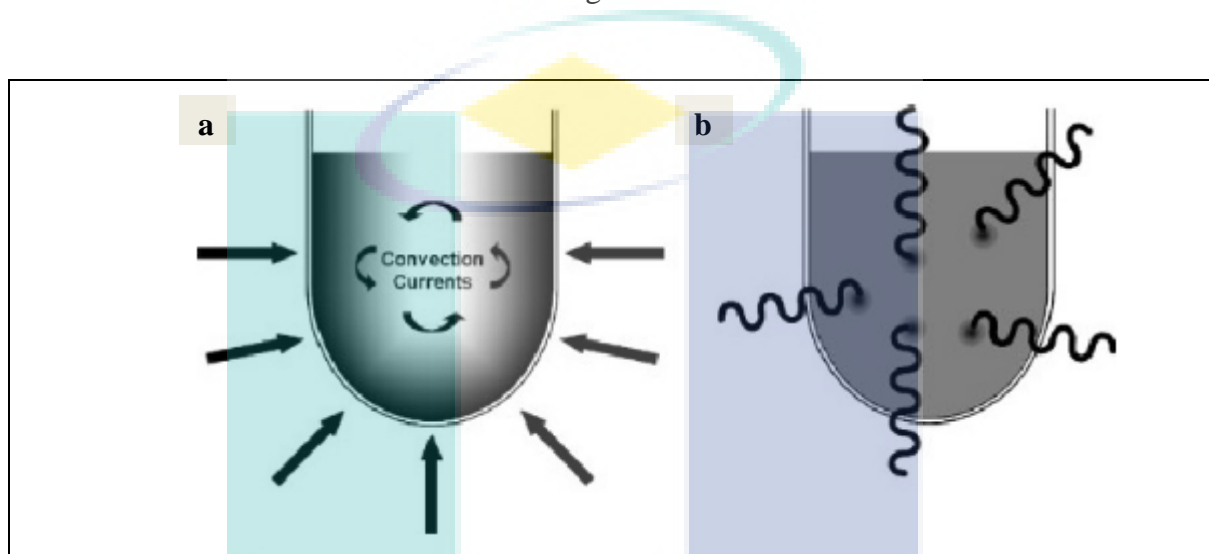


**Figure 2.1:** Comparison of conventional (a) and (b) microwave heating

**Source**: Kappe et al. (2009)

Since the reaction vessels employed in modern microwave reactors are typically made of (nearly) microwave transparent materials such as borosilicate glass, quartz or Teflon, the radiation pass through the walls of the vessel and an inverted temperature gradient as compared to conventional thermal heating results. If the microwave is well designed, the temperature increase will be uniform throughout the sample. The very efficient internal heat transfer results in minimized wall effects (no hot vessel surface) which may lead to the observation of the specific microwave effect (Kappe et al., 2009).
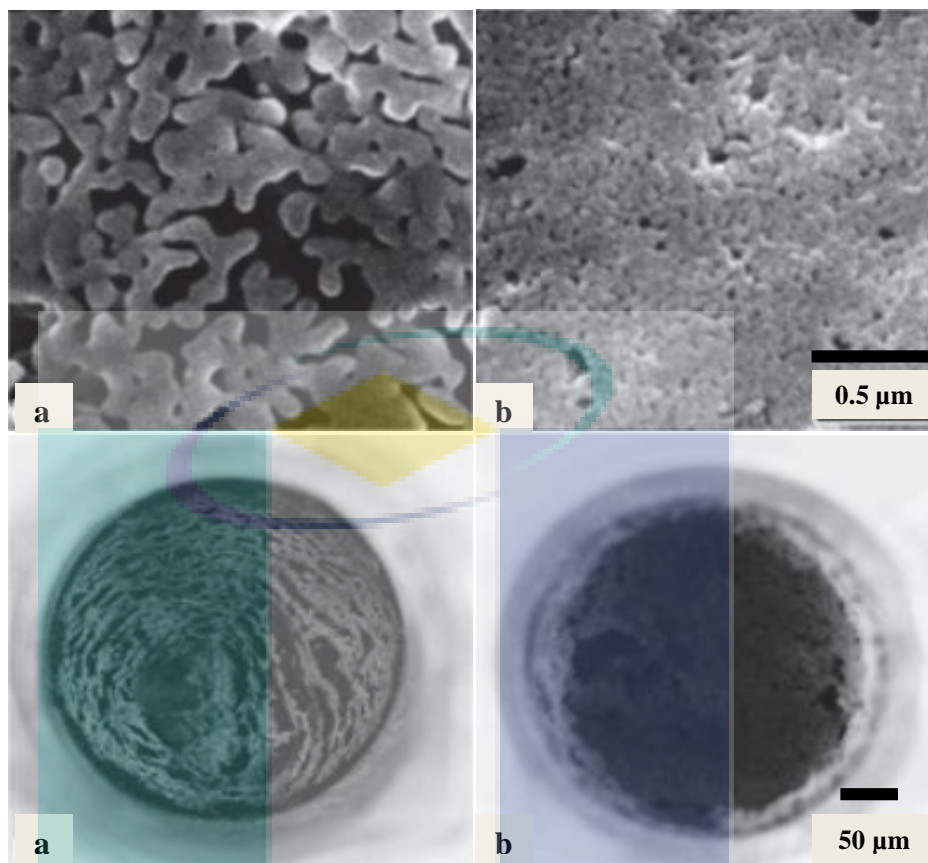
**Figure 2.2:** The effects of heating process (a) hot plate (b) microwave radiation on morphology of LaCrO$_3$

**Source**: Saxena and Usha Chandra (2010)

Figure 2.2 illustrates the merit of microwave heating over conventional heating method during the synthesis of lanthanum chromate (LaCrO$_3$) powder as homogeneous fine particles (Park et al., 1998). The mixed solution of the parent constituents was equally divided and heated separately on a hot plate and in a microwave oven. Heated products thus obtained were treated in a similar way and particles morphology was examined by scanning electron microscopy (SEM). The product obtained by hot plate heating is found to consist of hard agglomerates formed by the two dimensional interconnection of spherical particles. On the other hand product of microwave induced heating appears to be smaller in size and with reduced agglomeration (Saxena and Usha Chandra, 2010).

Thus, microwave irradiation has recently attracted the attention of chemists as a novel technique not only for synthesizing organic compounds but also for preparing inorganic samples especially the nano-sized materials. Many nano-sized inorganic materials with different morphologies were successfully prepared using microwave irradiation method such as nickel nanoparticles (Xu et al., 2008 and Eluri et al., 2012), nickel nanocrystals and nickel oxide composites (Panapoy et al., 2008) and palladium NPs (Li and Komarneni, 2008; Nadagouda et al., 2009; Yu et al, 2010 and Zhang et al., 2011).

*Ultrasonic irradiation*

Currently, there is an increase of interest in method for preparing nanoparticles. One of the novel and simple method for the synthesis of nanomaterial at low temperature is sonochemistry (Pradhan et al., 2008). Sonochemistry is an effective and powerful technique for the synthesis of different compounds under normal condition. Sonochemically synthesized materials are highly active catalysts due to their small particle size and high surface area (Rohani Bastami and Entezari, 2011).

The effect of ultrasound in chemical reactions is not well understood. It is believed that during sonication, the acoustic cavitations phenomenon occurs in the liquid solution of the reactants. The cavitations processes consist of the creation, growth and implosive collapse of gas vacuoles in the solution. The sonochemical method has some advantages, including uniformity of mixing, reduction of crystal growth and morphological control. Ultrasound can also fracture agglomerates to produce a uniform composition of products (Pinkas et al., 2008). The use of ultrasound radiation, during the homogeneous precipitation of the precursor, is expected to reduce the duration of the precipitation reaction of the precursor and to ensure homogeneity of the cations in the precursor (Zheng et al., 2008).

Moreover, the other advantage of using ultrasonic waves in reactions is the provision of high-intensity mixing especially in viscous media (Lepore et al., 2003) and improved dispersity of nanoparticles in solution (Yang et al., 2006). This would lead to an acceleration effect in chemical dynamics and higher rates of reactions.

Nagao et al. (2007) successfully synthesized carbon-supported Pt-Ru nanoparticles at high metal concentration. Figure 2.3a shows a TEM image of carbon supported metal particles prepared under ultrasonic irradiation by the reduction of hydrogen hexachloroplatinate(IV) hexahydrate ($H_2PtCl_6$) and ruthenium(III) chloride n-hydrate ($RuCl_3$) using sodium borohydride ($NaBH_4$) as reducing agent. Well dispersed black spots with a size range of 3-4 nm were observed on the carbon support, suggesting that the nanoparticles obtained under the ultrasonic irradiation were not aggregated. Figure 2.3b shows a TEM image of carbon supported metal particles formed without irradiation. Aggregation of metal nanoparticles on the carbon support was observed and single nanometer particles were scarcely obtained.
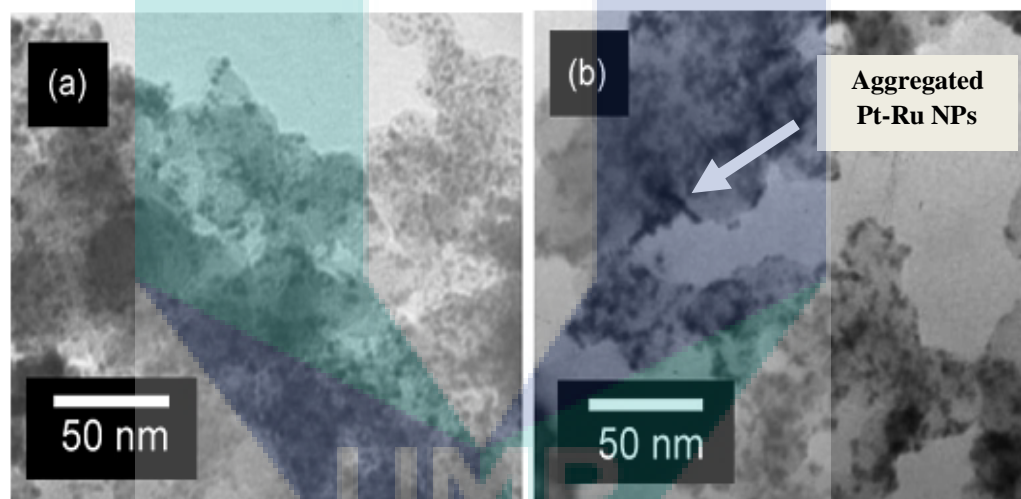


**Figure 2.3:** TEM images of carbon-supported Pt–Ru nanoparticles prepared with (a) and without (b) ultrasonication

**Source**: Nagao et al. (2007)

On the other hand, Lv et al. (2010) studied the effect of the sonochemical treatment on cobalt aluminate ($CoAl_2O_4$) particles size and composition. The TEM micrographs of $CoAl_2O_4$ powders prepared without and with 4 h of sonochemical treatment are shown in Figure 2.4. Figure 2.4b shows that the powder prepared using 4 h of sonication consist of ultrafine, well dispersed particles with uniform particle size of 9–38 nm. Whereas the powders synthesized without sonication (Figure 2.4a) consist of aggregated particles with particle size of 16–201 nm. The shape of the $CoAl_2O_4$ particles also varies from regular cubical shape (Figure 2.4b) to a less regular shape (Figure 2.4a).



(a)                                                          (b)
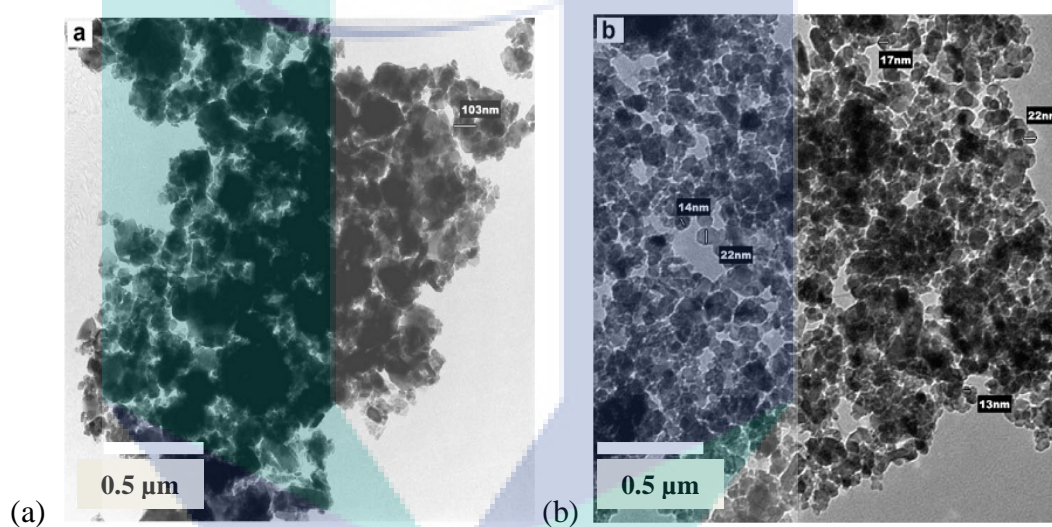
**Figure 2.4:** TEM image of $CoAl_2O_4$ nanosized powders obtained (a) without and (b) with 4 h of sonication

**Source**: Lv et al. (2010)

This observation is similar to that reported by Rohani Bastami and Entezari (2012) for their work on the synthesis of superparamagnetic husmannite ($Mn_3O_4$) NPs by ultrasonic bath. The properties, particles sizes, shape and purity of nanoparticles were not only dependent on solvent, chemical species and concentration in the reaction mixture but also sonication power and sonication time.

*i. Sonication power*

Park et al. (2006) successfully investigated the effect of ultrasonic power on the formation of Au-NPs. Figure 2.5 shows products formed using different ultrasonic irradiation powers (30–90 W). When a sample was irradiated with ultrasound at 30 W for 1 h, the particles had various shapes and forms such as rod, triangle, and disk (Figure 2.5a). In the case of 55 W of microwave irradiation, the formation of spherical Au-NPs having an average particles size of 20 nm was observed. In addition, triangular Au-NPs with edge lengths of 25 nm were observed (Figure 2.5b). Spherical and triangular Au-NPs co existed as main products. In the case of 90 W, the particles had uniform shape. The formation of spherical Au-NPs having an average particles size of 10 nm was observed (Figure 2.5c). The size of Au-NPs decreased with an increase in the ultrasonic irradiation power. These results were in agreement with the results obtained by Hassanjani-Roshan et al., 2011; Darroudi et al., 2012 and Esmaeili-Zare et al., 2012 in the synthesis of iron oxide, silver, and mercury selenide NPs respectively.
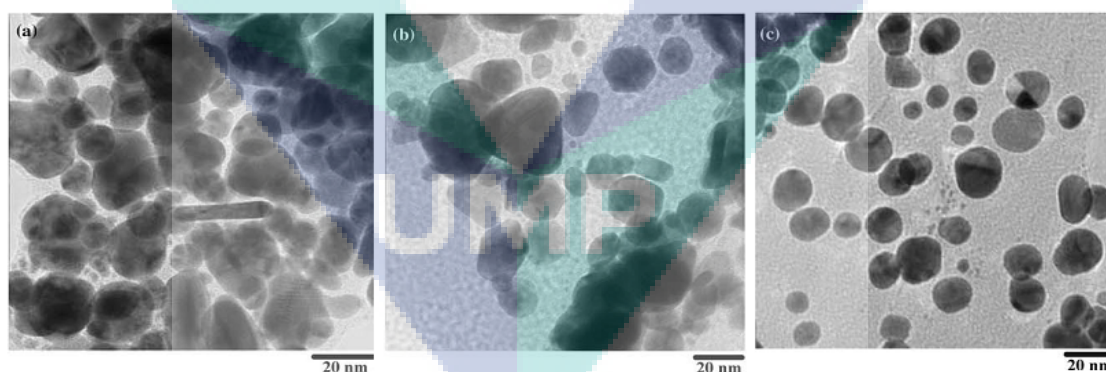


**Figure 2.5:** TEM images of Au-NPs prepared under 1 h ultrasonic irradiation of different powers: (a) 30 W, (b) 55 W, and (c) 90 W

**Source**: Park et al. (2006)

However, Abbasi and Morsali (2011) made the opposite observation. They found that, increase in ultrasound power resulted in an increase of solid solubility. As a result, small sizes nuclei may become unstable and dissolve back into the solution. The dissolved species will then deposit onto the surfaces of large particles. Thus, an increase of the power of ultrasound irradiation led to an increase of particle size.

### ii. Sonication time

The sonochemical reaction time is a key factor in controlling the aggregation and uniformity of particles size. Dang et al. (2011) reported the growth of barium titanate ($BaTiO_3$) NPs in ethanol-water solvent after different ultrasonication times. The formation process of the particles sonochemically synthesized in 30 vol. % ethanol-water solvent is shown in Figure 2.6.

When $BaTiO_3$ particles were synthesized in ethanol–water solvent, regular nanocrystals of about 10 nm were observed after 3 min of ultrasonication. On the other hand, no aggregation of nanocrystals was identified after long time of ultrasonication.
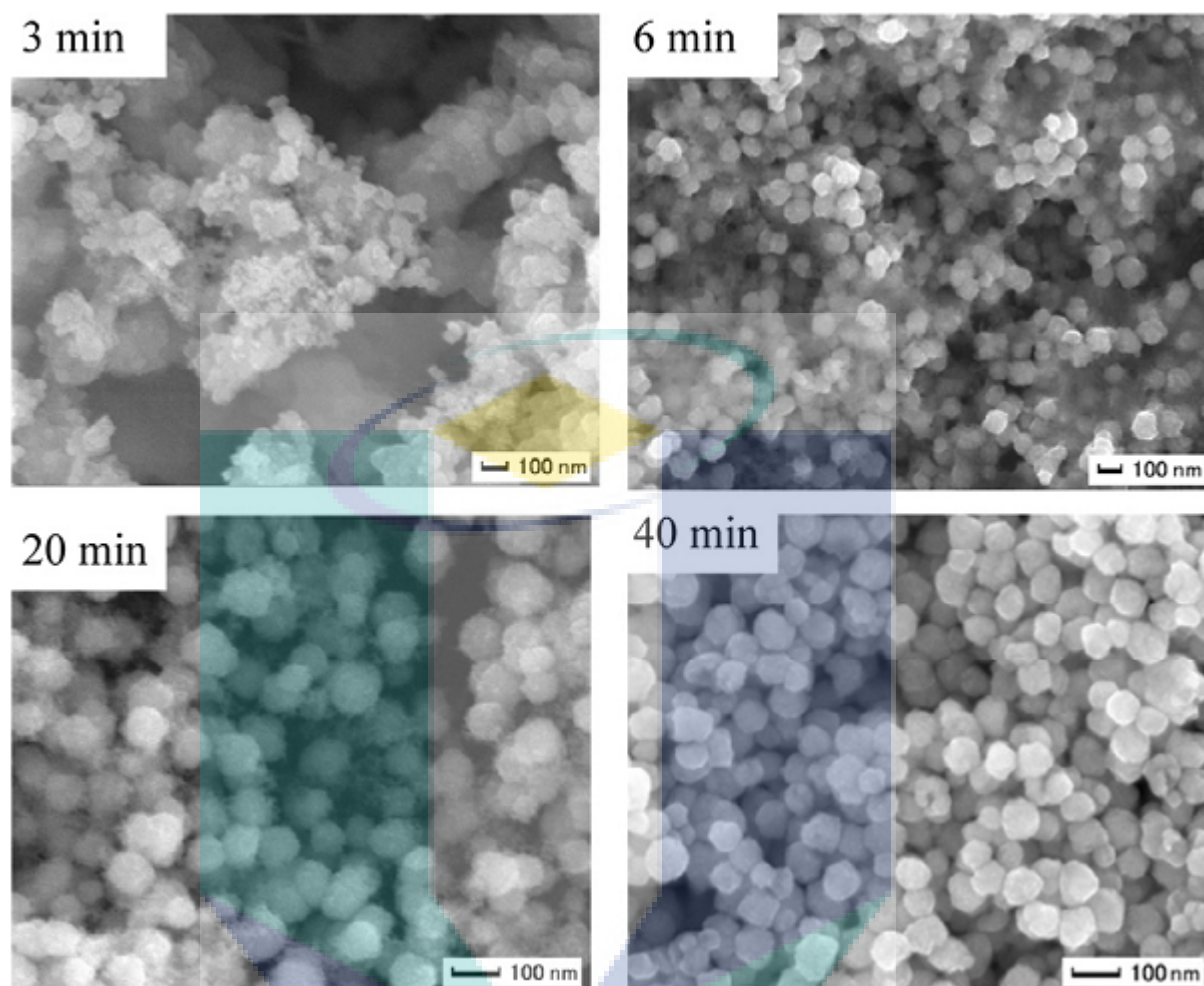
**Figure 2.6:** SEM photographs of particles sonochemically synthesized using 30 vol. % ethanol–water solvent at 50 $^o$C for 3, 6, 20 and 40 min

**Source**: Dang et al (2011)

Salavati-Niasari et al. (2011) successfully investigated the effect of sonication time on the morphology of lanthanum carbonate. They found that the particle sizes after 15 min of sonication were bigger than after 30 min. However, with increasing sonication time from 45 to 60 min, the NPs with average size of 100 nm in diameter were produced. These observations are in agreement with that of Darroudi et al., 2012. They concluded that in the synthesis of colloidal silver nanoparticles, increasing the ultrasonic irradiation time causes the particles size to become smaller.

## 2.2.2 Reducing Agents

Reducing agents could also affect the morphology and distribution of particles. Different reducing agents gave rise to different morphologies (Narayanan et al., 2004 and Hirai et al., 1979).

Choo et al. (2006) successfully investigated the effect of reducing agents towards the formation of palladium nanoparticles. Strong reducing agent was found to favor the formation of smaller size spherical or near-spherical particles. As the reducing ability of the agent decreased, particles with geometrical shapes appeared. In the presence of 2-methoxyethanol and 2-butoxyethanol, more particles with non-distinct outline were formed. Hexagonal shapes particles were dominant with the use of ethylene glycol. They also found that the use of different alcohols such as methanol, *n*-propanol and *i*-propanol as reducing agents at their respective refluxing temperature can affect the morphology of nanoparticles formed. Hydrogen gas and sodium borohydride ($NaBH_4$) that are strong reducing agents at ambient temperature were also used.

For the synthesis of chitosan-stabilized platinum and palladium NPs, $NaBH_4$ seemed to be a better reducing agent for palladium since the particle size and their distribution was smaller and narrower compared to the use of methanol-water and hydrazine as reducing agents (Adlim et al., 2004). Increasing the amount of reducing agents accelerated the reduction rate and produced more nuclei that led to the formation of smaller nanoparticles (Xu et al., 2008).

### 2.2.3 Types and amount of stabilizer or protective reagents

In most colloidal preparation methods, the use of protective agents avoids particles aggregation through the electrostatic and/or steric interaction (Nagao et al., 2007). The stability of the NPs is commonly achieved using different protective molecules, which binds to the NPs surface and avoiding their aggregation, making them soluble in given solvents (Oliveira et al., 2005).

Many polymers have been used for preparing nanocatalyst especially natural polymers that are biocompatible and non-toxic. Examples of biopolymers used are chitosan (Twu et al., 2008), arabic gum (Medina-Ramirez et al., 2009) and plant extracts such as the ones obtained from *Jatropha curcas* (Bar et al., 2009), *Murraya Koenigii* (Philip et al., 2011), *Magnifera indica* (Philip, 2010), *Cochlospermum gossypium* (Vinod et al., 2011) and *Rosa rugosa* (Dubey et al., 2010).

The natural rubber latex (NRL) extracted from *Hevea brasiliensis*, has also been used for synthesis of nanoparticles. NRL contains hundreds of individual amino acid residue linked together by peptide bonds (Abu Bakar et al., 2007 and Parella and Gaspari, 2002). Synthesis of silver NPs using NR and polyvinylpyrrolidone grafted natural rubber (PVP-g-NR) as a stabilizing agent has been done using photo reduction (Abu Bakar et al., 2007 and Bakar et al., 2010) and thermal treatment (Guidelli et al., 2011). They found that NRL molecules especially proteins plays an important role in the growth and stabilization of this Ag-NPs.
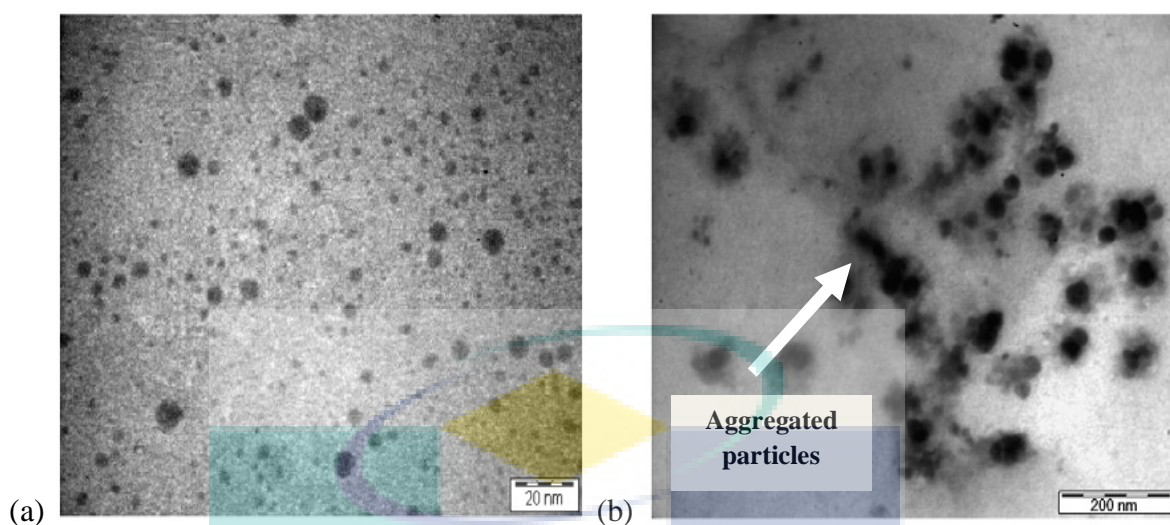
**Figure 2.7:** TEM images of silver nanoparticles in (a) Ag-NR and (b) Ag-DPNR films

**Source**: Abu Bakar et al. (2007)

Figure 2.7 shows the typical morphology of silver nanoparticles in the Ag-NR and deproteinized natural rubber Ag-DPNR films. Discrete globular silver nanoparticles are dispersed in the NR matrix as shown in Figure 2.7a. However, in Figure 2.7b aggregated particles are formed in the DPNR. It was concluded that DPNR is a less effective stabilizer due to the absence of protein molecules that act as protective reagents.

On the other hand, the morphology of particles was found to strongly depend on the amount of stabilizer. In the absence of stabilizer, submicrometer particles without a well-defined shape are formed (Harpeness et al., 2005 and Liu et al., 2008). The increasing amount of stabilizer such as PVP (Couto et al., 2007; Xu et al., 2008 and He et al., 2004a, b, 2007), oleic acid (Zhang et al., 2007) and polyacrylonitrile (PAN-b-PEG-b-PAN, PEA) would decrease the particle size. At lower stabilizer concentration, the stabilizers are not effectively distributed around the surface atoms of the particles, which cause the particles grow to become larger. At intermediate and higher stabilizer concentrations, the small particles formed are sufficiently stabilized, preventing their aggregation and hence resulting in smaller particle size (He et al., 2007).

In the synthesis of chitosan-stabilized platinum and palladium nanoparticles, Adlim et al. (2004) found that an increase in chitosan concentration did not affect the particle size of Me-NPs formed through reduction by methanol and $NaBH_4$. However, for Me-NPs reduced by hydrazine, the size of aggregated particles increased due to chemical interaction between polymer and the reducing agent.

### 2.2.4   Other factors

*pH*

It has been known that the presence of small amount of base in the reducing system could lead to smaller colloidal particles (Turkevich and Kim, 1970). Yu et al. (1999) successfully investigated the effect of base addition in the preparation of polymer-stabilized noble metal colloids. They found that, the average diameter of Pd colloidal particles decreases by increasing the amount of sodium hydroxide (NaOH) added into the reducing system. These as-prepared Me-NPs also exhibited higher activity for hydrogenation of olefins. They believed that the base will neutralize the proton released in the reduction process and accelerate the nucleation. As a result, large amount of nuclei will form resulting in smaller size colloidal particles. This result is in agreement to that obtained by He et al. (2004) for the synthesis of Ag NPs. However, Abbasi and Morsali (2010) found that an increase in pH caused an increase in particles size for the formation of silver iodide on silk fiber. Higher pH led to more deprotonation of carboxylic groups of the fiber's surface resulting in higher formation of AgI on silk surface.

The effect of pH on the stability of metal colloids has been studied by Wang et al. (2000). Ru nanoparticles were synthesized in the presence of NaOH and ethylene glycol as a solvent. As a result, they obtained stable colloidal solution of Ru under basic conditions without the presence of any stabilizer. The Ru metal particles have a strong affinity for anions and hence gave rise to electrostatic stabilization.

The presence of NaOH (base) and ammonia ($NH_3$) as weak bases could affect the morphology of Pd NPs (Choo et al., 2006). Geometrical shapes of Pd NPs disappeared when the pH of the solution increased from pH ~2.5 to 10.2. The particles formed became spherical or near-spherical due to the increase of the reduction rate associated with the increase of pH. In contrast, the reverse situation occurred with the presence of $NH_3$ during NPs formation. The presence of a complexing agent would also result in slower reduction rate and generated larger geometrical shaped particles.

As discussed above a number of studies on the effect of alkaline solution towards particle sizes have been reported. However, the effects of acidic solution are scarcely reported. He et al (2004) studied the effect of acidic conditions for the production of Ag NPs. They observed that, in the absence of HCl, the particle size became larger. The addition of very low concentration of HCl decreased the particle size but increasing the amount of HCl to $7.767 \times 10^{-7}$ M resulted in larger particles size. As a conclusion, the pH of the solution plays an important role on the morphology and distribution of particles.

*Concentration of precursor*

Tong et al. (2009) studied the effect of precursor concentration on the synthesis of pompon-like self-assemblies of Pd NPs under microwave irradiation. They found that, the sizes of pompon-like self –assemblies (nano-pompons) of Pd NPs are strongly dependent on the concentration of the precursor, palladium acetate. The increase of the precursor concentration increased the mean size of Pd self-assemblies. This result is in agreement to that reported for the synthesis of Pd-Sn NPs (Kim et al., 2009) and for the coating of stainless steel plate with silver nanoparticles (Soloviev and Gedanken, 2011). Moreover, the precursor's concentration could influence the morphology and distribution of metal nanoparticles and Choo et al. (2006) proved this in their work on synthesis of Pd NPs.

*Reaction temperature*

Abbasi and Morsali (2011) found that by increasing the temperature for the synthesis of silk yarn containing Ag NPs under ultrasound irradiation, the solubility of the solution also increased. High temperature reduces the supersaturation growth of the species in the solution. Unstable small sizes nuclei will dissolve back into the solution and deposit onto the surfaces of large particles. As a result, an increase of temperature led to an increase of particles sizes. These results are in agreement with that reported for the synthesis of cobalt aluminate (Lv et al., 2010), iron oxide (Hassanjani-Roshan et al., 2011) mercury selenide (Esmaeili-Zare et al., 2012) and Ru (Chen et al., 2008) NPs. Similarly, the NPs size distribution could also be affected by varying the reaction temperature as reported by Choo et al. (2006).

## 2.3     CATALYTIC HYDROGENATION OF NATURAL RUBBER (NR)

Chemical modification of rubber via catalytic hydrogenation is meant to enhance the physical and chemical properties of rubber. Catalytic hydrogenation can be achieved with either heterogeneous or homogeneous catalyst system. The present developments in the field of catalytic hydrogenation of synthetic *cis*-1,4-polyisoprene (CPIP), natural rubber and grafted natural rubber preferably apply homogeneous catalyst. These include Ziegler-natta type (Escobar Barrios et al., 2000a, b, 2003), ruthenium (Kongparakul et al., 2011), rhodium (Mao et al., 1998), and palladium (Bhattacharjee et al., 1993) complexes including catalyst comprising 5d transition metals: osmium (Mao et al., 2000 and Kongparakul et al. 2008a, b, 2011) and iridium (Mahittikul et al., 2009) complexes because of their high catalytic and selectivity. In addition, the reaction can be explained and understood at molecular level. Homogeneous catalysis also overcome the microscopic diffusion problems commonly presence in heterogeneous catalyst. The extent of hydrogenation depends on several reaction parameters such as catalyst loading, rubber concentration, acid addition, hydrogen pressure, temperature, impurity and solvent.

### 2.3.1 Catalyst loading

Mahittikul et al. (2009) found that the rate of hydrogenation of NRL exhibited first-order dependence on catalyst concentration. They suggested that the impurities in NRL might reduce the catalytic activity. This observation is consistent with the work on catalytic hydrogenation of methyl methacrylate-*g*-natural rubber (MMA-*g*-NR) (Kongparakul et al., 2008) and styrene-g-natural rubber (ST-*g*-NR) (Kongparakul et al., 2009) using osmium complexes.
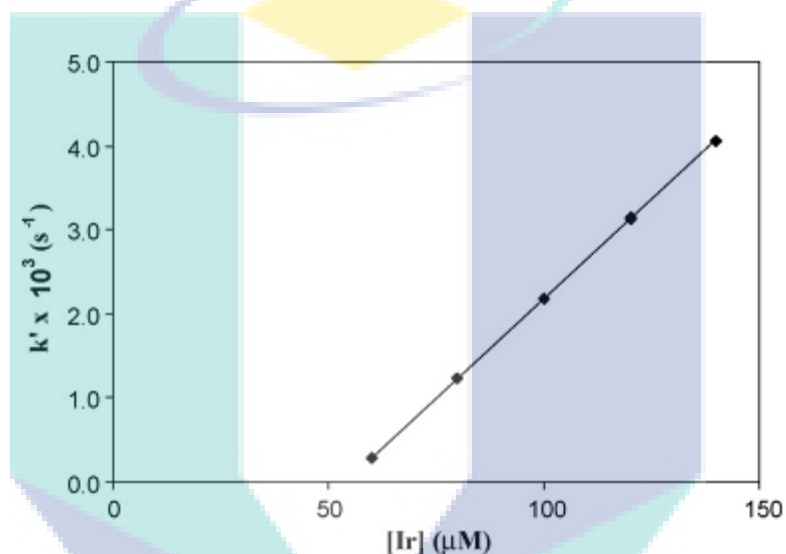


**Figure 2.8:** Effect of catalyst concentration on NRL hydrogenation rate

**Source**: Mahittikul et al (2009)

Figure 2.8 depicts the influence of catalyst concentration on the pseudo-first order rate constant for NRL hydrogenation. Rubber concentration, hydrogen pressure (41.4 bar), temperature (150 $^{o}$C) and other variables were kept constant while varying iridium catalyst concentration (60-140 μM) in monochlorobenzene. The NRL hydrogenation system requires a relatively high loading of iridium complex catalyst and some portion of catalyst, about 50 μM, appeared to be lost due to the impurities present within the NRL.

**2.3.2 Rubber concentration**

Kongparakul et al. (2008 and 2009) found that the rate of hydrogenation decreased with an increase in rubber concentration. Since proteins constitute a major impurity in NR, the catalytic activity of the osmium complex might be reduced by complexation with the amine contained in the protein structure. A steric effect may be a consequence of steric interaction in the bulk due to intermolecular interactions. This result is in agreement with the results obtained by Mahittikul et al. (2009) and Mao and Rempel (1998).
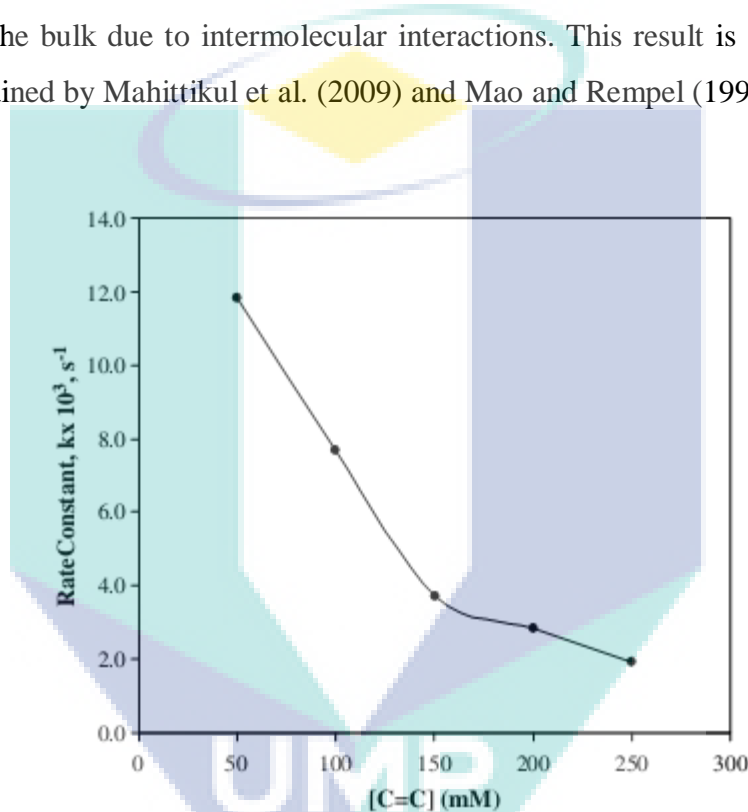


**Figure 2.9:** Effect of rubber concentration on the hydrogenation rate of MMA-g-NR

**Source**: Kongparakul et al. (2008)

Figure 2.9 shows the effect of rubber concentration on the rate constant of MMA-g-NR hydrogenation by osmium complex. The experiments were done with rubber concentration in the range of 50-200 mM, catalyst concentration of 100 μM, *p*-TSA concentration of 2 mM, hydrogen pressure of 20.4 bar and reaction temperature of 140 $^{o}$C.

The rate constant for MMA-g-NR hydrogenation decreased with an increase in rubber concentration.

### 2.3.3 Acid addition

Acid addition improves the catalytic activity of olefinic hydrogenation. Guo and Rempel (1998) reported the effectiveness of carboxylic acids in preventing the poisoning of the catalyst by impurities in the emulsion system. Selective entrapment of the phospine ligand and the formation of a highly active 14-electron ruthenium-monophosphine species during acid addition in the alkene hydrogenation catalyzed by ruthenium complexes resulted in the enhancement of catalytic activity as reported by Yi et al. (2000). However, too high concentration of these acids in the system may cause partial or total deactivation of the catalyst, presumably due to the coordination with the metal sites (Gilliom, 1989).

### 2.3.4 Hydrogen pressure

The effect of hydrogen pressure towards the rate of hydrogenation depends on polymer and catalyst types. Hydrogenation behavior of diene-based polymers such as NRL (Mahittikul et al., 2006), nitrile-butadiene rubber (NBR) (Parent et al., 2001) and *cis*-1,4 polyisoprene (CIP) (Charmondusit et al., 2003) catalyzed by osmium complexes exhibited a second order dependence on hydrogen pressure. At high hydrogen pressure, the reaction turns to zero order with respect to hydrogen pressure. Catalytic hydrogenation of MMA-g-NR (Kongparakul et al., 2008) and ST-g-NR (Kongparakul et al., 2009) in the presence of the same catalyst system showed that the rate of hydrogenation was first order with respect to hydrogen pressure and change to zero order at higher hydrogen pressure. Similarly, in the hydrogenation of NRL (Mahittikul et al., 2009) and solution of NR (Hinchiranan et al., 2006) in the presence of iridium complexes, the rate of hydrogenation was first-order with respect to the hydrogen pressure. These results are consistent to that reported by Hu et al. (2005) for hydrogenation of nitrile butadiene rubber (NBR).
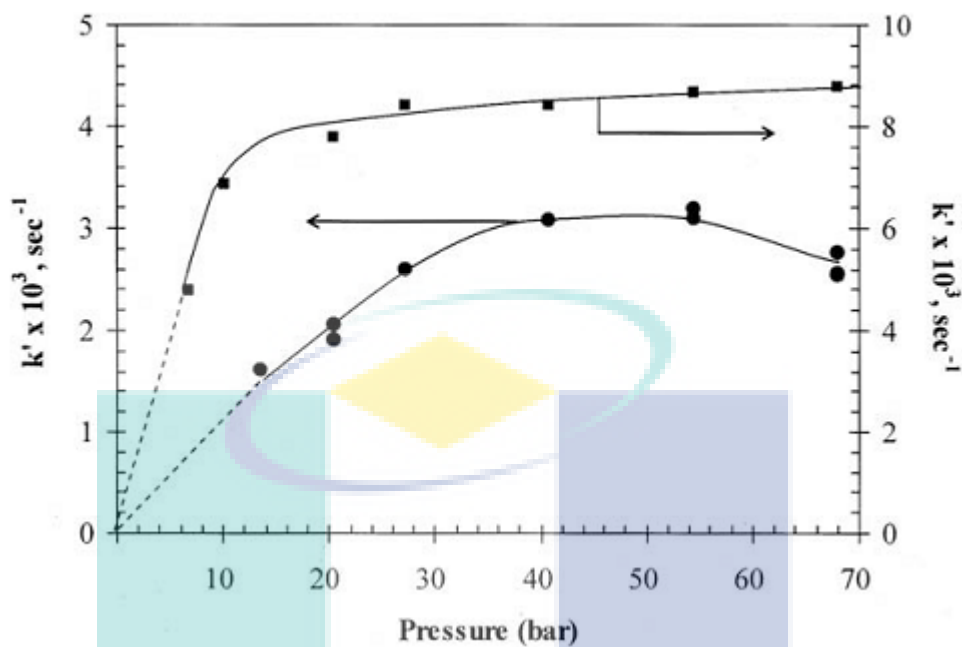
**Figure 2.10:** The effect of hydrogen pressure on the rate constant for (●) ST- g-NR and (■) MMA-g-NR hydrogenation

**Source**: Kongparakul et al. (2009)

Figure 2.10 illustrated the effect of hydrogen pressure on the rate of ST-g-NR hydrogenation using osmium complexes. The experiments were conducted over hydrogen pressure range of 13.6-68.0 bar at 140 $^{\circ}$C while other variables were kept constant. The hydrogenation reaction exhibited a first order dependence on hydrogen pressure at low pressure and change to zero order at high pressure.

### 2.3.5   Temperature

Generally, an increase in reaction temperature results in increase in the rate of hydrogenation. This is true for the experiments occurring under chemical reaction control where mass transfer limitation and the diffusion of the reactants was not the main rate-determining factor under these conditions (Kongparakul et al., 2008 and Mahittikul et al., 2009). However, the differences of chemical structure of polymers such as NR, MMA-g-NR and ST-g-NR would influence the activation energy for reaction. The higher activation energy for hydrogenation of ST-g-NR (83.3kJ/mol) compared to MMA-g-NR hydrogenation that was 70.3 kJ/mol (Kongparakul et al., 2008), but lower than that of NR hydrogenation (122.8kJ/mol) (Hinchiranan et al., 2006) proved this point.
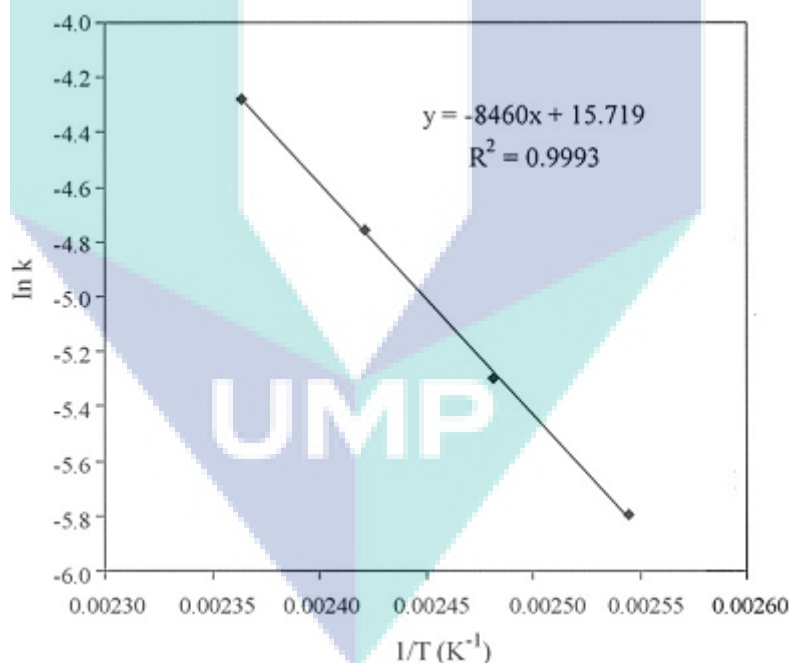


**Figure 2.11**: Arrhenius plot for hydrogenation of MMA-g-NR

**Source**: Kongparakul et al. (2008)

Figure 2.11 shows an Arrhenius plot for the effect of reaction temperature on the hydrogenation of grafted NR using osmium complex. The experiments were conducted over the range of 120-160 $^{\circ}$C at 27.2 bars, while other variables were kept constant. The rate of hydrogenation increased as the reaction temperature increased. The ln k versus 1/T plot was linear and apparent activation energy of 70.3 kJ/mole was obtained from the slope of this plot.

## 2.3.6 Impurity

The presence of impurities in NRL decreases the hydrogenation rate. Mahittikul et al. (2009) showed that deproteinized natural rubber (DPNRL) exhibited higher degree of hydrogenation than NRL under the same reactions conditions with the use of iridium and osmium (Mahittikul et al., 2006) complexes as catalyst system. This observation is attributed to the lower amount of protein n the system.

## 2.3.7 Solvent system

Solvent plays an important role in chemical reactivity. Solvents can affect solubility, stability and reaction rates and choosing the appropriate solvent allows thermodynamic and kinetic control over a chemical reaction. The next sub-section discusses the effect of solvent system towards the hydrogenation of NRL.

### *Organic solvents*

Mahittikul et al. (2009) reported that monochlorobenzene are viable solvents for catalytic hydrogenation of NRL in the presence of iridium complex. However, the use of others solvent such as toluene, hexane, and xylene could not completely dissolve the cationic iridium catalyst. This observation is similar to that of Crabtree et al. (1977). For the hydrogenation of CPIP and NR using osmium catalyst, the strong coordinating solvent (tetrahydrofuran) was reported to be an efficient solvent system but hinder the performance

of Crabtree's catalyst (Hinchiranan et al., 2006). However, the use of non-coordinating solvents lead to higher activity of Crabtree's catalyst as found by Hu et al. (2005).

*Green solvents*

Catalysis in green solvent systems consists of asymmetric catalysis in solvent free and highly concentrated reactions, catalyzed reactions in ionic liquids, supercritical fluids and water. However, the greenest solvent of all is water. Water is the most abundantly existing liquid solvent, nontoxic, nonflammable and environmentally benign. It has unique reactivity and selectivity that result from the hydrophobic effects.

Reactions in water generally involved low solubility of either the reactants and reagents or the products. This could be solved by new technologies such as combined microwave and ultrasonic irradiation (Wang, 2008).

Parmar et al (2003) successfully hydrogenated various types of unsaturated hydrocarbons using synthesized water-soluble $RuCl_2(TPPTS)_3$ in aqueous medium. Lu et al. (2008) reported on high hydrogenation activity of phenol containing wastewater using aqueous solution containing synthesized chain like Ru nanoparticles. Hydrogenation of cylohexenone (Musselwhite et al., 2011) and nitroarenes to arylamines (Sreedhar et al., 2011) were successfully investigated in aqueous medium condition with the use of synthesized Pt nanoparticles. On the other hand, methathesis hydrogenation of DPNRL exhibited more than 97% hydrogenation under mild conditions and without organic solvent addition than that used to dissolve $2^{nd}$ generation of Grubb's catalyst (Kongparakul et al., 2011). These observations indicated the potential of green catalytic approach for converting unsaturated hydrocarbons and polymers into more stable product with the use of water soluble nanocatalyst.

## 2.4 Catalytic hydrogenation using metal nanoparticles

Me-NPs have been attracting great attraction because of their remarkable catalytic performance in hydrogenation, oxidation, and reduction reactions (Tian et al., 2007; Nolte et al., 2008; Schrinner et al., 2009). Literatures reported that Pd, Pt, Rh, Ru, Au, and Ni nanoparticles exhibited higher catalytic activity for hydrogenation (Telkar et al., 2004). It includes the hydrogenation of octene (Adlim et al., 2004) using Pt, quinoline (Sanchez-Delgado et al., 2007) using Ru, $CO_2$ to methane (Adlim et al., 2004) using Rh and 1, 3-butadiene using Pd NPs (Silvestre-Albero et al., 2006). Others include hydrogenation of ethene (Binder et al., 2009), styrene and nitrobenzene (Harraz et al., 2012) using Pd, and with the use of Ni nanoparticles for converting $p$-nitrophenol to $p$-aminophenol (Wang et al., 2009; Wu et al., 2012). However, the activity and selectivity of Me-NPs are believed to be strongly dependent on their size and shape (Telkar et al., 2004; Yu and Yam, 2005; Rashid and Mandal, 2007).

### 2.4.1 Effects of particle sizes

Boitiaux et al. (1983) have investigated the effect of average metal particle sizes of a supported palladium catalyst. They found that metal dispersion above 20% led to decrease in activity for hydrogenation of but-1-yne because of stronger complexation of the alkyne to the metal when the particles were smaller and therefore, more electron deficient. The activity decreased with decreasing particle sizes. On the other hand, Bennett et al. (2009) found that the higher catalytic performance for hydrogenation of 2-pentyne catalyzed by smaller size alumina particles was the result of larger surface area for external mass transfer. The rate of hydrogenation of ethene catalyzed by palladium slightly depends on the size of supported and unsupported Pd (Binder et al., 2009). Particles size, the support, and the presence of additional metal (promoters) have a significant effect on both catalytic and selectivity of the hydrogenation reaction (Silverstre-Albero et al., 2006).

Besides that, Hoxha et al. (2009) have successfully investigated the remarkable particle sizes effect in Rh catalyzed enantioselective hydrogenation. They found that Me-NPs with a particle size of about 2 nm or below seems to be non-beneficial in line with earlier observation for the same hydrogenation reaction over Pt (Wehrli et al., 1990) and Ir (Marzialetti et al., 2008) catalyst. Abe et al. (2009) found that a highly dispersed supported Ru NPs forming small particles to be more active than large metal ensembles. $CO_2$ hydrogenation to methane was found to not depend on particle sizes at high temperatures but favored high activity at low temperature using supported Ru NPs (Karelovic and Raiz, 2009).

Wang et al. (2009) have investigated the role of Ni NPs in catalytic hydrogenation of p-nitrophenol to p-aminophenol. They found that the catalytic activity and selectivity of Ni NPs increased with decreasing particle size compared to Raney Ni catalyst. Mayne et al. (2011) described the effect of Ni particle size on the sulfur-tolerance of ceria-zirconia supported Ni catalyst during autothermal reforming (ATR) of isooctane. They found that, larger Ni NPs proved to be more vulnerable to sulfur poisoning. The poor ATR activity of small Ni particles can be attributed either to a lack of sufficiently large nickel surface enambles, or to their higher propensity to form nickel oxides under reaction conditions. As a result, more highly dispersed Ni catalyst will not result in elevated sulfur tolerance under typical ATR conditions. Thus, it can be concluded that size control of Ni NPs is a best strategy to optimize metal catalyst for catalytic reactions (Wu et al., 2012).

In these perspectives, microwave assisted ultrasonic irradiation synthesis of Me-NPs may fulfill these requirements to produce smaller nanoparticles with prompt start up, uniform heating and very short heating time. This work describes the synthesis, characterization and study of nickel and palladium nanoparticles obtained under microwave assisted ultrasonic irradiation route, starting from nickel chloride and palladium chloride as precursor, sodium borohydride ($NaBH_4$) as reducing and NRL as protective agent. This study will synthesize Me-NPs and determine their catalytic activity for the hydrogenation of NRL.

# CHAPTER 3

## METHODOLOGY

## 3.1    INTRODUCTION

This chapter will present the detail of experimental procedures including the preparation and characterization of colloidal Me-NPs, the hydrogenation reaction system and catalytic hydrogenation reaction condition, analysis of catalytic activity and characterizations of hydrogenated NRL.

The colloidal Me-NPs were prepared using conventional heating, microwave and ultrasonic irradiation methods. The catalytic activities of the prepared catalysts for catalytic hydrogenation reaction of NRL were determined.

TEM was used not only to determine the particles size and particle size distribution but also the shape of particles. The interaction of NPs with NRL and hydrogenated products were also investigated with FTIR spectroscopy. The structures of NRL - nanoparticles composite and the extent of hydrogenation were analyzed using electron microscopy (SEM and FESEM) and $^1$H NMR respectively. The thermal stability studies of hydrogenated products were done using TGA.

## 3.2 MATERIALS

NRL with 40% dry rubber content (DRC) used in this study was collected from an estate in Gambang, Kuantan. Sodium borohydride 96% (GR for analysis), nickel(II) chloride 98% (anhydrous for synthesis), palladium(II) chloride 59% Pd (anhydrous for synthesis), monochlorobenzene 99% for synthesis, acetic acid glacial 100% (anhydrous for analysis), ammonia solution 25% for analysis, chloroform-D1 (0.03 vol. % TMS), were purchased from Merck (Hohenhurnn, Germany). Ethanol (Industrial Grade) was from Taat Bestari Sdn. Bhd. (Ampang, Selangor Darul Ehsan). Air Products Malaysia Sdn. Bhd. (Gebeng, Pahang Darul Makmur) supplied 99.99% oxygen-free hydrogen gas for the hydrogenation experiments and nitrogen built in purifier. All reagents and chemicals were used without further purification.

## 3.3 REAGENT PREPARATIONS

Nickel ions stock solutions with concentration of 0.003 M (SS1), 0.005 M (SS2) and 0.008 M (SS3) were prepared and kept under constant magnetic stirring for 30 min at room temperature of $25 \pm 2$ $^{o}$C. Using the same preparative condition, 0.003 M of palladium ions stock solution was prepared and labeled as SS4. The aqueous stock solutions were prepared from synthesis grade $NiCl_2$ and $PdCl_2$. The latex solution used to stabilize the metallic nanoparticles was prepared by diluting 1 ml of crude natural rubber latex (NRL) to 300 ml using triply distilled de-ionized water and was adjusted to the desired pH using ammonia solution. This stock solution was purged with nitrogen for half an hour at 60 ml/min flow rate while kept under constant magnetic stirring and labeled as SS5.

**3.4     EXPERIMENTAL PROCEDURES**

This section will focus on the experimental procedures to synthesize the metal nanoparticles and to determine its catalytic activity towards the hydrogenation of NRL.

**3.4.1   Synthesis of metal nanoparticles**

The metal nanoparticles were prepared using chemical reduction method. $NaBH_4$ and water function as reducing agent and solvent respectively, whereas latex solution stabilizes metallic nanoparticles from agglomerating. Different synthesis parameters or reaction conditions were used to optimize the reaction conditions.

*Effect of synthesis method*

The effect of synthesis method such as conventional heating, microwave and ultrasonic irradiation were investigated to compare the rate of reduction and their effect on the size and distribution of nanoparticles formed.

*i. Conventional heating*

Metal nanoparticles (Me-NPs) were synthesized according to the following: 10 ml of SS1 (Nickel) stock solution was mixed with 30 ml of SS5 stock solution. Further, the reducing agent, $NaBH_4$ was then added in a mole ratio of 10 with respect to the metal salt. Mixture was heated using oil bath at the reflux temperature which is 80 $^oC$ with constant magnetic stirring. Heating was discontinued when the colloidal solution changed into strong grey color.

## ii. Ultrasonic irradiation

Me-NPs were synthesized according to the following: 10 ml of SS1 (Nickel) stock solution was mixed with 30 ml of SS5 stock solution. Further, the reducing agent, $NaBH_4$ was added in a mole ratio of 10 with respect to the metal salt. Mixture was irradiated in ultrasonic bath at 80 $^{o}$C. Heating was discontinued when the colloidal solution changed into strong grey color.

## iii. Microwave irradiation

Me-NPs were synthesized according to the following: 10 ml of SS1 (Nickel) stock solution was mixed with 30 ml of SS5 stock solution. Further, the reducing agent, $NaBH_4$ was added in a mole ratio of 10 with respect to the metal salt. The mixture was irradiated with microwave radiation at 300 W. Heating was discontinued when the colloidal solution changed into strong grey color.

## Effect of Ni precursor concentration

The 0.003 M (SS1), 0.005 M (SS2) and 0.008 M (SS3) nickel ions solutions were used to investigate the influence of metal precursor concentration towards the formation of nanoparticles. 10 ml of SS1 (Ni) was mixed with 30 ml of SS5 stock solution. Further, the reducing agent, $NaBH_4$ was added in a mole ratio of 10 with respect to the metal salt. The mixture was stirred constantly for half an hour and sonicated for 15 min. Then, the mixture was irradiated with microwave radiation at 300 W for one min. A strong grey color formed after the reduction process and indicated the formation of Ni-NRL. The process was repeated for SS2 and SS3 solutions.

*Effect of volume ratio of latex to metal precursor*

Me-NPs were synthesized according to the following: 10 ml of SS1 (Ni) or SS4 (Pd) stock solution was mixed with 30 ml of SS5 stock solution. Further, the reducing agent, $NaBH_4$ was added in a mole ratio of 10 with respect to the metal salt. The mixture was stirred continuously for half an hour and sonicated for 15 min. Then, the mixture was irradiated with microwave radiation at 300 W for one min. A strong grey color formed after the reduction step and indicated the formation of Me-NPs. The process was repeated for other volume ratio of stabilizer to metal ions precursor of 20:20 and 10:30.

*Effect of sonication time*

To investigate the effect of sonication time, 10 ml of (SS1) was mixed with 30 ml of SS5 stock solution. Further, the reducing agent, $NaBH_4$ was added in a mole ratio of 10 with respect to the metal salt. The mixture was continuously stirred for half an hour and sonicated for 15, 60 and 90 min. Then, the mixture was irradiated with microwave radiation at 300 W for one min. A strong grey colour formed after the reduction process and indicated the formation of Ni-NRL.

*Effect of pH*

The effect of (pH) toward the formation of nickel nanoparticles (Ni-NRL) involves varying the pH of the colloid system to 10.37, 11.5, 11.76 and 12.19 using ammonia solution. The ratio of stabilizer to nickel ion precursor (SS1) was 30:10 and the $NaBH_4$ was added in a mole ratio of 10 with respect to the nickel salt. The mixture was continuously stirred for half an hour and sonicated for 15 minutes. Then, the mixture was irradiated with microwave radiation at 300 W for one minute. A strong grey color formed after the reduction process and indicated the formation of Ni-NRL.

All the preparation and synthesis process of these Me-NPs involve the use of commercial microwave oven (Samsung (MW71E), Triple Distribution System, 2450 MHz, and 800 W) and ultrasonic (Branson2510R-DTH, Danbury, USA).

### 3.4.2 Hydrogenation of natural rubber latex (NRL)

The hydrogenation set-up comprised of a three-neck round bottom glass flask with capacity of 250 ml with hydrogen gas continuously bubbled through the mixture. The necks were respectively inserted with thermometer, condenser and glass hollow tube inside the reaction vessel for the hydrogen gas flow. All the necks were clamped using conical joints clips. Hydrogen gas was supplied using the silicon tube connected from hydrogen tank to the glass tube inside the reaction vessel.

The hydrogenation reaction mixture was continuously stirred and the reaction set-up is summarized and illustrated in Figure 3.1 and 3.2 respectively. In addition, the 250 ml three-neck round bottom flask was immersed in the oil bath (3 quarters of the total vessel volume). 30 µl of NRL in 50 ml of solvent with the desired amount of colloidal catalyst was injected into the reaction vessel. The mixtures were degassed with nitrogen gas for half an hour. The reactor was then heated to the desired temperature, with hydrogen gas being bubbled into the reaction mixture at 58-60 ml/min flow rate throughout the required reaction duration. The reaction mixture was kept under constant magnetic stirring until the completion of the reaction. The reactor was cooled and the hydrogenated product was isolated by precipitation with ethanol and then dried in vacuum. A series of catalytic experiments to study the effects of catalyst amount, solvent and NPs sizes were carried out for both Ni and Pd nanoparticles to determine the degree of hydrogenation and differentiate their catalytic performances.
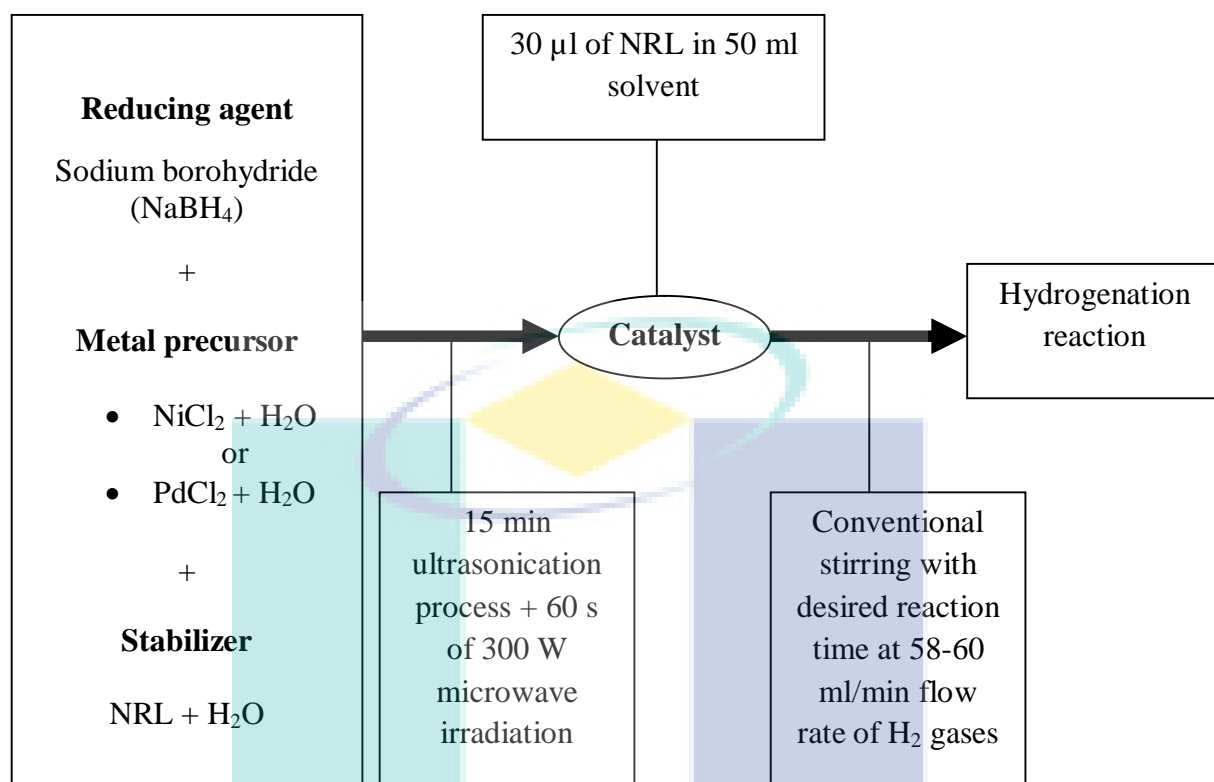
**Figure 3.1:** Process flow for hydrogenation reaction of NRL
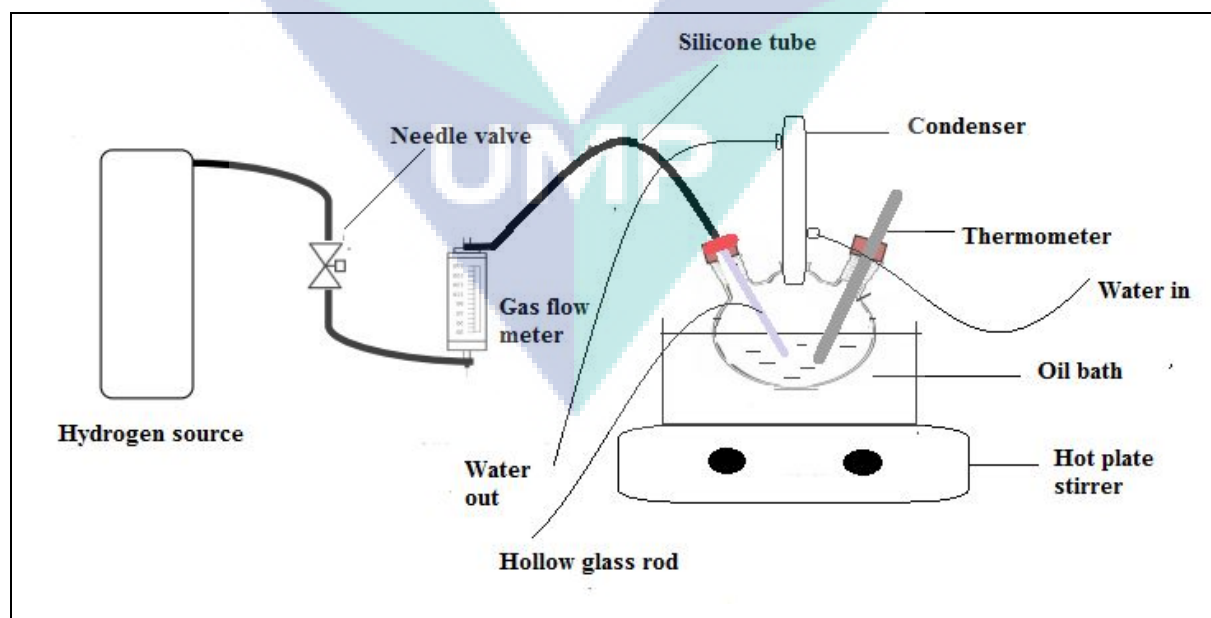


**Figure 3.2:** Reactor set-up for hydrogenation of NRL

*Catalytic activity of Ni and Pd nanoparticles towards hydrogenation of NRL*

Hydrogenations of NRL using Ni and Pd nanoparticles in monochlorobenzene were done by varying the reaction conditions such as amount of catalyst and nanoparticles sizes.

*i) Effect of catalyst amount (Monochlorobenzene)*

A series of 0.75 x $10^{-7}$, 1.5 x $10^{-6}$ and 6 x $10^{-6}$ mole of both nanocatalysts towards hydrogenation of 30 µl of NRL in 50 ml monochlorobenzene were carried out in order to investigate the influence of catalyst amount. The hydrogen gas was flowing at 58-60 ml/min and the temperature was kept constant at 120 $^{o}$C for 720 min.

*ii) Effect of particle size*

To investigate the influence of particle size of Me-NPs on NRL hydrogenation, all the reaction conditions were kept constant except the nanoparticle sizes. The different particle sizes were obtained by varying the volume ratio of latex stabilizer to metal precursor. The comparisons involved data after 360 min of reaction. The flow rate of hydrogen gas, temperature, catalyst concentration and rubber concentration were 58-60 ml/min, 120 $^{o}$C, and 30 µl of NRL in 50 ml of monochlorobenzene with addition of 6 x $10^{-6}$ mole of catalyst.

*Catalytic hydrogenation of NRL in aqueous medium*

Hydrogenation of NRL using Ni and Pd nanoparticles in aqueous medium was done by varying the reaction conditions such as solvents and amount of catalyst

*i) Effect of solvents*

The effects of water and monochlorobenzene (MCB) as solvent for NRL on the hydrogenation of 30 µl of NRL in 50 ml for each solvent in the presence of $6 \times 10^{-6}$ mole of Ni-NRL and Pd-NRL as nanocatalyst were investigated at atmospheric pressure and the mixture boiling point. The boiling point of aqueous solution and monochlorobenzene are 100 $^o$C and 120 $^o$C respectively. The flow rate of hydrogen gas flowing was kept constant at 58-60 ml/min for 720 min.

*ii) Effect of catalyst amount (Aqueous)*

Hydrogenation reaction involves of $6 \times 10^{-6}$, $1.2 \times 10^{-5}$, $1.8 \times 10^{-5}$ and $2.4 \times 10^{-5}$ mole of nanocatalyst and 30 µl of NRL in 50 ml aqueous solution were done to investigate the influence of catalyst concentration on the hydrogenation reaction. The hydrogen flow rate, reaction temperature and reaction duration were 58-60 ml/min, 100 $^o$C and 720 min respectively.

**3.5      CHARACTERIZATION**

**3.5.1    Characterization of synthesized metal nanoparticles**

A transmission electron microscopy (TEM) LEO 912AB energy filter instrument was used to determined the morphology and size of Ni-NRL and Pd-NRL nanoparticles. A drop of the colloidal solution was placed on a copper grid under ambient condition, followed by solvent evaporation. Typically, the TEM micrographs of each sample were taken at multiple, random locations in the sample to ensure that the images are representative. The individual particle diameters ($d_i$) were measured from the enlarged micrographs using a computer program "Gatan: Digital Micrograph". The average particle size ($d$) and standard deviation ($\sigma$) were obtained from at least 300 particles. The interaction between natural rubber latex and the nanoparticles was also investigated with a FTIR Perkin Elmer Spectrum 100 spectrometer.

**3.5.2    Characterization of hydrogenated natural rubber latex**

The hydrogenated samples were characterized by FTIR spectroscopy, SEM and FESEM while the degree of olefin hydrogenation was determined by ^{1}H NMR spectroscopy using Bruker 500-MHz spectrometer. The NMR determinations were carried out by dissolving $3 \pm 0.1$ mg of sample in 1000 µl of chloroform-D1 (CDCl$_3$).

The thermal stability studies were performed with TGA/DSC 1 high resolution thermogravimetric analyzer from Mettler Toledo using $3 \pm 0.1$ mg of sample. The temperature was increased under nitrogen atmosphere from room temperature to 800 $^0$C at a constant heating rate of 20 $^0$C/min. The nitrogen gas flow rate used was 45 ml/min.

*Calculation for the degree of hydrogenation*

The degree of hydrogenation for hydrogenated natural rubber by Ni-NRL and Pd-NRL nanoparticles was determined by calculating the differences in the percentage of olefinic proton (with respect to total proton signal) of blank NRL sample (A) against that of the catalyzed sample (B). The equation is as follow:

$$\frac{\dfrac{Total_{>5.15\ ppm}}{Total}_A - \dfrac{Total_{>5.15\ ppm}}{Total}_B}{\dfrac{Total_{>5.15\ ppm}}{Total}_A} \times 100\% = \%\ \text{Conversion B}$$

Where,

A = Blank NRL

B = Hydrogenated NRL (HNRL)

# CHAPTER 4

## RESULTS AND DISCUSSION

## 4.1 INTRODUCTION

This chapter will present and discuss the experimental results from this research. It consists of the synthesis and characterization of synthesized metal nanoparticles and their catalytic activity for the hydrogenation reaction of NRL.

The characterization of nanoparticles involved the use of transmission electron microscopy (TEM) to determine the size and distribution of particles. The Fourier transform infrared (FTIR) spectra of samples were analyzed to identify the interaction between nanoparticles (NPs) and the NRL.

The catalytic hydrogenation reaction of NRL was conducted under conventional stirring at solvent boiling temperature and atmospheric pressure. The extent of hydrogenation under different reaction conditions were determined and compared. The relationship between catalytic activity and catalyst characteristics will be discussed in order to explain the catalytic behavior of the catalysts. The FTIR, SEM and FESEM data will be used to characterize hydrogenated NRL. Finally, the decomposition of the hydrogenated in thermogravimetric analyzer (TGA) would also elucidate the nature of the hydrogenated product.

## 4.2 SYNTHESIS AND CHARACTERIZATION OF METAL NANOPARTICLES

The metal nanoparticles of Ni and Pd were synthesized by chemical reduction method using reducing agent as described in section 3.4.1. Firstly, the Ni nanoparticles were formed under different synthesis parameters to optimize the reaction conditions. These include the effect of synthesis method, Ni precursor, volume ratio of latex to metal precursor, sonication time and pH. Then, the optimum reaction conditions of Ni nanoparticles were used to synthesis Pd nanoparticles for catalytic study.

The most important characteristics of metal nanoparticles are morphology, particle size distribution and the interaction between Me-NPs with stabilizer. The techniques used in this study to characterize Me-NPs include transmission electron microscopy (TEM) and Fourier transform infrared (FTIR) spectroscopy. The findings from these analyses are discussed in the next sub sections.

### 4.2.1 TEM analysis

*Effect of synthesis method*

Typical micrographs and particle size distribution for Ni nanoparticles prepared through different synthesis methods are shown in Figures 4.1 (a-c). Figure 4.1a shows the TEM images of monometallic Ni nanoparticles prepared using conventional heating (reflux) method. The particles are aggregated with diameter ranging from 25-50 nm. Meanwhile, under ultrasonic (Figure 4.1b) and microwave (Figure 4.1c) irradiation methods, the average diameters of particles were 10-20 nm and 8-10 nm respectively.
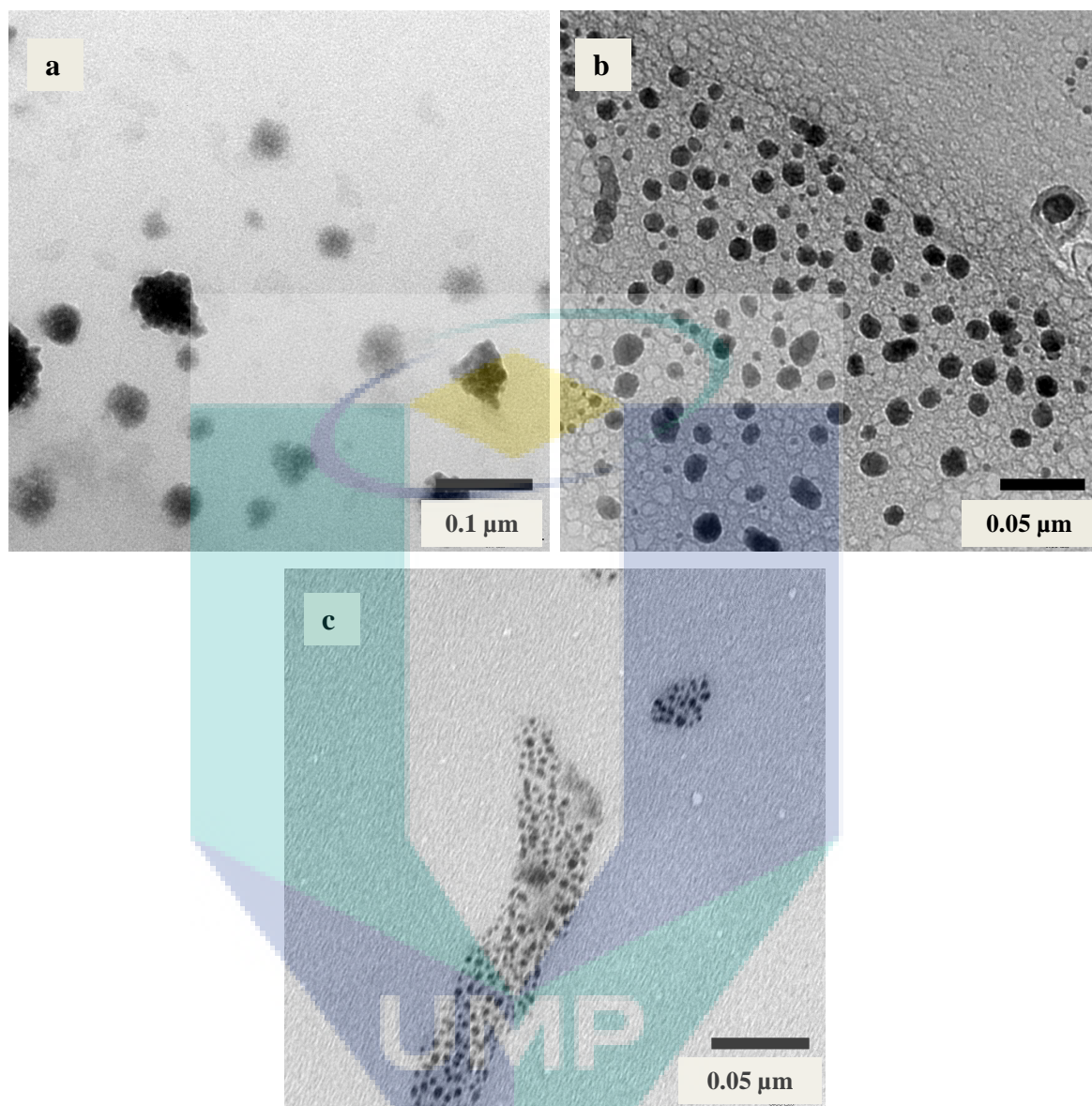
**Figure 4.1:** TEM images of Ni nanoparticles synthesized using (a) conventional heating, (b) ultrasonic irradiation and (c) microwave irradiation method

Microwave irradiation method resulted in smallest particle sizes for Ni nanoparticles followed by ultrasonic irradiation and refluxing method. The ultrasonic irradiation produces the most well dispersed Ni nanoparticles. All the TEM images show spherical and nearly spherical shape particles. The time required to reduce Ni nanoparticles was 90 min at 80 $^{\circ}$C of refluxing, 30 min at 80 $^{\circ}$C of ultrasonication process and 60 s of 300 W of microwave irradiation method. Table 4.1 summarized the formation of Ni nanoparticles through the different synthesis methods.

**Table 4.1:** Formation of Ni nanoparticles using different synthesis methods

| Synthesis Method | Temperature | Time Required | Mean Diameter, $d$ (nm) |
|---|---|---|---|
| Conventional Heating | 80 $^{\circ}$C | 90 min | 25-50 (Aggregated) |
| Ultrasonic Irradiation | 80 $^{\circ}$C | 30 min | 10-20 |
| Microwave Irradiation | 300 W | 60 s | 8-10 |

TEM analysis indicated that the microwave irradiation method can produce smaller nanoparticles with shorter reaction time in comparison with the conventional heating and ultrasonic irradiation process. Meanwhile, the ultrasonic irradiation method produced highly dispersed nanoparticles. Thus, the use of microwave irradiation in combination of ultrasonic irradiation at ambient temperature may fulfill the requirements to produce good dispersion of nanoparticles with short reduction time and low energy requirements.

*Effect of Ni precursor concentration*

Figures 4.2 (a-c) show typical TEM images of Ni nanoparticles prepared from different concentrations of the precursor with the same volume ratio of stabilizer/Ni(II) of 30/10 (but decreasing molar ratio of latex: Ni due the increase in concentration of Ni) using microwave heating for 60 s and 15 min ultrasonication process. The mean particle sizes of different precursors were tabulated in Table 4.2. TEM analysis indicated that, when the concentration of nickel chloride was 0.003, 0.005 and 0.008 M, the mean size of the as-prepared nanoparticles was 10.8±0.3 nm, 48.2±4.3 nm and 73.7±7.0 nm respectively as shown in Figure 4.2 (a-c).
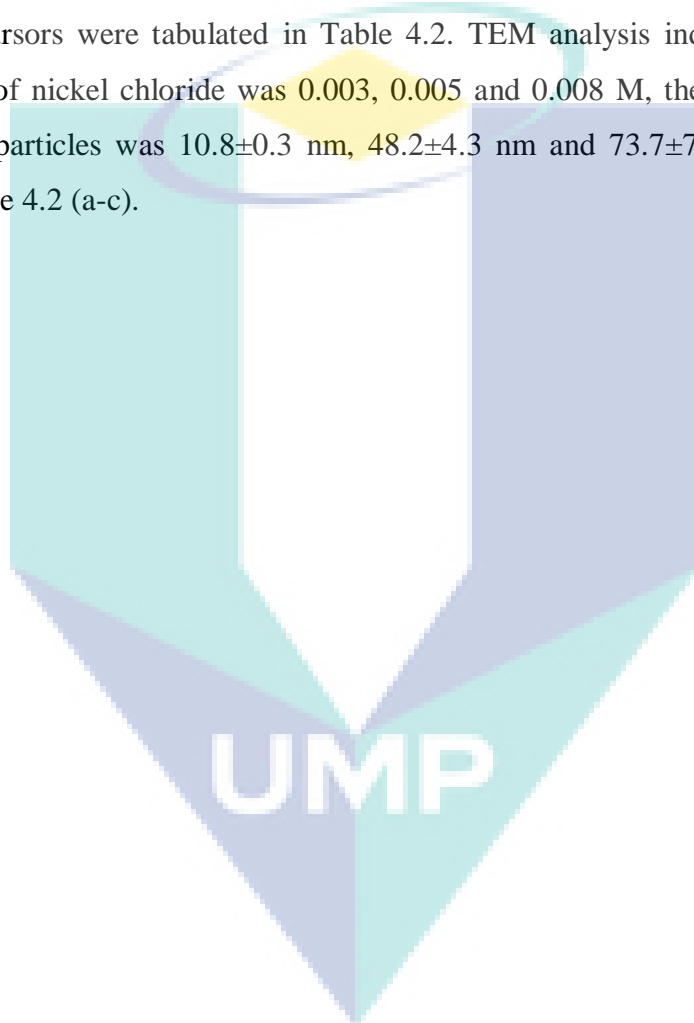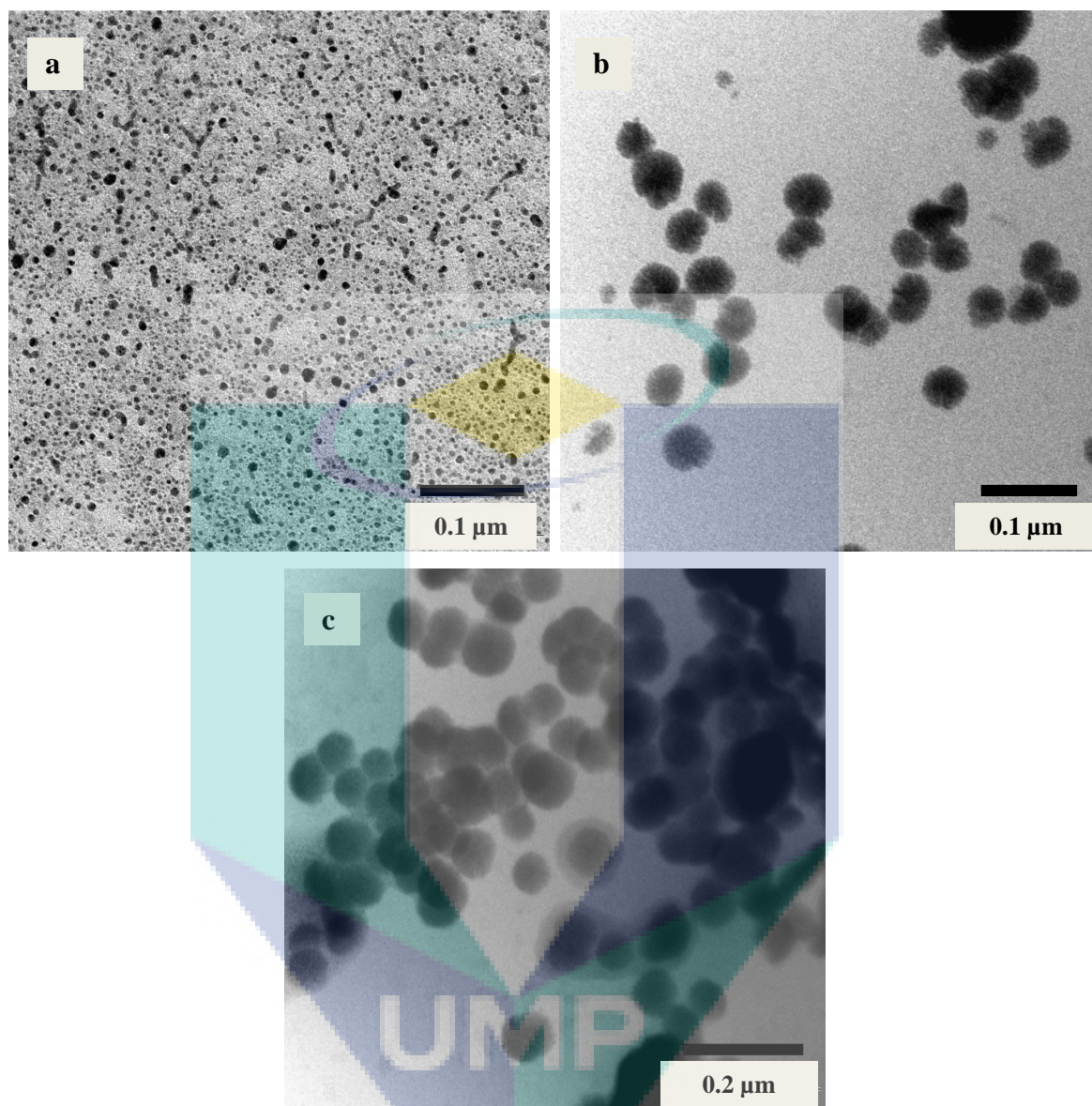
**Figure 4.2:** TEM images of Ni nanoparticles synthesized using (a) 0.003 M, (b) 0.005 M, and (c) 0.008 M of Ni precursor

**Table 4.2:** The size of Ni nanoparticles prepared using different concentrations of Ni precursor

| Concentration | Mean Diameter, $d$ (nm) | Standard Deviation, $\sigma$ (nm) |
|---|---|---|
| 0.003 M | 10.8 | 0.3 |
| 0.005 M | 48.2 | 4.3 |
| 0.008 M | 73.7 | 7.0 |

The size distributions of the particles formed from different precursor concentrations are shown in Figure 4.3. Almost all of the particles in the colloidal system with stabilizer: Ni(II) ratio of 30:10 (0.003 M) has spherical or nearly spherical shape with diameter of 10-11 nm. However, for synthesis starting with precursor concentrations of 0.005 M to 0.008 M, most particles have mean diameters in the range of 40-60 nm and 60-90 nm respectively.
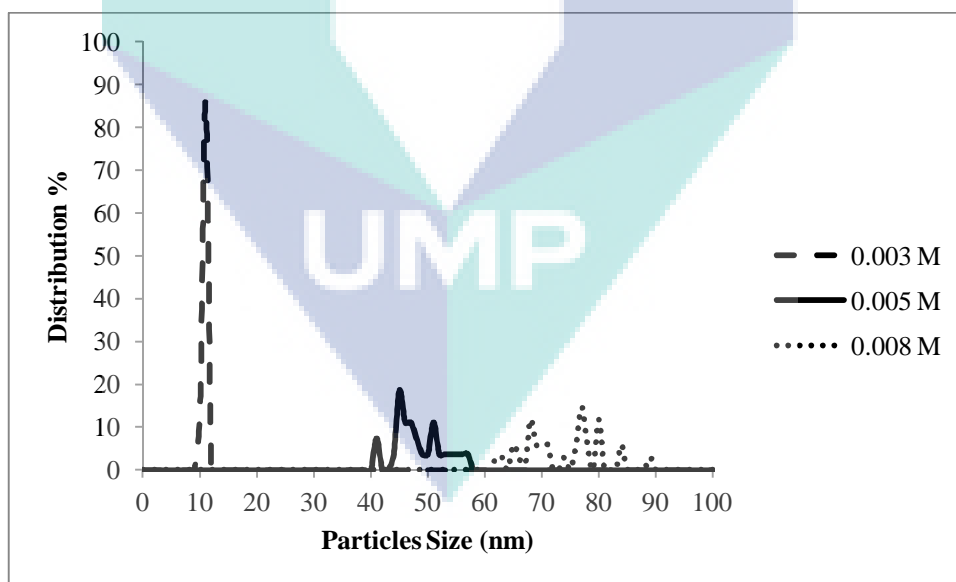


**Figure 4.3:** Size distribution of Ni nanoparticles synthesized using different concentrations of Ni precursor

At low precursor concentration, lesser amount of Ni is formed resulting in smaller particles. With the increase of nickel chloride concentration, more metallic Ni are formed and these nanoparticles and have more opportunity to agglomerate to form large aggregates. At higher Ni concentration, the stabilizer is unable to stabilize the metal with the increase of precursor concentration and decease in molar ratio of latex to Ni. In conclusion, the size of Ni nanoparticles formed is strongly dependent on the precursor concentration and this is consistent with the findings of Kim et al. (2009), Abbasi and Morsali (2010) and Tong et al. (2012).

### *Effect of volume ratio of latex to metal precursor*

Figure 4.4 (a-c) shows the TEM images and mean particle size of Ni nanoparticles prepared with the different volume ratios of latex to metal precursor. The ratio of latex to metal precursor has a drastic effect on the size distribution of nickel nanoparticles. Volume ratio of latex solution to that of metal precursor of 30:10, 20:20 and 10:30 gave rise to average sizes of 10.8±0.3 nm, 13.4±0.4 nm and 26.0±2.6 nm respectively. The mean particle sizes are summarized in Table 4.3 while Figure 4.5 illustrates the size distribution of Ni nanoparticles formed with different latex to metal precursor ratios. It is observed that higher volume ratio of stabilizer to Ni precursor produces smaller Ni nanoparticles with narrower size distribution.
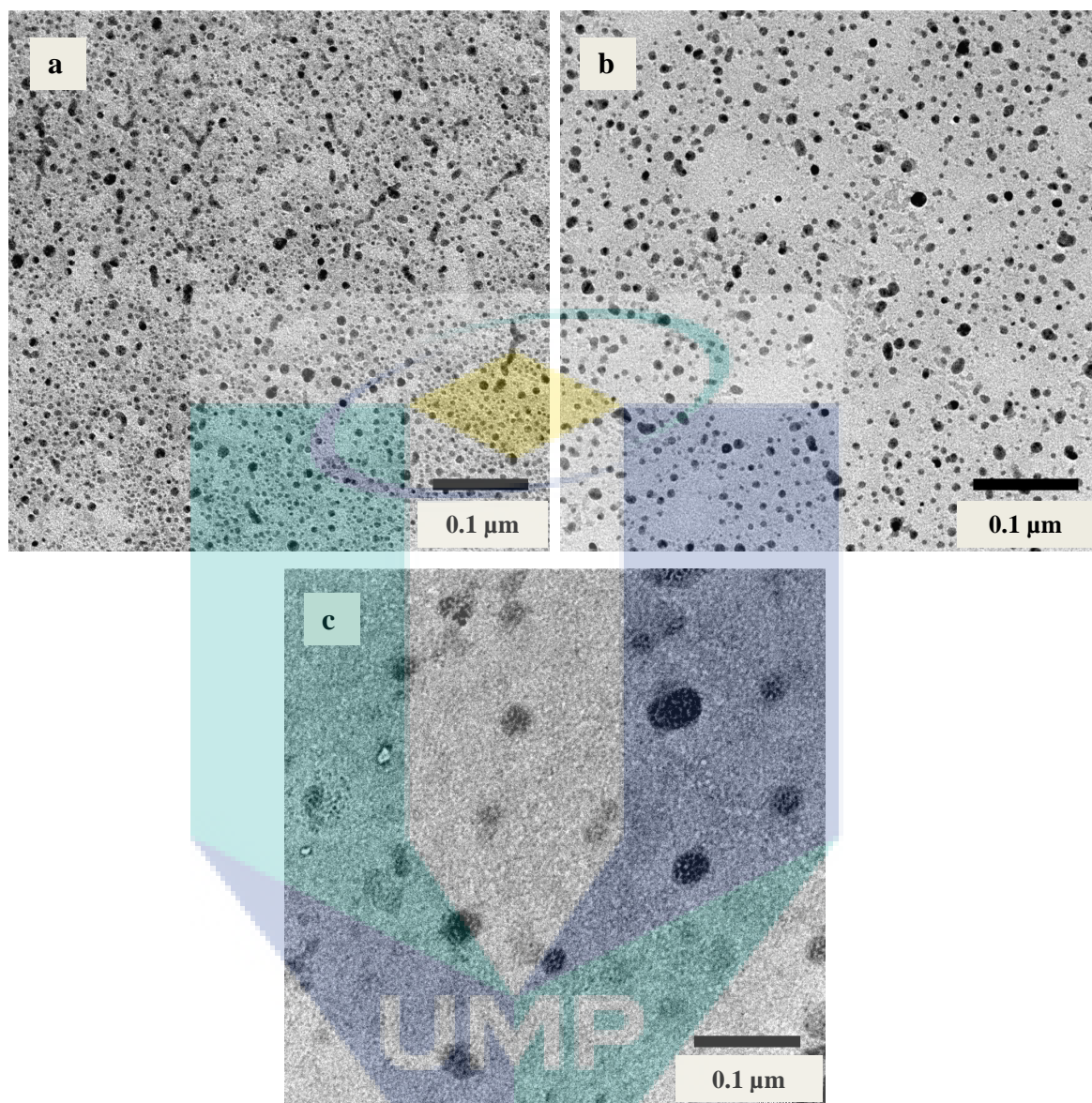
**Figure 4.4:** TEM images of Ni nanoparticles synthesized with volume ratio of latex solution to that of Ni precursor of (a) 30:10, (b) 20:20 and (c) 10:30

**Table 4.3:** The effect of volume ratio of latex solution to metal solution on the sizes of Ni nanoparticles

| Latex solution/ 0.003 M Ni(II) | Mean Diameter, $d$ (nm) | Standard Deviation, $\sigma$ (nm) |
|---|---|---|
| 30:10 | 10.8 | 0.3 |
| 20:20 | 13.4 | 0.4 |
| 10:30 | 26.0* | 2.6 |

\* Agglomerates
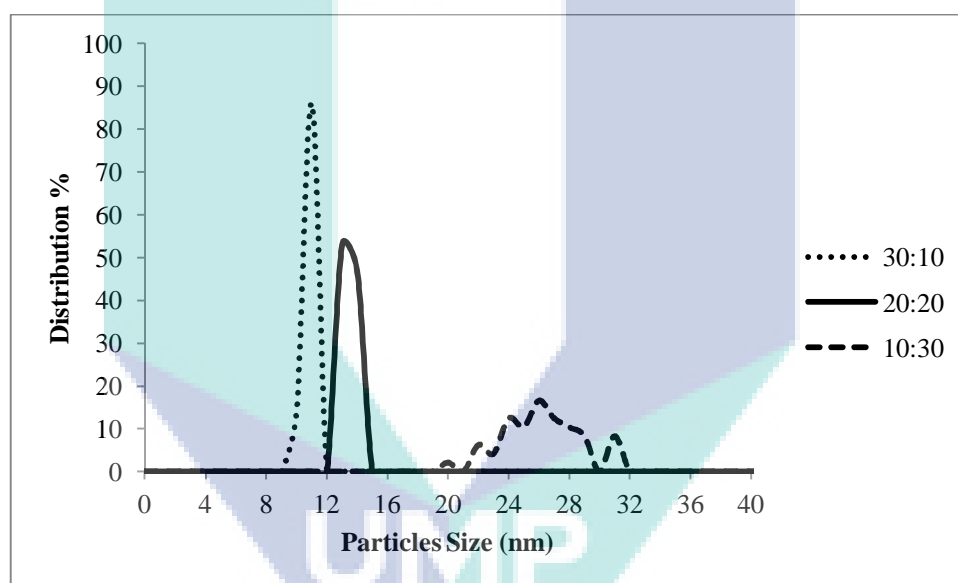


**Figure 4.5:** Size distribution of Ni nanoparticles as a function of volume ratio of latex solution to that of Ni precursor

Figures 4.6 (a-c) shows the typical TEM images of Pd nanoparticles prepared under similar condition as that for Ni as presented above. The mean particle sizes are summarized in Table 4.4 while Figure 4.7 illustrates the size distribution of Pd nanoparticles prepared using different latex to metal precursor ratios. Volume ratios of latex solution to that of metal precursor of 30:10, 20:20 and 10:30 gave rise to average particle size of 30.6±2.9 nm, 56.7±6.1 nm and 73.9±7.7 nm respectively. Generally, the average particle sizes of Pd

nanoparticles are larger than that of nickel. The increasing amount of latex compared to Pd resulted in smaller particle size while smaller quantity of latex used resulted in agglomeration of the nanoparticles produced. These results are consistent with the findings reported by Harpeness et al. (2005) and Liu et al. (2008).
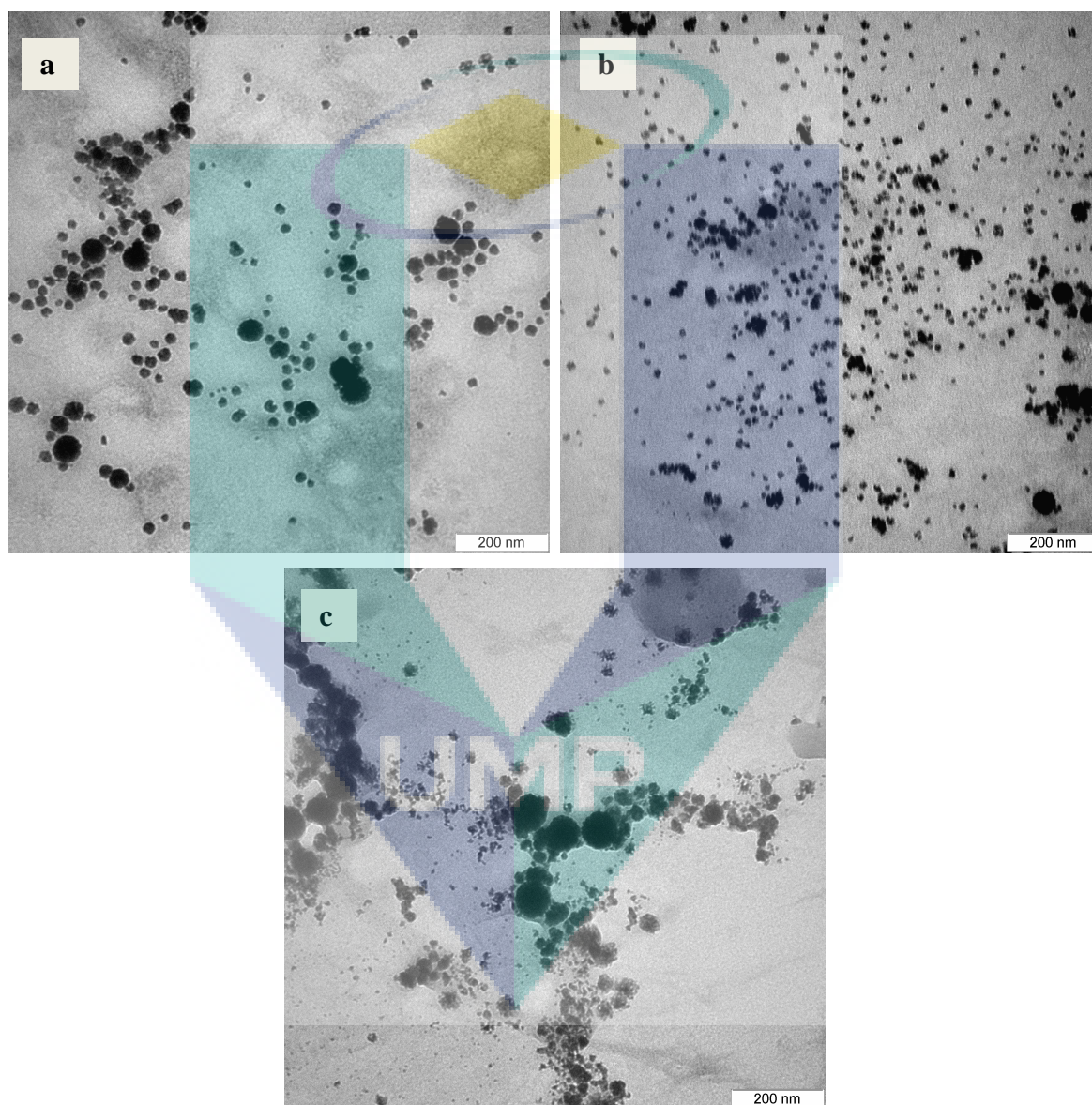


**Figure 4.6:** TEM images of Pd nanoparticles synthesized with volume ratio of latex solution to that of Pd precursor of (a) 30:10, (b) 20:20 and (c) 10:30

**Table 4.4:** The effect of volume ratio of latex solution to that of Pd precursor on the sizes of Pd nanoparticles

| Latex solution/ 0.003 M Pd(II) | Mean Diameter, $d$ (nm) | Standard Deviation, $\sigma$ (nm) |
|---|---|---|
| 30:10 | 30.6 | 2.9 |
| 20:20 | 56.7 | 6.1 |
| 10:30 | 73.9* | 7.7 |

*Agglomerated
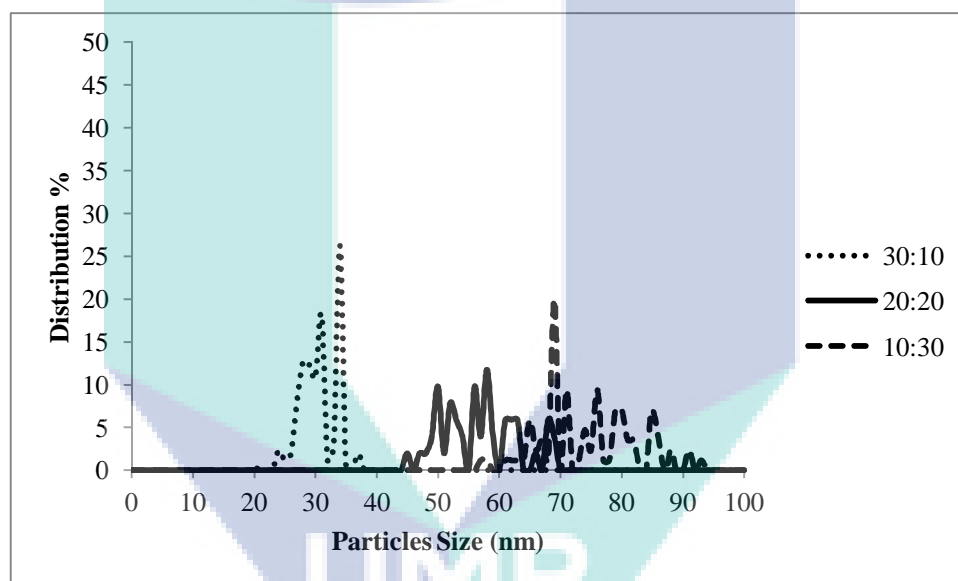


**Figure 4.7:** Size distribution of Pd nanoparticles as a function of volume ratio of latex solution to that of Pd precursor

*Effect of sonication time*

To investigate the effect of sonication time on the morphology and distribution of particle size, the duration of ultra sonic irradiation treatment prior to microwave irradiation was varied to be 15, 60 and 90 min. Other parameters were kept constant as described in section 3.4.1. The TEM micrographs of Ni nanoparticles prepared with different durations of sonication treatment are shown in Figure 4.8 (a-c) and their mean particle sizes are summarized in Table 4.5.
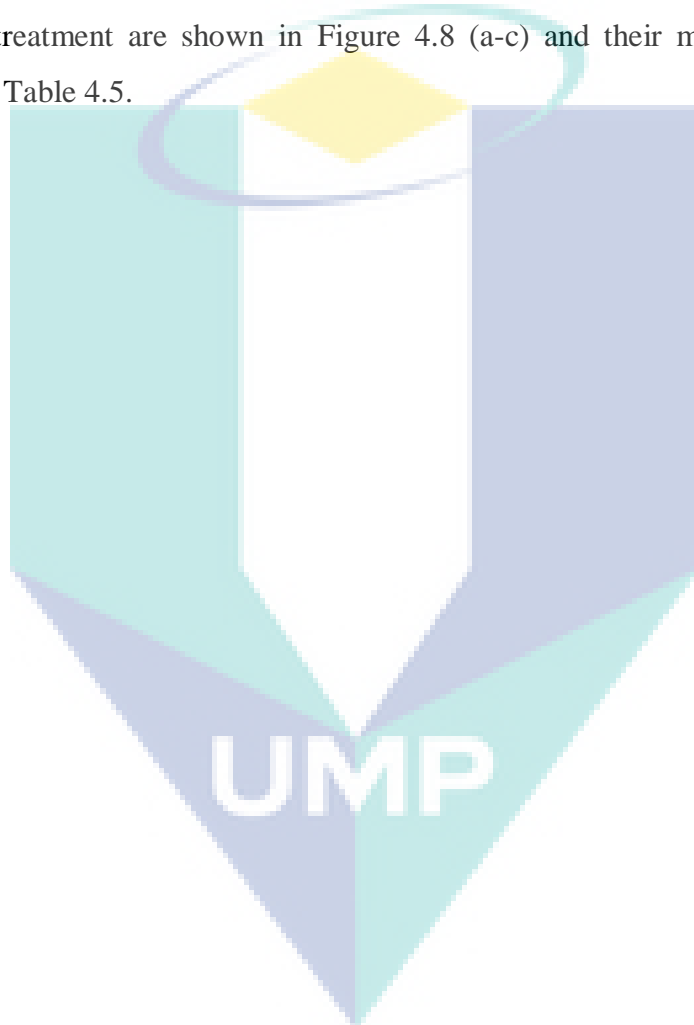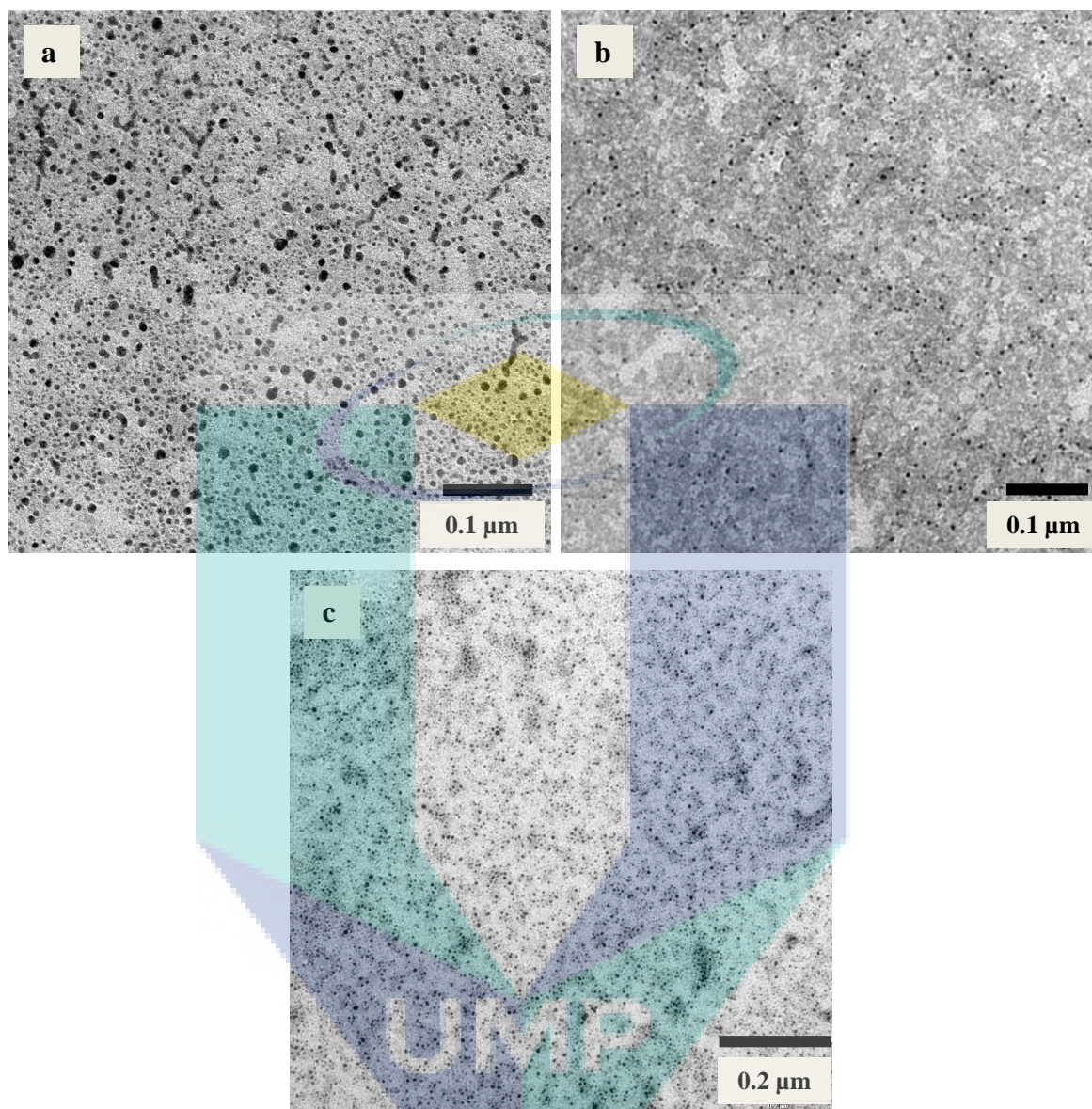
**Figure 4.8:** TEM images of Ni nanoparticles synthesized using (a) 15 min, (b) 60 min and (c) 90 min of sonication time

**Table 4.5:** The effect of sonication time on the sizes of Ni nanoparticles

| Sonication Time (min) | Mean Diameter, $d$ (nm) | Standard Deviation, $\sigma$ (nm) |
|---|---|---|
| 15 | 10.8 | 0.3 |
| 60 | 6.7 | 0.6 |
| 90 | 4.0 | 0.3 |

Homogeneous nanoparticles having mean diameter of 10.8±0.3 nm were formed after 15 min of ultrasonication (Figure 4.8a). The mean particle sizes after 60 min (Figure 4.8b) and 90 min (Figure 4.8c) of sonication are 6.7±0.6 nm and 4.0±0.3 nm respectively. The size distributions of Ni nanoparticles formed after different sonication time are presented in Figure 4.9.
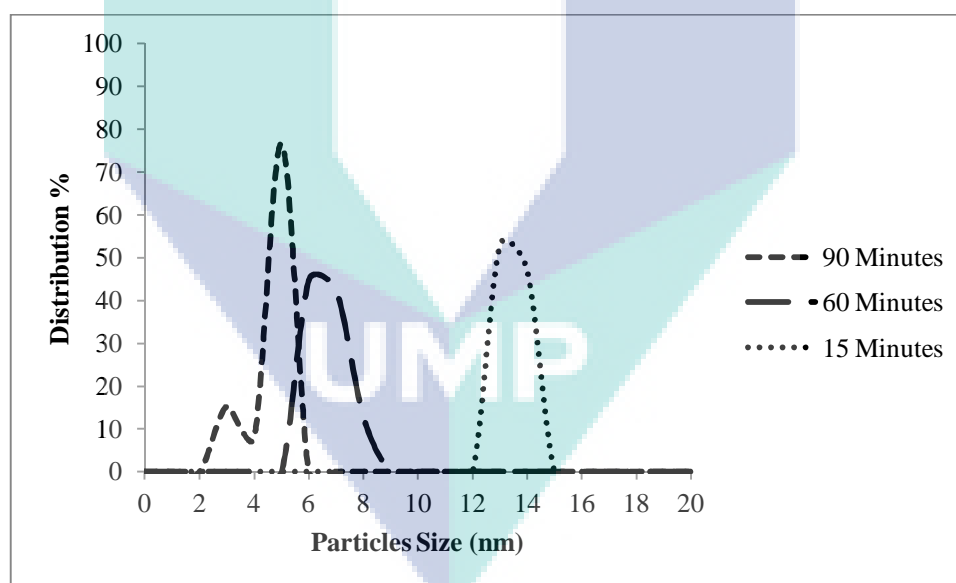


**Figure 4.9:** Size distribution of Ni nanoparticles prepared with different duration of sonication

It can be observed that most of the nanoparticles have particle size of 2-5 nm for 90 min ultrasonication process compared to 6-8 nm for 60 min and 10-11 nm for 15 min of sonication. The nanoparticle size decreases with the increased of sonication time. On the other hand, no aggregation and changes of nanoparticles shape were observed after long duration ultrasonication. It showed that sonochemical treatment could play an important role in controlling the aggregation and uniformity of the nanoparticles. These results are in agreement with that reported by Darroudi et al. (2012) for the synthesis of colloidal silver nanoparticles by sonochemical method.

*Effect of pH*

Figures 4.10 (a-d) show the TEM images of Ni nanoparticles prepared at different pHs using the same volume ratio of stabilizer/(0.003 M)Ni (II) of 30/10 after 15 min of ultrasonication and 60 s microwave heating. The mean diameter and standard deviation of the particle are presented in Table 4.6. At lower pH 10.30, aggregated Ni nanoparticles were formed (Figure 4.10a). Well dispersed Ni nanoparticles with uniform size having diameter of 10.8±0.3 nm were produced when the pH was 11.50 (Figure 4.10b). It is observed that when the pH of solution was increased from 11.50 to 11.80 and 12.30, the nanoparticles exhibited two particle distributions which were small (0-9 nm) and large (10-20 nm) spherical and nearly spherical shapes. The mean diameter at pH 11.80 (Figure 4.10c) and 12.30 (Figure 4.10d) were 10.8±2.8 nm (large), 4.3±0.3 nm (small) and 12.3±4.7 nm (large), 4.7±0.7 nm (small) respectively. This indicates that higher pH facilitates the formation of more regular particles. These particles however undergo agglomeration to form the dual particle size distribution. This may relate to the increasing stability of the colloidal system of latex at higher pH that then influences the rate of reduction of the metal ions.
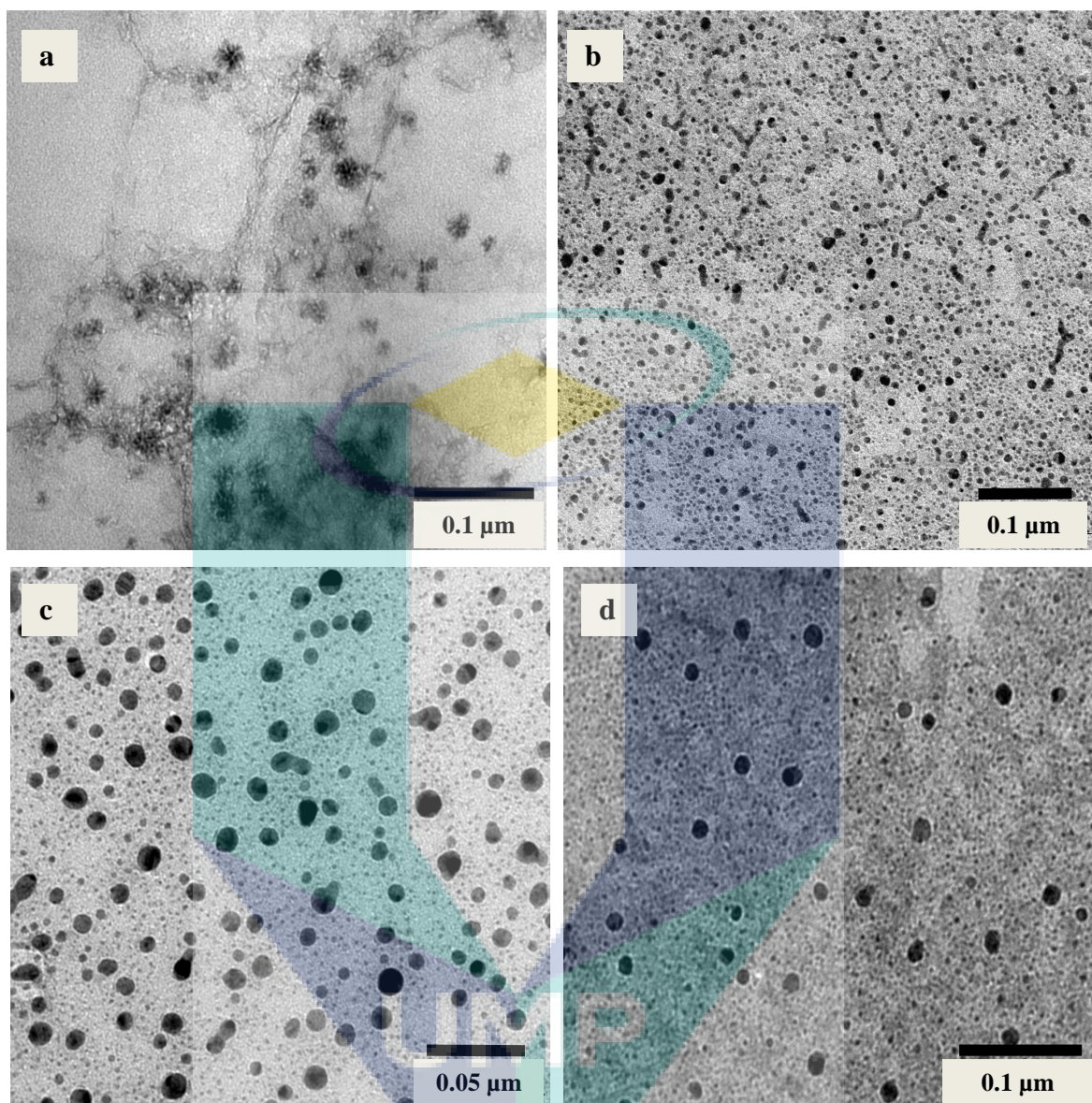
**Figure 4.10:** TEM images of Ni nanoparticles synthesized at (a) pH 10.30, (b) pH 11.50, (c) pH 11.80 and (d) pH 12.30

**Table 4.6:** The size of Ni nanoparticles synthesized at different pHs

| pH | Mean Diameter, $d$ (nm) | Standard Deviation, $\sigma$ (nm) |
|---|---|---|
| 11.50 | 10.8 | 0.3 |
| 11.80 | 10.8 (L):4.3 (S) | 2.8 (L):0.3 (S) |
| 12.30 | 12.3 (L):4.7 (S) | 4.7 (L):0.7 (S) |

When the amount of ammonia ($NH_3$) added into the colloidal mixture was increased, the smaller spherical or nearly spherical shape nanoparticles were the most frequently observed, while larger particles were rarely found. The distributions of Ni nanoparticles at pH 11.50, 11.80 and 12.30 are illustrated in Figure 4.11. It can be seen that, almost all of the particles have uniform size with diameter of 10-11 nm at pH 11.50. However, at pH 12.30, about 90 % of smaller spherical or nearly spherical shapes were found compared to 70 % at pH 11.80.
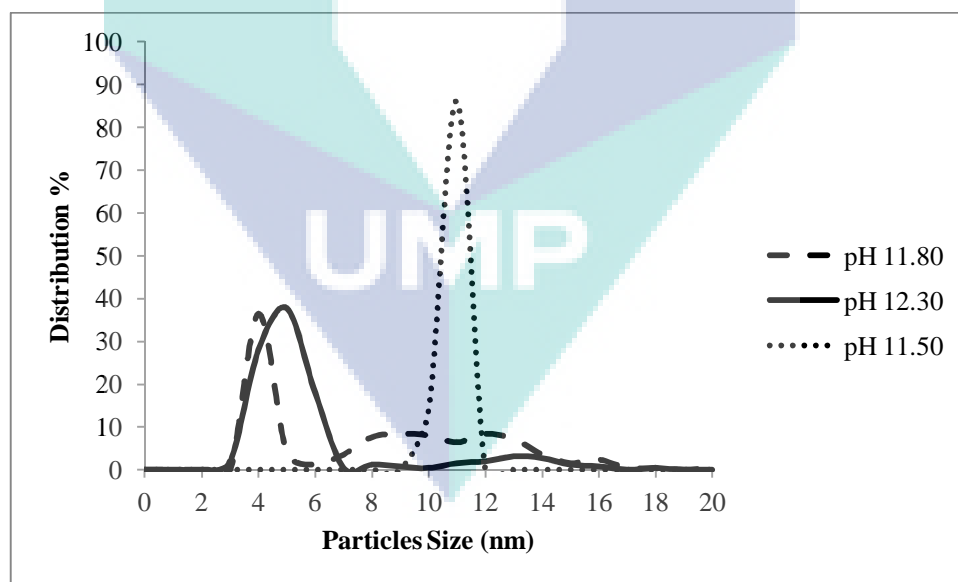


**Figure 4.11:** Size distribution of Ni nanoparticles synthesized at different pHs

It can be concluded that, the pH of the colloidal system affects the morphology and distribution of Ni nanoparticles. At high pH, base presence would neutralize the proton released in the reduction process and accelerated nucleation. This result is consistent with the findings reported by He et al. (2004) and Choo et al. (2006).
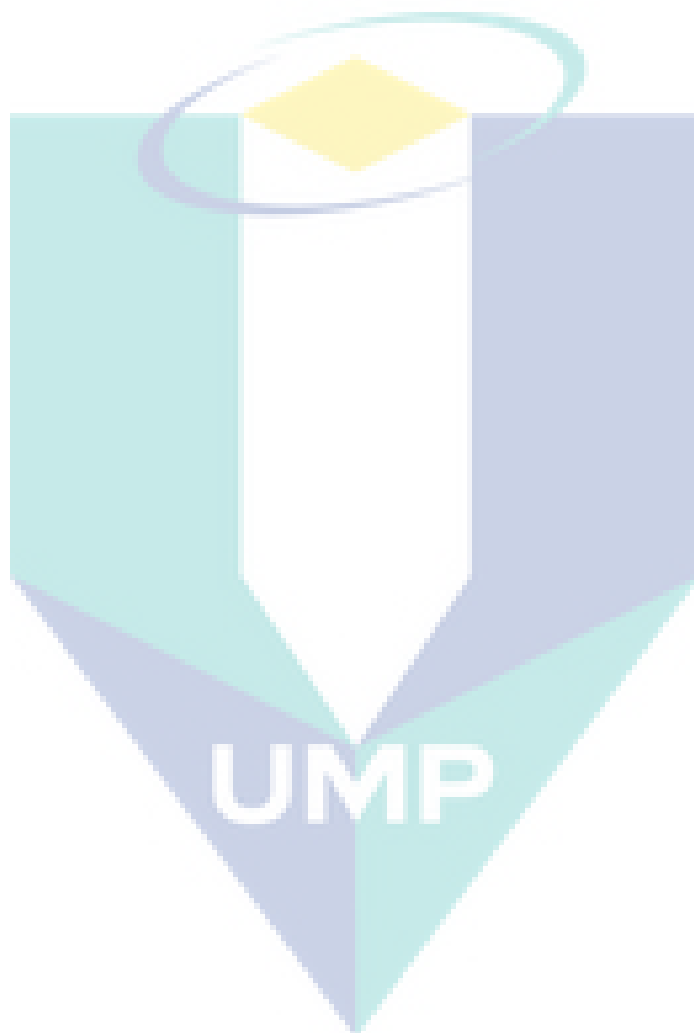
### 4.2.2 FTIR analysis

Figures 4.12 and 4.13 present the infrared spectra of fresh NRL, NRL blank (without metallic nanoparticles but undergone the same treatment as that for nanoparticles preparation), Ni-NRL and Pd-NRL samples. The assignment of the fundamental vibration modes of NRL blank, Ni-NRL, and Pd-NRL samples are shown in Table 4.7. The FTIR spectrum of fresh and blank NRL have similar characteristic with the FTIR spectrum reported in the literature for cis-isoprene structure (Guidelli et al., 2011). The main vibration bands of NRL blank are associated with the C–H stretching at 2961 cm$^{-1}$, the symmetric and asymmetric stretching of the CH$_3$ group at 2915 and 2853 cm$^{-1}$. The symmetric and asymmetric bending of the CH$_3$ group is in the region of 1447 and 1376 cm$^{-1}$ and the C=C stretching and olefinic C–H bending are located at 1664 and 836 cm$^{-1}$ respectively. On the other hand, the vibration bands at 1739 cm$^{-1}$, 1543 cm$^{-1}$ and 1243 cm$^{-1}$ are assigned to C=O stretching, N-H bending and O-P-O asymmetric stretching respectively.

In general, the FTIR spectra of the sample of nanoparticles synthesized in the presence of NRL are broader and less resolved. The intensities of the bands at 2961, 2915, and 2853 cm$^{-1}$ decrease dramatically, whereas the bands at 1447 and 1376 cm$^{-1}$ become broader and more intense. A shift of the bands at 1664, 1447, 1376, 1083 and 836 cm$^{-1}$ toward a smaller wavenumber for different ratios of latex to metal precursor are shown in Table 4.7. The peaks associated to C=O stretching, N-H bending and O-P-O tend to be more intense in the presence of metal nanoparticles especially at smaller ratio of latex to metal.

New peaks appear in the region of 3100–3600 cm$^{-1}$. The broad band at 3100–3600 cm$^{-1}$ is associated with the retention of water in the NRL matrix during the synthesis. The band in this region is also related to the N–H stretching as the NRL was conserved in ammonia. This suggests that the amine group interacted with the nanoparticles surfaces.
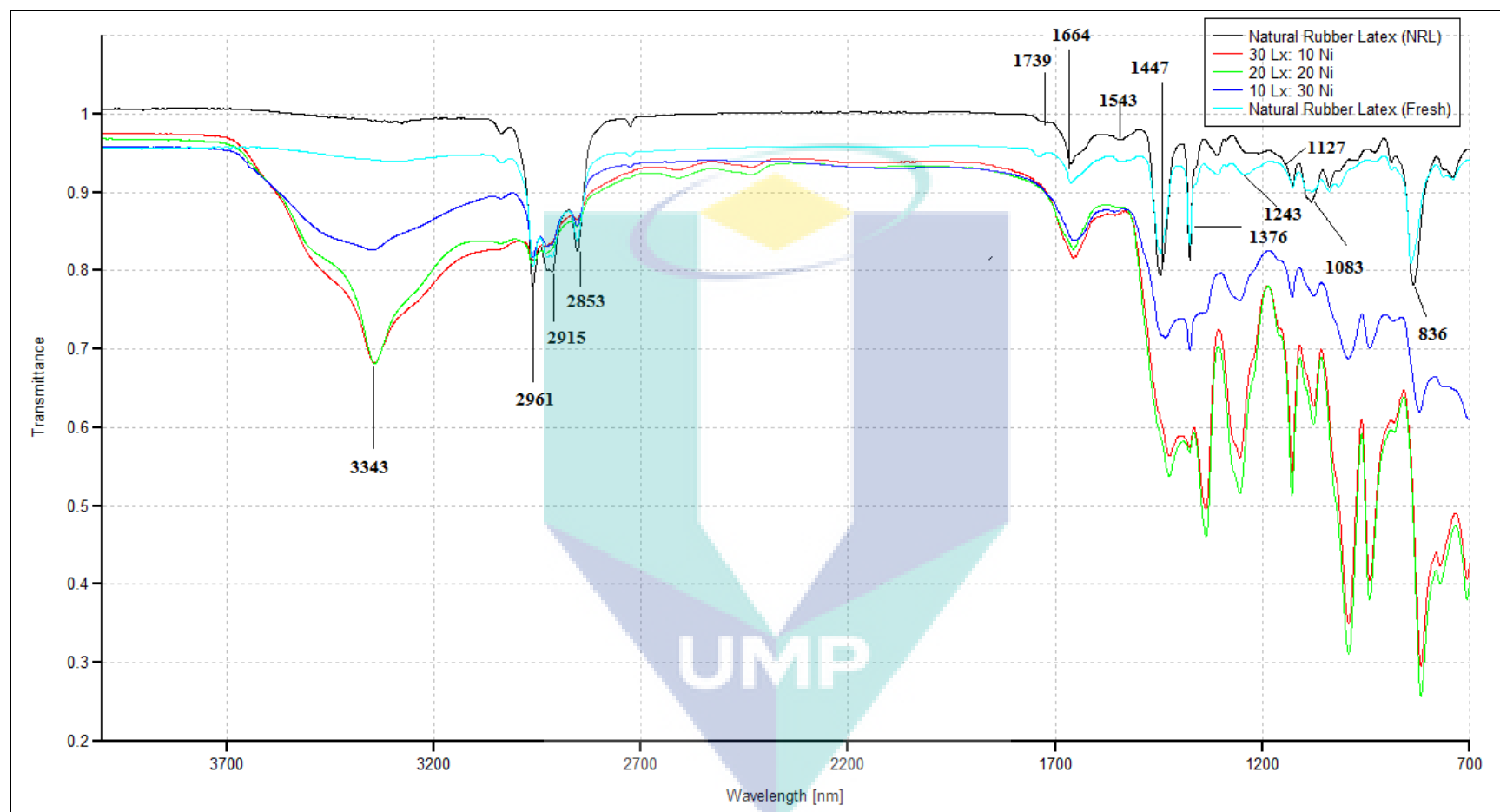
**Figure 4.12:** FTIR spectra of NRL blank and Ni-NRL samples
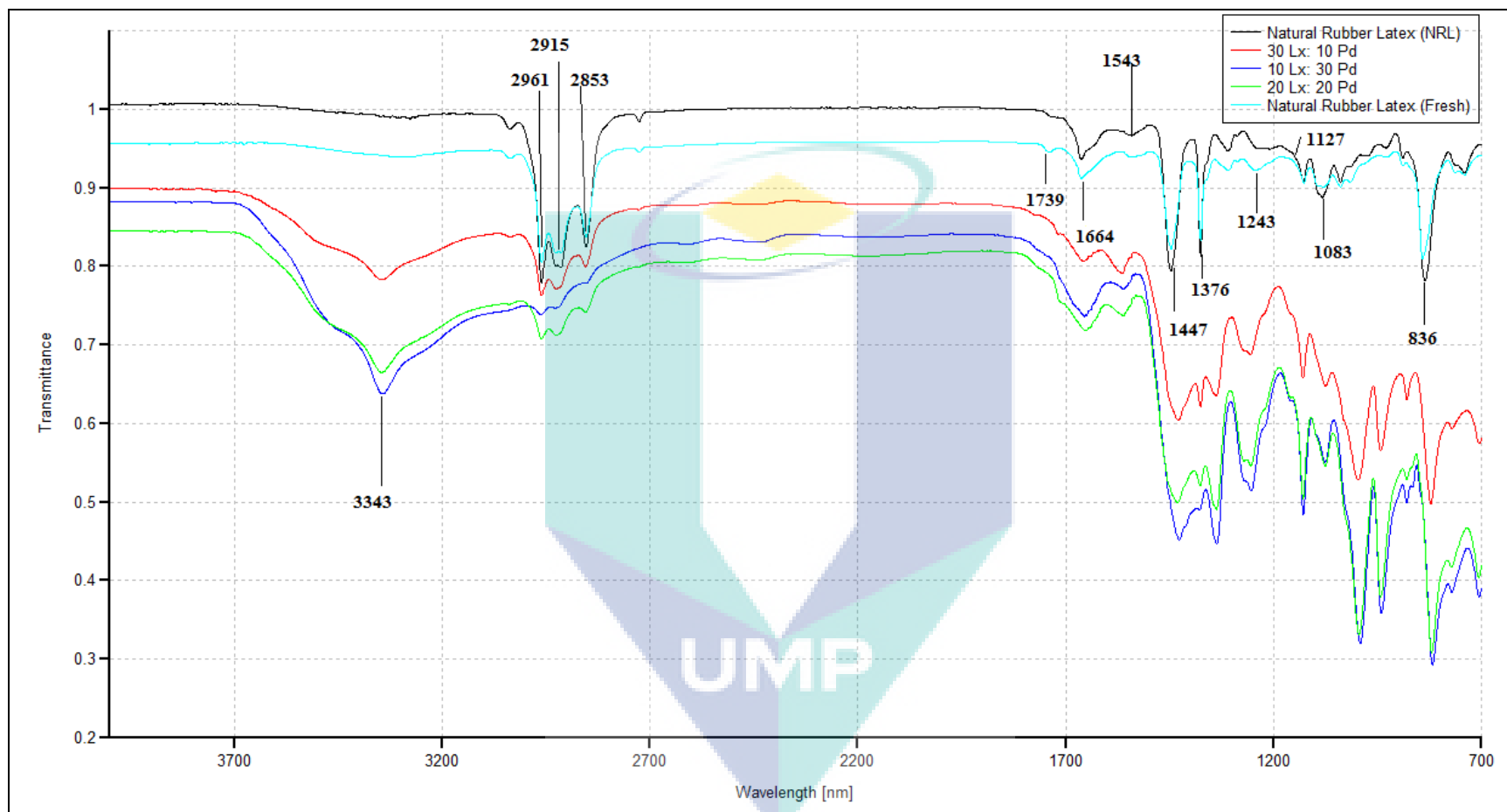
**Figure 4.13:** FTIR spectra of NRL blank and Pd-NRL samples

**Table 4.7**: Assignment of the fundamental vibration modes for NRL blank, Ni-NRL, and Pd-NRL samples

| Assignment | NRL Blank (cm⁻¹) | 30 Lx: 10 Ni (cm⁻¹) | 30 Lx: 10 Pd (cm⁻¹) | 20 Lx: 20 Ni (cm⁻¹) | 20 Lx: 20 Pd (cm⁻¹) | 10 Lx: 30 Ni (cm⁻¹) | 10 Lx: 30 Pd (cm⁻¹) |
|---|---|---|---|---|---|---|---|
| O – H Stretching | - | 3100-3600 | 3100-3600 | 3100-3600 | 3100-3600 | 3100-3600 | 3100-3600 |
| $CH_3$ Stretching | 2961 | 2961 | 2961 | 2961 | 2961 | 2961 | 2962 |
| $CH_2$ Asymmetric Stretching | 2915 | 2930 | 2925 | 2929 | 2926 | 2927 | 2928 |
| $CH_2$ Symmetric Stretching | 2853 | 2854 | 2854 | 2855 | 2855 | 2854 | - |
| C=O Stretching | 1739 | - | 1717 | - | 1717 | - | 1717 |
| C=C Stretching | 1664 | 1655 | 1656 | 1655 | 1650 | 1657 | 1654 |
| N-H Bending | 1543 | 1555 | 1562 | 1557 | 1561 | 1557 | 1560 |
| $CH_2$ Bending | 1447 | 1424 | 1429 | 1425 | 1430 | 1435 | 1427 |
| C-H Asymmetric Bending | 1376 | 1337 | 1339 | 1337 | 1338 | 1375 | 1338 |
| O-P-O Asymmetric Stretching | 1243 | 1254 | 1256 | 1254 | 1255 | 1256 | 1254 |
| $CH_2$ Wagging | 1127 | 1128 | 1129 | 1128 | 1129 | 1128 | 1128 |
| $C-CH_2$ Stretching | 1083 | 1077 | 1075 | 1077 | 1076 | 1076 | 1076 |
| C=C-H Bending | 836 | 818 | 822 | 818 | 820 | 822 | 818 |

It can be observed that in Pd-NRL the peak at 1739 $cm^{-1}$ shifted to the smaller wavenumber to 1717 $cm^{-1}$. For Ni-NRL, the vibration cannot be detected as it merged with other vibrational band. On the other hand, the vibrational bands of Ni-NRL and Pd-NRL at 1543 $cm^{-1}$ and 1243 $cm^{-1}$ become more intense and wider compared to the NRL blank. The position and changes of transmittance peak of the carbonyl group associated to fatty acids at 1739-1742 $cm^{-1}$, 1543 $cm^{-1}$ (N-H stretching) and that of phosphate group at 1243 $cm^{-1}$ in the Pd-NRL and Ni-NRL samples suggest that the functional group interacted with the nanoparticles. It is known that these functional groups have strong affinities for metals, thus preventing their agglomeration as reported by Guidelli et al. (2005). The FTIR spectra support the hypothesis that the cis-isoprene molecules of the NRL act as a capping agent, thereby avoiding agglomeration of the nanoparticles (Abu Bakar et al., 2007 and Bar et al., 2009).

On the whole, these changes suggest an interaction between the metal nanoparticles and the cis-isoprene molecules present in the NRL. The substantial lowering of the C=C stretching peak suggests that the interaction between natural rubber latex and the metallic nanoparticles may also involve the C=C functional group.

*Summary: Effect of reaction condition on the size of Me-NPs and its characterization*

TEM analysis indicated that microwave irradiation method resulted in smallest particle size for Ni-NRL nanoparticles, followed by ultrasonic irradiation and refluxing method. The ultrasonic irradiation method produces the most well dispersed Ni-NRL nanoparticles. The particle sizes of the NPs decreases with pH, sonication time, and stabilizer concentration. The particle size increases with the increased of metal ions precursor concentration. At optimum reaction conditions, the average particle sizes of Pd-NRL are larger than that of Ni-NRL nanoparticles. On the other hand, from FTIR analysis, it can be observed that, there is an interaction between NPs and the cis-isoprene molecules of the NRL. Thus, it can be concluded that latex was able to stabilize the Me-NPs and prevent their agglomeration.

## 4.3 CATALYTIC ACTIVITY OF NI AND PD NANOPARTICLES TOWARDS HYDROGENATION OF NATURAL RUBBER LATEX (NRL)

The hydrogenation of NRL catalyzed by as-prepared Ni and Pd nanoparticles having diameter of 10.8±0.3 nm and 30.6±2.9 nm respectively were done. The degree of hydrogenation of latex were calculated based on the integrated peak area of C=CH-(olefinic) proton using $^1$H NMR spectroscopic technique. The effect of catalyst amount and nanoparticle sizes was carried out. All catalytic experiments were done under constant flow of hydrogen and under vigorous mixing. Since $H_2$ was bubbled through-out the reaction, the concentration of $H_2$ was assumed to remain constant during the course of the reaction in the continuous batch reactor. Calculation for the degree of hydrogenation was described in section 3.5.2.

### *Catalyst amount*

The effect of $0.75 \times 10^{-7}$, $1.5 \times 10^{-6}$, and $6 \times 10^{-6}$ mole of nanocatalyst towards the hydrogenation of 30 µl of NRL in 50 ml monochlorobenzene were determined in order to investigate the influence of catalyst amount. The flow rate of hydrogen was kept constant at 58-60 ml/min while the reaction temperature was at 120 $^{\circ}$C throughout the 720 minutes of reaction. The effects of catalyst amount on hydrogenation of NRL are summarized in Tables 4.8 and illustrated in Figure 4.14.

**Table 4.8:** The effect of Ni and Pd catalyst amount on the hydrogenation of 30 µl of NRL in 50 ml monochlorobenzene

| Exp. | Catalyst Amount (Mole) | Reaction Time (Min) | % Hydrogenation Ni-HNRL/Pd-HNRL | |
|------|------------------------|---------------------|------------------|------|
| 1 | $0.75 \times 10^{-7}$ | 720 | 13.7 | 33.6 |
| 2 | $1.50 \times 10^{-6}$ | 720 | 23.2 | 40.0 |
| 3 | $6.00 \times 10^{-6}$ | 720 | 62.0 | 70.0 |
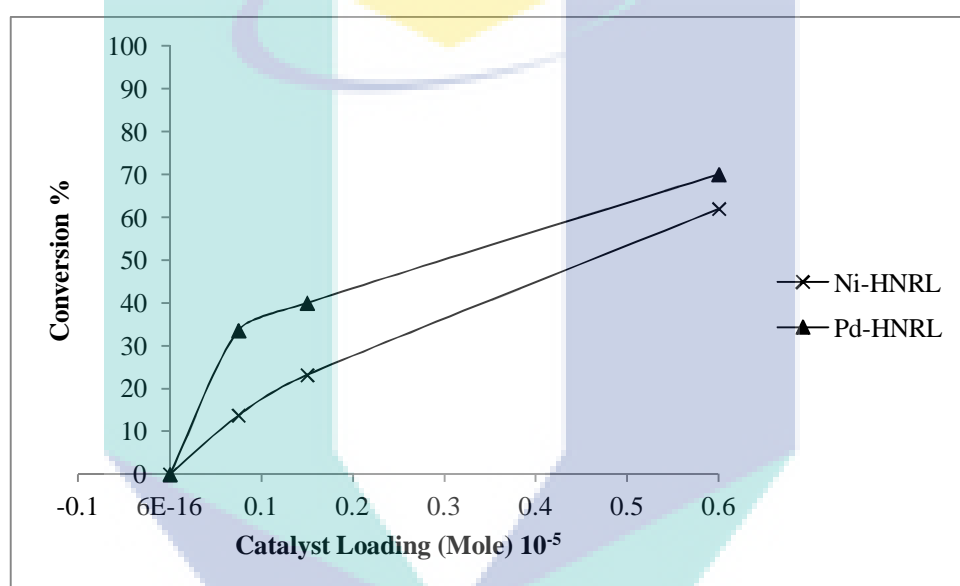


**Figure 4.14**: Effect of catalyst loading on the hydrogenation of NRL in monochlorobenzene

Results show that the hydrogenation of NRL catalyzed by Ni-NRL causes 13.7% conversion compared to Pd-NRL which is 33.6% when $0.75 \times 10^{-7}$ mole of catalyst was used. However, by increasing the amount of catalyst from $1.50 \times 10^{-6}$ to $6.00 \times 10^{-6}$ mole, the extents of hydrogenation increased from 23.2% to 62.0% for Ni-NRL and from 40.0% to 70.0% for Pd-NRL. The extent of hydrogenation increases with the increased of catalyst amount as it have sufficient amount of catalyst to catalyze the hydrogenation of NRL. Moreover, Pd-NRL tends to exhibit higher conversion compared to Ni-NRL as Pd is known to be more active metal and exhibits high catalytic activity compared to Ni.

*Particle size*

The influence of the size of metal nanoparticles prepared and described as in Table 4.3 and 4.4, on NRL hydrogenation was investigated. The reaction time was 360 min. The flow rate of hydrogen gas, temperature, catalyst and rubber amount were 58-60 ml/min, 120 $^{\circ}$C, and 30 µl of NRL in 50 ml of monochlorobenzene respectively while the amount of catalyst used was 6 x 10$^{-6}$ mole catalyst.

**Table 4.9**: The effect of particle sizes on the hydrogenation of NRL in monochlorobenzene by 6 x 10$^{-6}$ mole of Ni catalyst

| Exp. | NP Size (nm) | Reaction Time (Min) | % Hydrogenation |
|------|--------------|---------------------|-----------------|
| 1 | 10.8±0.3 | 360 | 23.7 |
| 2 | 13.4±0.4 | 360 | 45.0 |
| 3 | 26.0±2.6 | 360 | 61.5 |

**Table 4.10**: The effect of particle sizes on the hydrogenation of NRL in monochlorobenzene by 6 x 10$^{-6}$ mole of Pd catalyst

| Exp. | NPs Size (nm) | Reaction Time (Min) | % Hydrogenation |
|------|---------------|---------------------|-----------------|
| 1 | 30.6±2.9 | 360 | 31.6 |
| 2 | 56.7±6.1 | 360 | 35.8 |
| 3 | 73.9±7.7 | 360 | 37.0 |

Tables 4.9 and 4.10 summarize the effect of particle sizes of Ni-NRL and Pd-NRL towards the hydrogenation of NRL. Hydrogenation of NRL using Ni-NRL having mean diameter of $10.8\pm0.3$ and $13.4\pm0.4$ nm exhibits about 23.7% and 45.0% conversion respectively. However, with the use of aggregated Ni-NRL with mean diameter of $26.0\pm2.6$ nm, the extent of hydrogenation slightly increased to 61.5%. Hydrogenation of NRL using Pd-NRL having diameter of $30.6\pm2.9$, $56.7\pm6.1$ nm and $73.9\pm7.7$ nm exhibits about 31-37% conversion. Results showed that the extent of hydrogenation increased with the increase of nanoparticle sizes for hydrogenation of NRL catalyzed by Ni-NRL. The same trend was observed with the use of Pd-NRL. The extent of hydrogenation slightly increased with the increase of particle size. This indicates that the larger particles have higher proportion of free metal surface available to catalyze the hydrogenation reaction compared to smaller sizes nanoparticle samples. The larger particles have better interaction with the rubber particles enabling the hydrogenation to take place more effectively. On the other hand the smaller particles have limited interaction especially with the double bond of rubber. This observation is in agreement with the findings as reported by Campbell et al. (2010) and Mayne et al. (2011)

## 4.4    CATAYTIC HYDROGENATION OF NRL IN AQUEOUS MEDIUM

Hydrogenation of NRL using nanocatalyst especially in aqueous phase has not been reported. Thus, further investigation has been done to study the ability of the prepared nanocatalyst to catalyze the hydrogenation of NRL in aqueous medium. The hydrogenations of NRL catalyzed by as-prepared Ni and Pd nanoparticles having diameter of 10.8±0.3 nm and 30.6±2.9 nm respectively were done. The degree of hydrogenation of latex were calculated based on the integrated peak area of C=CH- (olefinic) proton using $^1$H NMR spectroscopic technique. The effects of solvents and catalyst amount were carried out. All catalytic experiments were done under constant flow of hydrogen and under vigorous mixing. The concentration of $H_2$ was assumed to remain constant during the course of the reaction in the continuous batch reactor. Calculation for the degree of hydrogenation was described in section 3.5.2.

### *Solvents*

The effects of water and monochlorobenzene as solvent on the hydrogenation of 30 µl of NRL in 50 ml solvent in the presence of $6 \times 10^{-6}$ mole of Ni and Pd nanoparticles were investigated at atmospheric pressure and the solvents boiling point. The flow rate of hydrogen gas was kept constant at 58-60 ml/min for 720 min.

**Table 4.11**: Hydrogenation of NRL in different solvents by $6 \times 10^{-6}$ mole of catalyst

| Exp. | Solvent | Catalyst | Reaction Time (Min) | % Hydrogenation |
|------|---------|----------|---------------------|-----------------|
| 1 | Water | Ni-NRL | 720 | 30.4 |
| 2 | Water | Pd-NRL | 720 | 36.0 |
| 3 | Monochlorobenzene | Ni-NRL | 720 | 62.0 |
| 4 | Monochlorobenzene | Pd-NRL | 720 | 70.0 |

The effects of solvent on the hydrogenation activity are summarized in Table 4.12. Hydrogenation of NRL in monochlorobenzene catalyzed by Pd-NRL causes 70.0% conversion compared to Ni-NRL that is 62.0%. The use of aqueous medium resulted in 30.0-36.0% conversion over both catalysts. Results show that the Pd-NRL has slightly higher catalytic activity than Ni-NRL for the hydrogenation of NRL in aqueous and monochlorobenzene as Pd nanoparticles is a more active metal compared to nickel. Nevertheless, the solvent has larger effect on the hydrogenation reaction than that of different metal nanoparticles. Chlorinated solvents led to high catalytic hydrogenation of NRL using Ni-NRL and Pd-NRL as also observed by Mahittikul et al. (2009). However, the potential of water as a solvent system could be considered for green catalytic hydrogenation approach. Water is most abundantly existing liquid solvent, nontoxic, nonflammable and environmentally benign but it generally low solubility of either the reactants and reagents or the product. The combination of microwave and ultrasonic method could increase the solubility of water as a solvent system thus converts NRL into more stable product.

*Catalyst loading*

The effects of $6.0 \times 10^{-6}$, $1.2 \times 10^{-5}$, $1.8 \times 10^{-5}$ and $2.4 \times 10^{-5}$ moles of nanocatalyst on the hydrogenation of 30 µl of NRL in 50 ml aqueous solution were determined in order to investigate the influence of catalyst loading on the green catalytic hydrogenation approach for NRL. The flow rate of hydrogen gas flowing and temperature were kept constant at 58-60 ml/min at 100 $^{\circ}$C for 720 min.

**Table 4.12:** The effect of Ni and Pd catalyst amount on the hydrogenation of NRL in aqueous medium

| Exp. | Catalyst Amount (Mole) | Reaction Time (Min) | % Hydrogenation Ni-HNRL/Pd-HNRL | |
|---|---|---|---|---|
| 1 | $6.0 \times 10^{-6}$ | 720 | 30.4 | 36.0 |
| 2 | $1.2 \times 10^{-5}$ | 720 | 62.9 | 80.6 |
| 3 | $1.8 \times 10^{-5}$ | 720 | 66.0 | 83.7 |
| 4 | $2.4 \times 10^{-5}$ | 720 | 90.5 | 92.3 |

The effect of catalyst loading towards the degree of hydrogenation is illustrated in Figure 4.15 and summarized in Table 4.12. The result shows that the extent of hydrogenation increases with increasing catalyst concentration. Hydrogenation of NRL using Pd-NRL exhibits higher performance compared to Ni-NRL up to $1.8 \times 10^{-5}$ mole catalyst concentration. However, at $2.4 \times 10^{-5}$ mole, the performance of this nanocatalyst seems to be similar to each other.
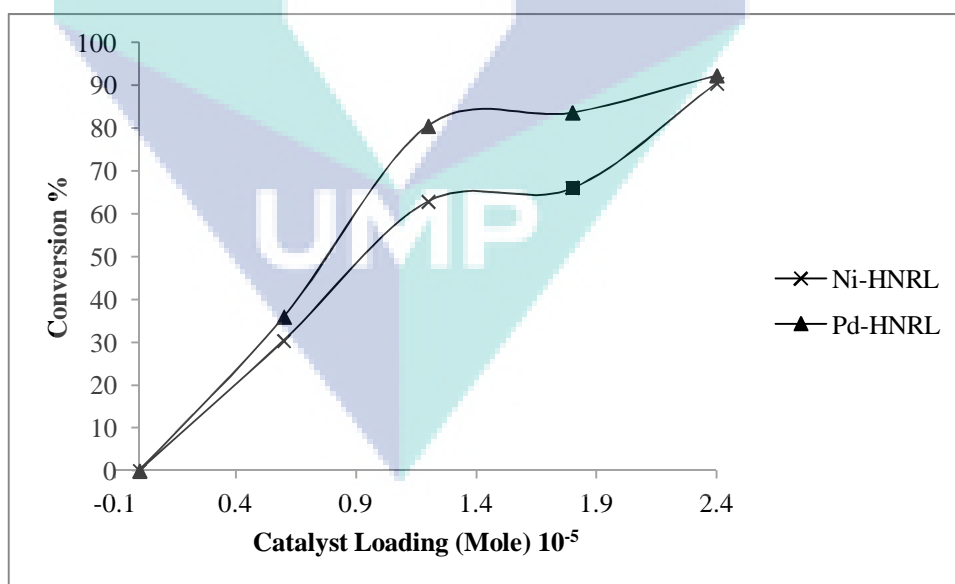


**Figure 4.15:** Effect of catalyst loading on the hydrogenation of NRL in aqueous medium

NRL hydrogenation in aqueous medium requires a relatively higher loading of catalyst compared to that in organic solvent medium to achieve similar conversion at the same reaction conditions. Generally, hydrogenation of NRL was strongly dependent on catalyst concentration. On the other hand, it is believed that impurities in NRL might reduce the catalytic activity (A. Mahittikul et al., 2006 and 2009). They also found that catalytic activity decreased with an increase in the rubber concentration which implied that increase of impurities contents.

## 4.5    CHARACTERIZATION OF HYDROGENATED NATURAL RUBBER LATEX (HNRL)

The structures, interaction between the catalyst and natural rubber particles, surface morphology and thermal properties of the hydrogenated product were characterized by NMR, FTIR, scanning electron microscopy (SEM), field emission scanning electron microscopy (FESEM) and thermogravimetric analyzer (TGA) respectively.

### 4.5.1    Structure characterization of natural rubber and hydrogenated natural rubber latex (Monochlorobenzene)

*NMR analysis*

The structures of both NRL and HNRL were previously investigated by ^{1}H NMR spectroscopy by Mahittikul et al. (2009). ^{1}H NMR spectra of NRL before and after hydrogenation reaction are show that the intensities of olefinic proton, unsaturated methylene and unsaturated methyl signal at 5.15, 2.04-2.10, and 1.60-1.70 ppm respectively, are reduced. The remaining signals show very low intensity which confirms that most carbon-carbon double bonds in NRL were hydrogenated. HNRL shows new strong signals in the range of 0.80-1.40 ppm which are attributed to methine, methylene and methyl groups (Appendix A (1-4)).

*FTIR analysis*

The FTIR spectra of hydrogenated NRL in monochlorobenzene (Figures 4.16 and 4.17) show that the absorption bands corresponding to C=C stretching, olefinic C-H bending, and $-(CH_2)_3-$ are located at 1664, 836 and 739 cm$^{-1}$, respectively. The characteristic peak of unsaturation, 1664 and 836 cm$^{-1}$, are lower in the hydrogenated NRL while an intense signal appeared at 739 cm$^{-1}$ due to saturated carbon formed through hydrogenation.

It has been reported that phospholipids shows C=O stretching band for associated fatty acid and ester in the range of 1738-1742 cm$^{-1}$ (Dupont et al., 1976). Moreover, the absorption peak at 1243 cm$^{-1}$ was assigned to O-P-O asymmetric stretching of phospholipids (Wong and Mantsch, 1988). This assignment of FTIR spectrum corresponds to the structure of phospholipids at the rubber chain-end by Tarachiwin et al. (2005). It is found that, in this work, the hydrogenation of NRL using both nanoparticles enhances the absorption peaks at 1739 cm$^{-1}$ and 1243 cm$^{-1}$. However, the intensity of Pd-HNRL was higher compared to that of Ni-HNRL for these vibration bands. As a result, most of the performances of Ni and Pd to catalyze the hydrogenation of NRL quite similar to each other although Pd is known to be more active metal compared to Ni. It indicated that Pd-HNRL has strong interaction with the NRL matrix, and this is likely to contribute to the inhibition of catalytic activity due to the coverage of the metallic surface.
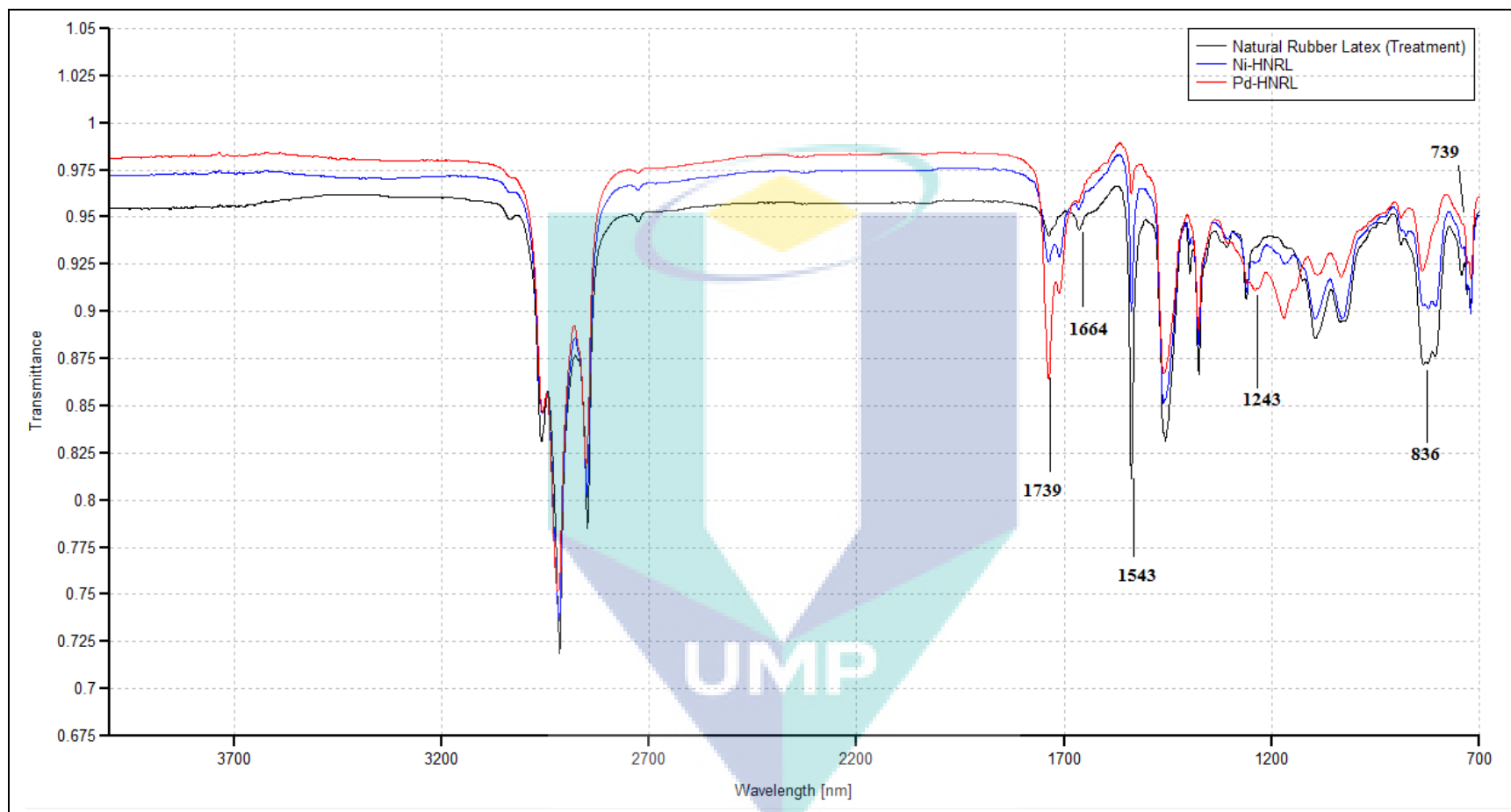
**Figure 4.16:** FTIR spectra of natural rubber latex (NRL) and hydrogenated natural rubber latex (HNRL) in monochlorobenzene at 4000-700 cm$^{-1}$
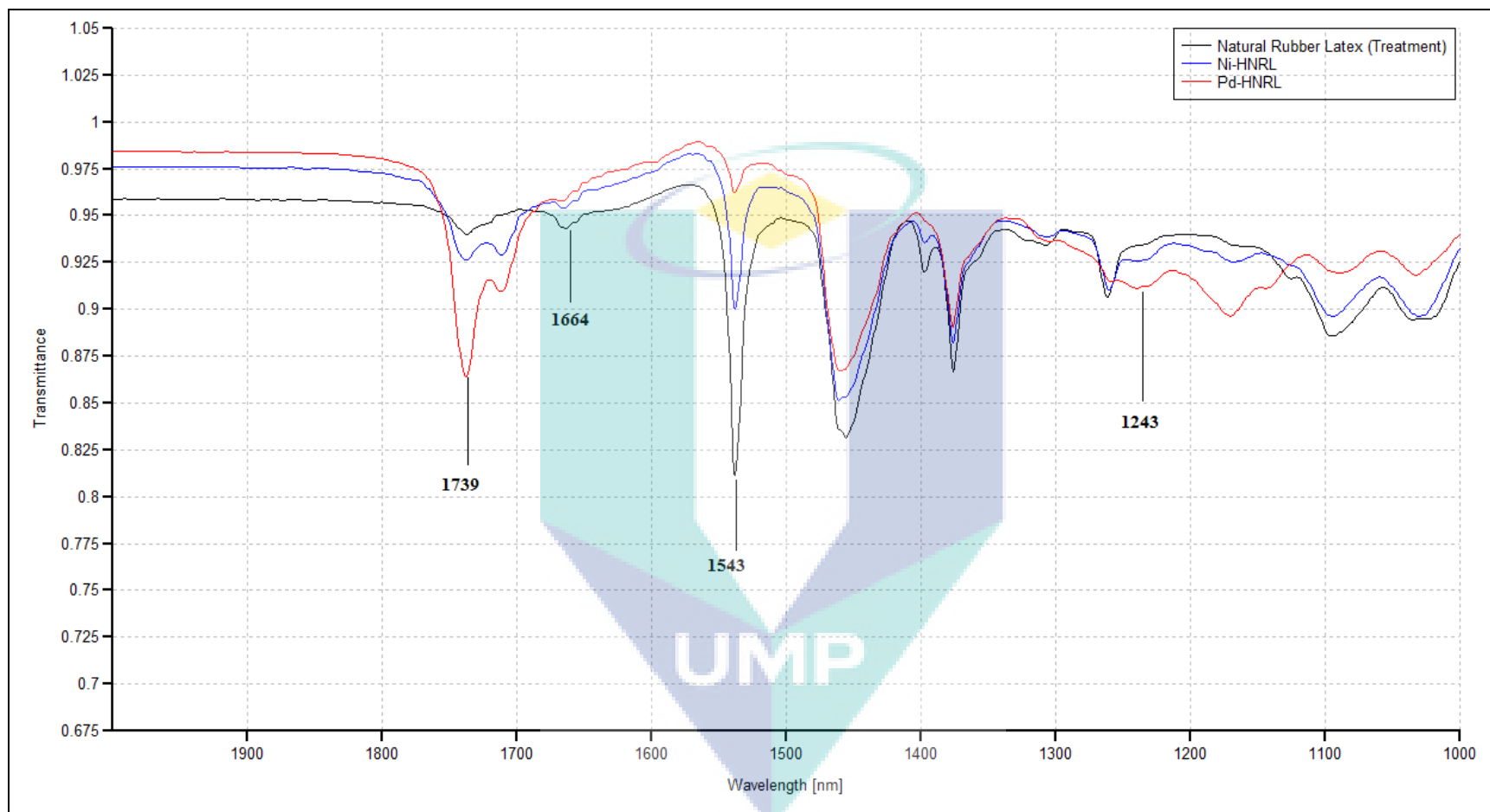
**Figure 4.17:** FTIR spectra of natural rubber latex (NRL) and hydrogenated natural rubber latex (HNRL) in monochlorobenzene at 2000-1000 cm$^{-1}$

### *Microstructure studies: FESEM and SEM analysis*

The surface morphology of Ni-HNRL and Pd-HNRL in monochlorobenzene was characterized using SEM and FESEM. Figure 4.18 shows the lower magnification images whereas Figure 4.19 shows the higher magnification images of SEM. Figure 4.18a and 4.19a shows the images of blank NRL matrix used as a control for comparison with other samples at low and high magnifications. The surface morphology of Ni-HNRL (Ni-NRL/NRL of wt. 2.9%) differs from that of Pd-HNRL (Pd-NRL/NRL of wt. 5.3%). It appear that the surface morphology of Ni-HNRL (Figure 4.18b and 4.19b) is relatively smooth than Pd-HNRL (Figure 4.18c and 4.19c). The formation of bulk agglomerated particles probably the catalyst embedded in the HNRL products appeared in Pd-HNRL surface morphology (yellow rectangle area) make it less ordered compared to that of Ni-HNRL. Overall observation from Figures 4.18 and 4.19 indicates that the morphology of Ni-HNRL and Pd-HNRL changes when the hydrogenation process takes place.
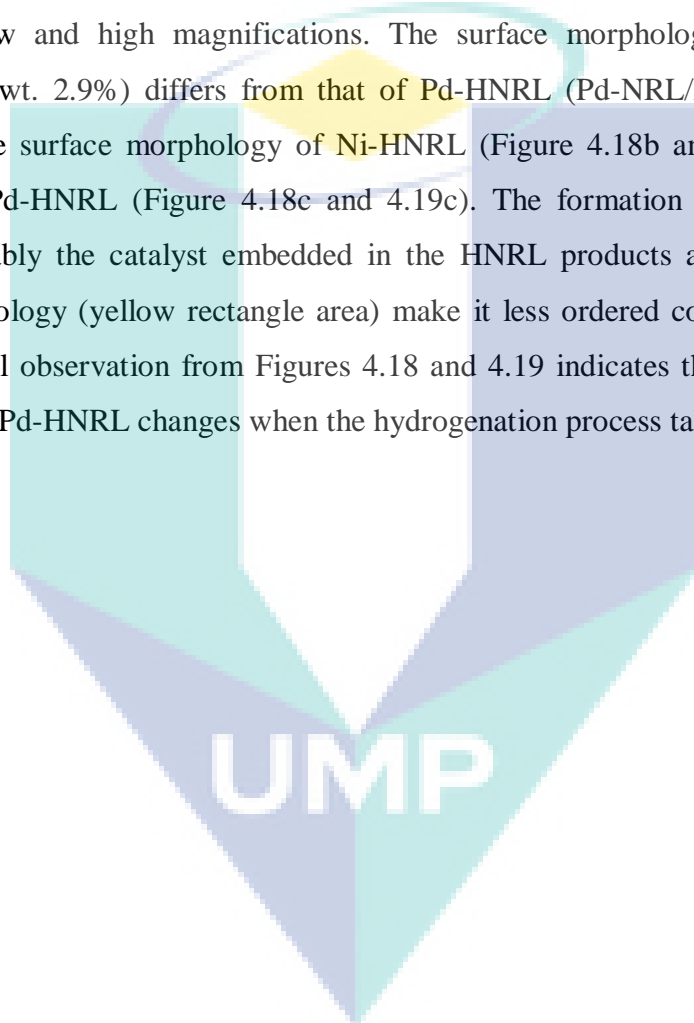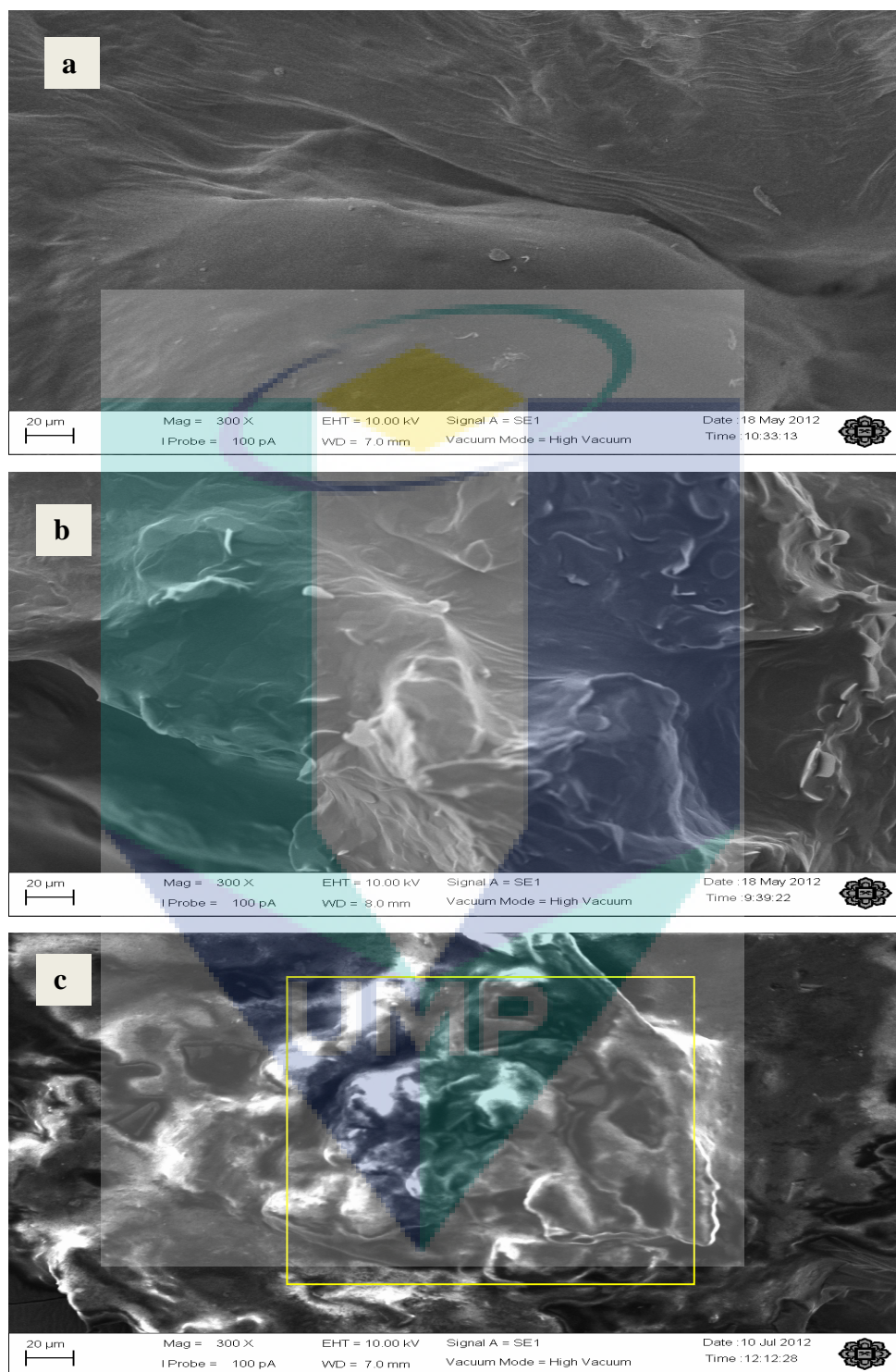
**Figure 4.18:** SEM micrographs of (a) NRL (Blank), (b) Ni-HNRL (Monochlorobenzene) and (c) Pd-HNRL (Monochlorobenzene) at low magnification (300X)

**Figure 4.19:** SEM micrographs of (a) NRL (Blank), (b) Ni-HNRL (Monochlorobenzene) and (c) Pd-HNRL (Monochlorobenzene) at high magnification (2300X)

Further investigation on the surface morphology of Ni-HNRL and Pd-HNRL in monochlorobenzene has been done using FESEM, where these samples were coated with platinum. Figure 4.20 showed the images using secondary electron whereas Figure 4.21 (low magnification) and Figure 4.22 (high magnification) using backscattered techniques. The surface of Ni-HNRL (Figure 4.20-4.22a) appears to be smoother with existing of smooth area (red triangle area) with small lines compared to that of Pd-HNRL (Figure 4.20-4.22b). The Pd-HNRL surfaces seem to be rougher (lack of smooth area) with bigger lines. The images also consist of white and dark spots as shown in Figure 4.22.

The identity of the white and dark spots in Ni-HNRL and Pd-HNRL sample was studied using energy-dispersive x-ray (EDX) techniques and found to be crystallites of calsium. As illustrated in Figures 4.24 and 4.26, it can be seen that the dark spots area dominantly consisted of C and O and it indicated the surface of HNRLs. Compared to the white spot (Figure 4.23 and 4.25), the significant amount of Ca was attributed to the formation of calcium crystallites as reported by Rippel et al., 2005. The result also indicates that Ni-NRL and Pd-NRL nanoparticles were not present on the surface of HNRLs. This suggests that the nanoparticles of Ni and Pd are encapsulated within HNRLs matrix.
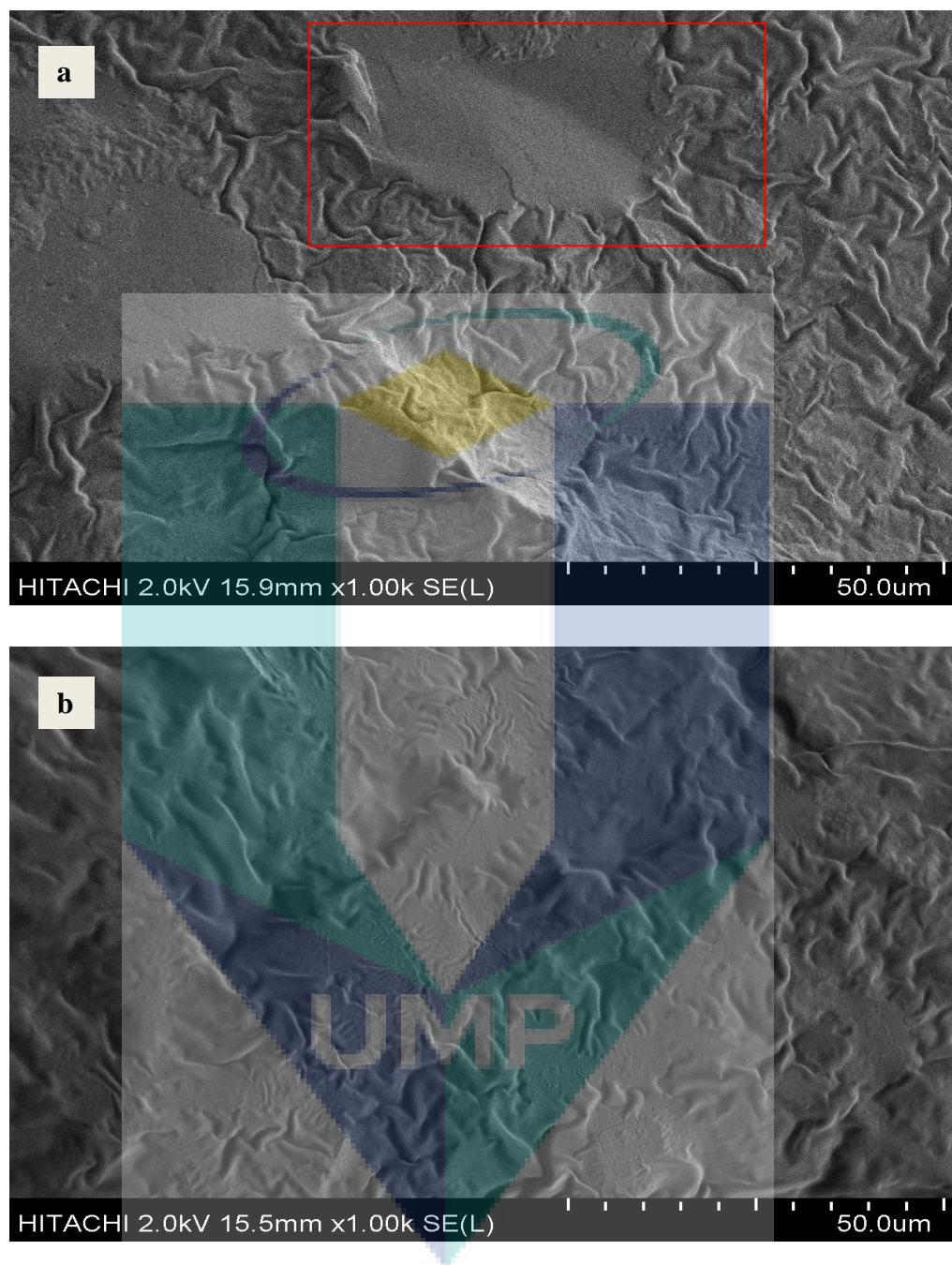
**Figure 4.20:** FESEM micrographs of (a) Ni-HNRL (Monochlorobenzene) and (b) Pd-HNRL (Monochlorobenzene) using secondary electron techniques
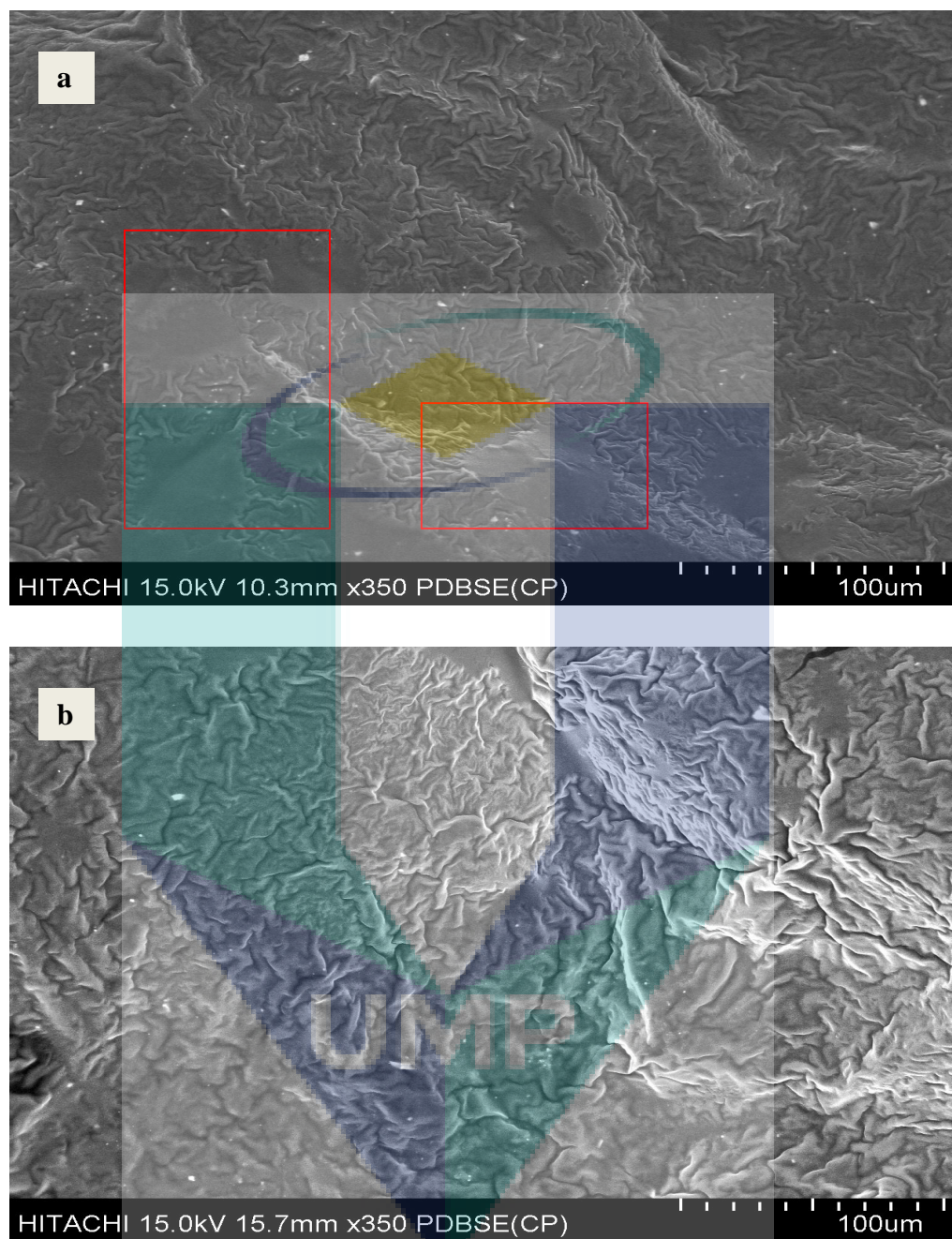
**Figure 4.21:** FESEM micrographs of (a) Ni-HNRL (Monochlorobenzene) and (b) Pd-HNRL (Monochlorobenzene) at low magnification using backscattered techniques
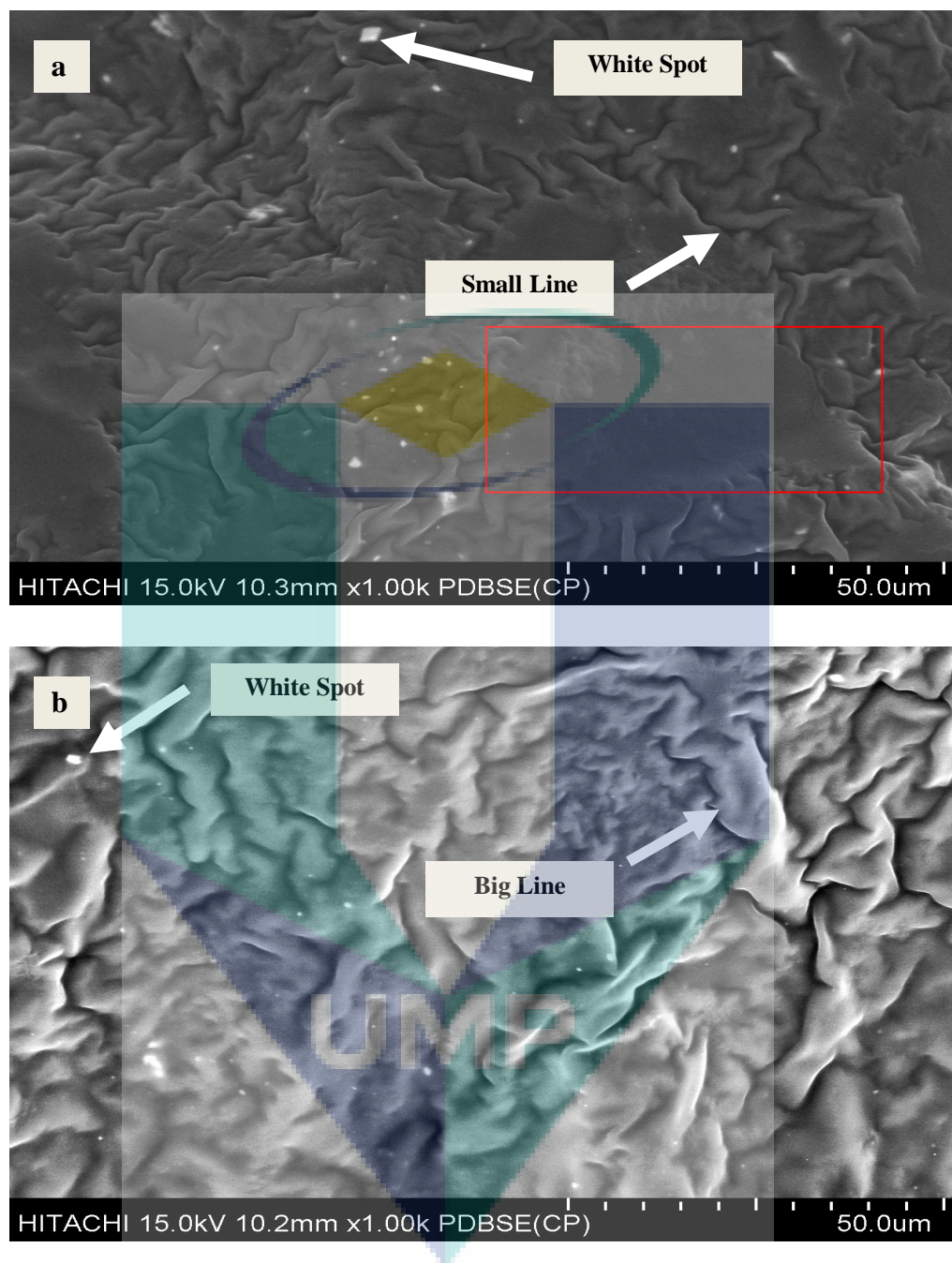
**Figure 4.22:** FESEM micrographs of (a) Ni-HNRL (Monochlorobenzene) and (b) Pd-HNRL (Monochlorobenzene) at high magnification using backscattered techniques
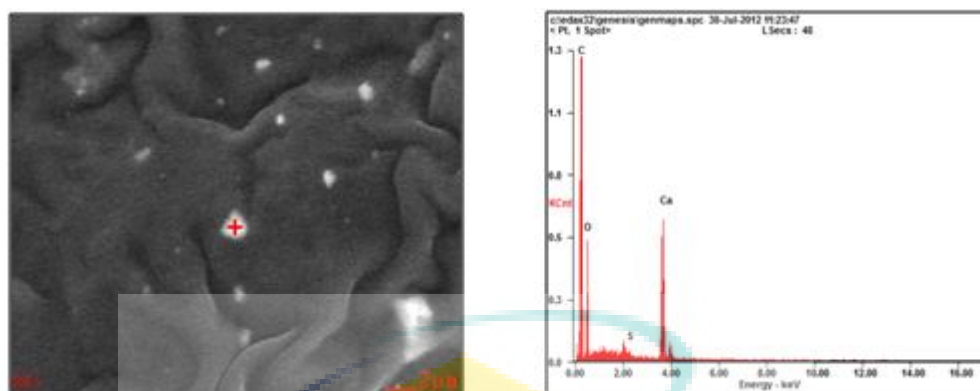
| Element | Wt% | At% |
|---|---|---|
| CK | 55.58 | 69.04 |
| OK | 25.67 | 23.94 |
| SK | 00.47 | 00.22 |
| CaK | 18.29 | 06.81 |
| Matrix | Correction | ZAF |

**Figure 4.23:** EDX analysis on white spot of Ni-NRL (Monochlorobenzene)
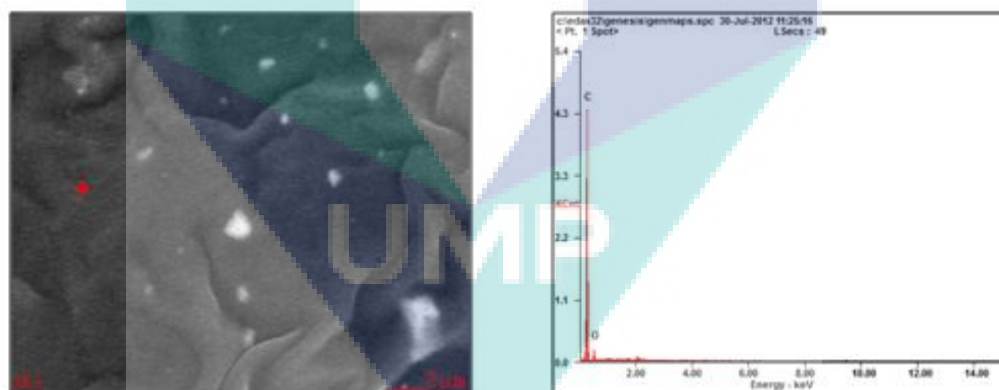


| Element | Wt% | At% |
|---|---|---|
| CK | 87.37 | 90.21 |
| OK | 12.63 | 09.79 |
| Matrix | Correction | ZAF |

**Figure 4.24:** EDX analysis on dark spot of Ni-NRL (Monochlorobenzene)
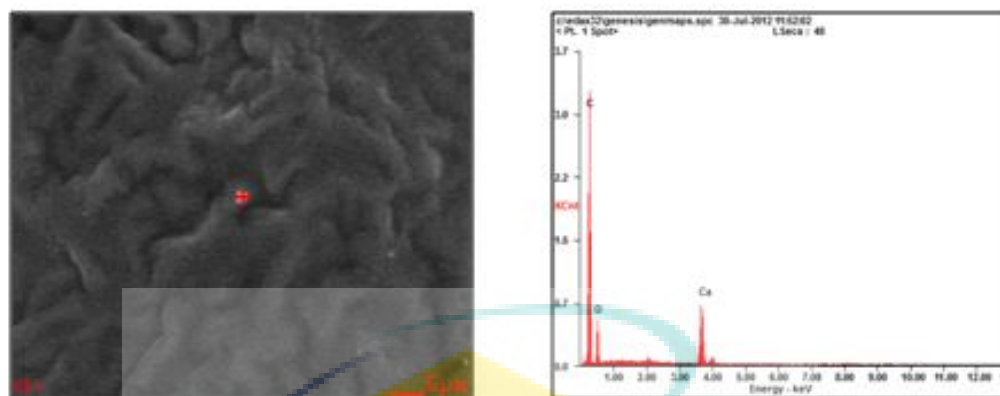
| Element | Wt% | At% |
|---|---|---|
| CK | 55.59 | 69.32 |
| OK | 25.04 | 23.44 |
| CaK | 19.36 | 07.24 |
| Matrix | Correction | ZAF |

**Figure 4.25:** EDX analysis on white spot of Pd-NRL (Monochlorobenzene)
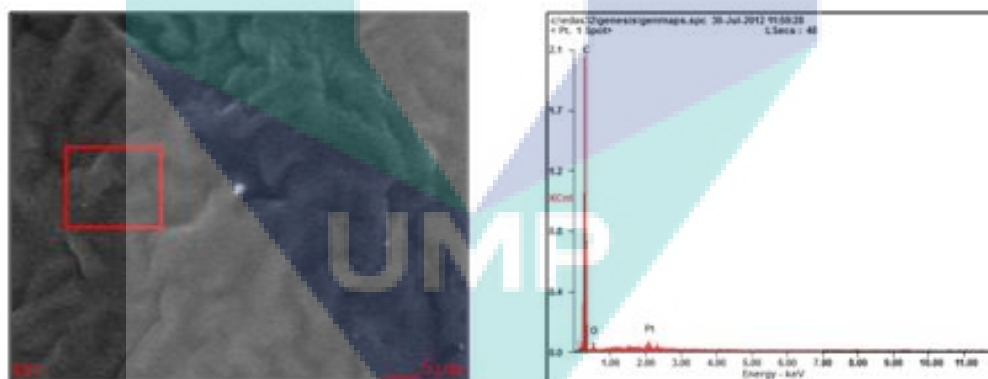


| Element | Wt% | At% |
|---|---|---|
| CK | 94.51 | 95.82 |
| OK | 05.49 | 04.18 |
| Matrix | Correction | ZAF |

**Figure 4.26:** EDX analysis on dark surface of Pd-NRL (Monochlorobenzene)

*TGA analysis*

Thermogravimetric analyses (TGA and DTGA) plots for natural rubber (NRL), hydrogenated natural rubber catalyzed by nickel nanoparticles (Ni-HNRL) and hydrogenated natural rubber catalyzed by palladium nanoparticles (Pd-HNRL) are shown in Figure 4.27 and the percentage weight loss in the respective temperature range are given in Table 4.13. The TG curves have two large plateaus while the DTG curve show two degradation peaks. The lower degradation peak is at about 290-310 $^{o}$C while the higher temperature degradation peak is at 370-380 $^{o}$C.

The weight loss at the lower temperature is higher for Pd-HNRL than Ni-HNRL followed by NRL. The opposite trend is observed for the weight loss due to degradation at higher temperature. The total weight losses for all the three samples are relatively similar to each other. At 800 $^{o}$C, the residual mass is 6.78% for NRL, 5.99% for Ni-HNRL and 4.95% for Pd-HNRL. The hydrogenated latex tends to have lower decomposition temperature than that of natural latex that has undergone similar treatment except for the presence of catalyst.

**Table 4.13:** Proximate analysis of NRL, Ni-HNRL and Pd-HNRL at various temperatures

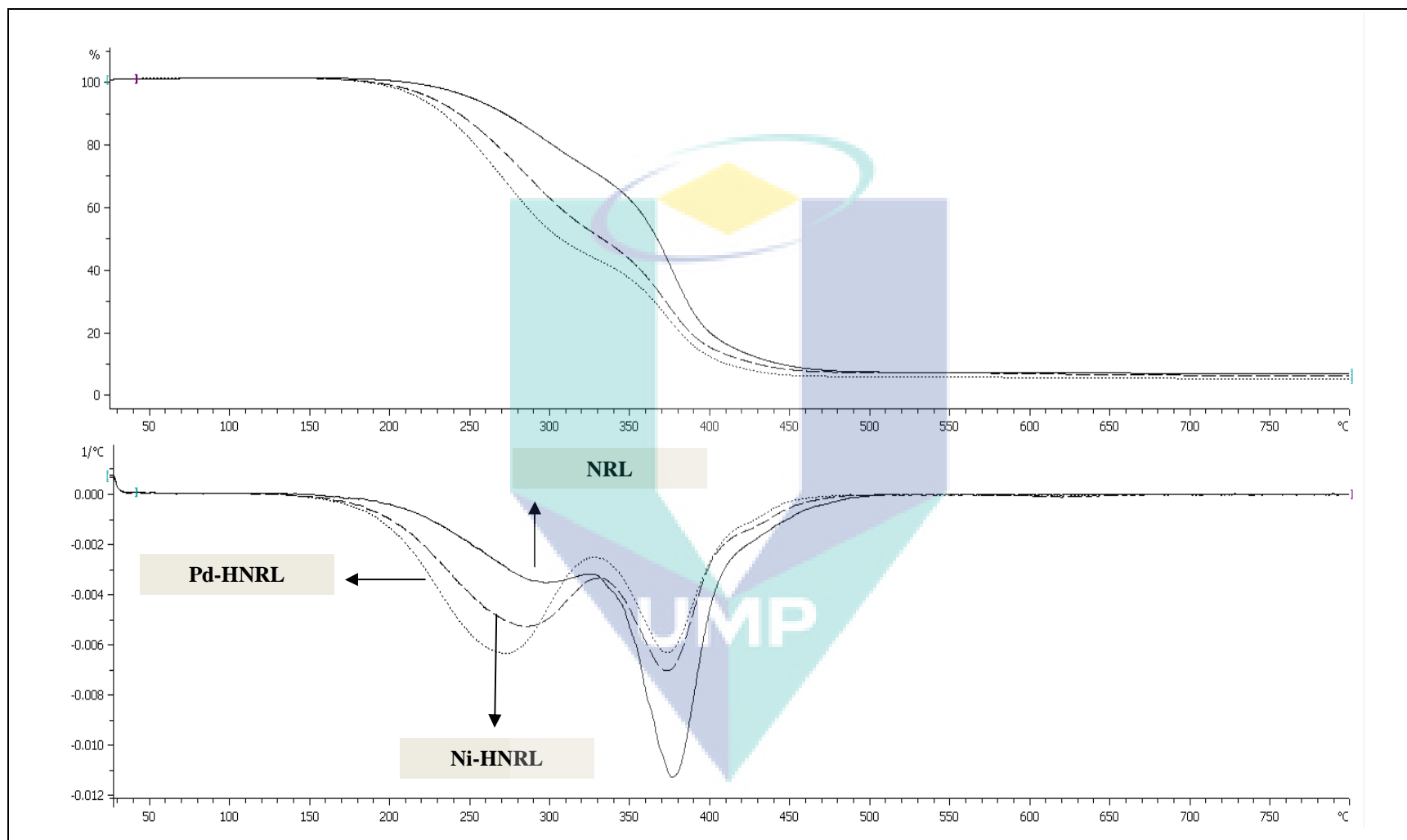| Sample Code | Moisture, % < 150 $^{o}$C | Volatile, % 150-330 $^{o}$C | Rubber Degradation, % 330-800 $^{o}$C | Residues, % 800 $^{o}$C |
|---|---|---|---|---|
| NRL | 0.33 | 30.65 | 63.56 | 6.78 |
| Ni-HNRL | 0.19 | 50.40 | 44.46 | 5.99 |
| Pd-HNRL | 0.13 | 58.17 | 37.82 | 4.95 |

**Figure 4.27:** Plot of TGA and DTG which (a) ___ NRL, (b) - - - Ni-HNRL and (c) … Pd-HNRL

**4.5.2 Structure characterization of natural rubber and hydrogenated natural rubber latex (Aqueous)**

*NMR analysis*

^{1}H NMR spectra of NRL before and after hydrogenation reaction show that the intensity of olefinic proton, unsaturated methylene and unsaturated methyl signal at 5.12-5.40, 2.04-2.07, and 1.59-1.71 ppm respectively, are reduced. The remaining signals show very low intensity which confirms that most carbon-carbon double bonds in NRL were hydrogenated. HNRL shows new strong signals in the range of 0.80-1.40 ppm which are attributed to methine, methylene and methyl groups (Appendix A (5-8)).

*FTIR analysis*

The FTIR spectra of NRL before and after hydrogenation are shown in Figures 4.28 and 4.29. For samples prepared in aqueous phase, the FTIR spectra shows that the absorption bands corresponding to the O-H (H-bonded), C=C stretching, and olefinic =C-H bending are located at 3200-3700, 1664 and 836 cm$^{-1}$ respectively. The intensity of 3200-3700 cm$^{-1}$ becomes broader because HNRL is saturated with O-H species and easier to form hydrogen bonds. The characteristic peak related to unsaturation, 1664 and 836 cm$^{-1}$ are lower in the HNRL due to hydrogenation. The broadening and increase in the intensity of peak in the 1000 region is in-line with the hydrogenation that has taken place in NRL. The enhancement of the peaks at region 1739 and changes at 1243 cm$^{-1}$ for Ni-HNRL and Pd-HNRL confirmed the interaction of Ni-NRL and Pd-NRL NPs with the NR matrix as has been discussed in section 4.2.2.
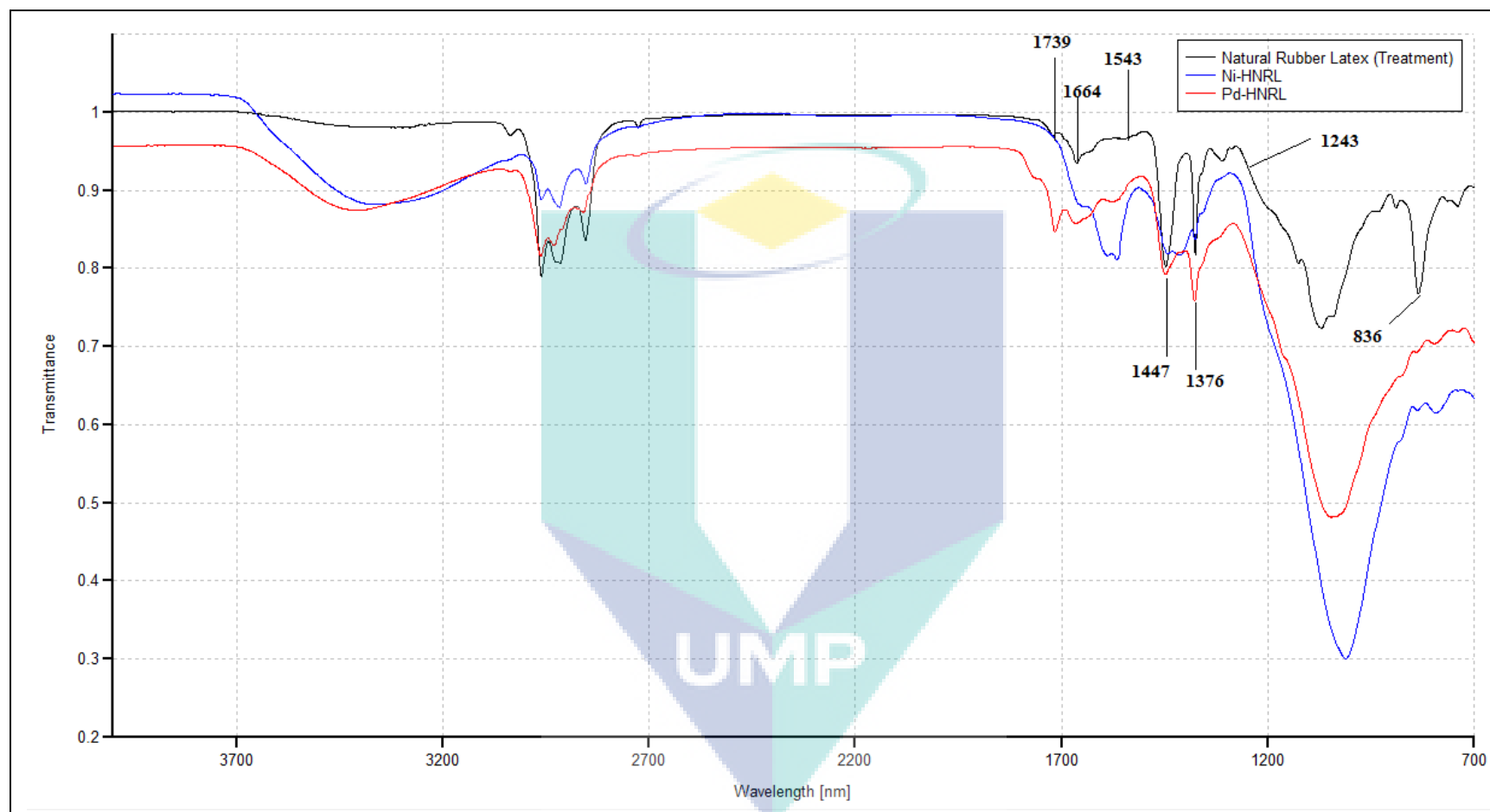
**Figure 4.28:** FTIR spectra of natural rubber latex (NRL) and hydrogenated natural rubber latex (HNRL) in aqueous solution at 4000-700 cm$^{-1}$
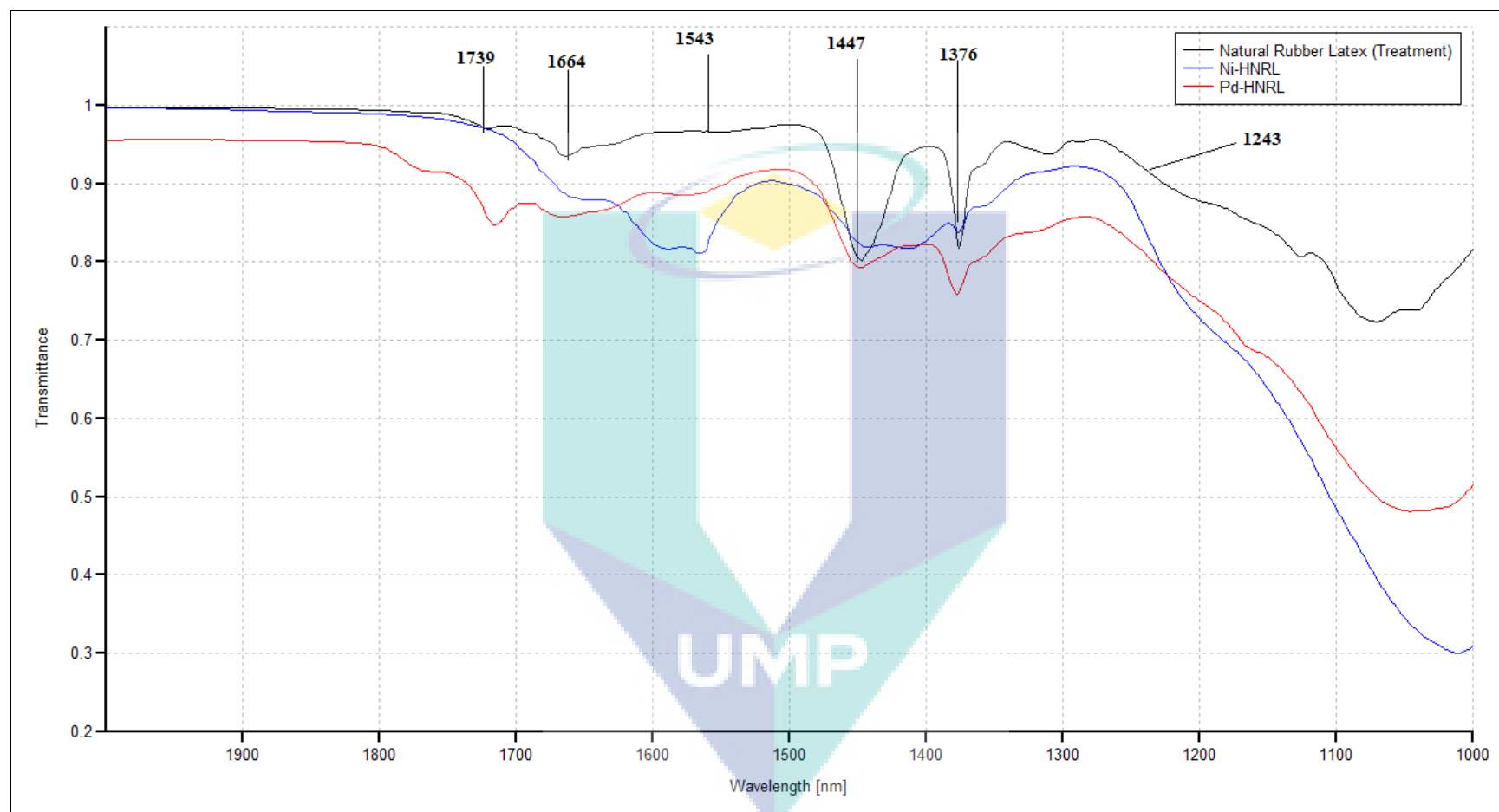
**Figure 4.29:** FTIR spectra of natural rubber latex (NRL) and hydrogenated natural rubber latex (HNRL) in aqueous solution at 2000-1000 cm$^{-1}$

*SEM analysis*

*Effect of different solvents*

Figures 4.30 and 4.31 show the surface morphology of Ni-HNRL (Ni-NRL/NRL of wt. 2.9%) and Pd-HNRL (Pd-NRL/NRL of wt. 5.3%) operated in aqueous medium. Figure 4.30a demonstrates a smooth surface area of Ni-HNRL compared to Pd-HNRL (Figure 4.30b). On the other hand, small and short lines are observed for Ni-HNRL instead of big lines for Pd-HNRL. This observation is quiet similar with that of HNRLs in monochlorobenzene as shown before. Thus, it can be concluded that the morphology of HNRLs are weakly dependent with the type of solvents used.
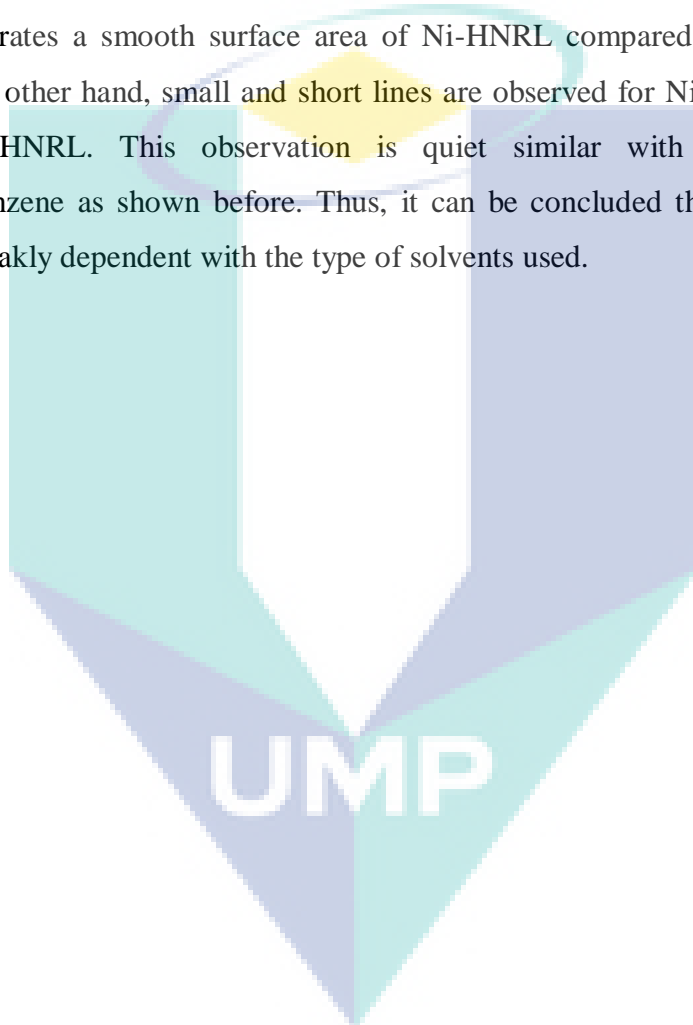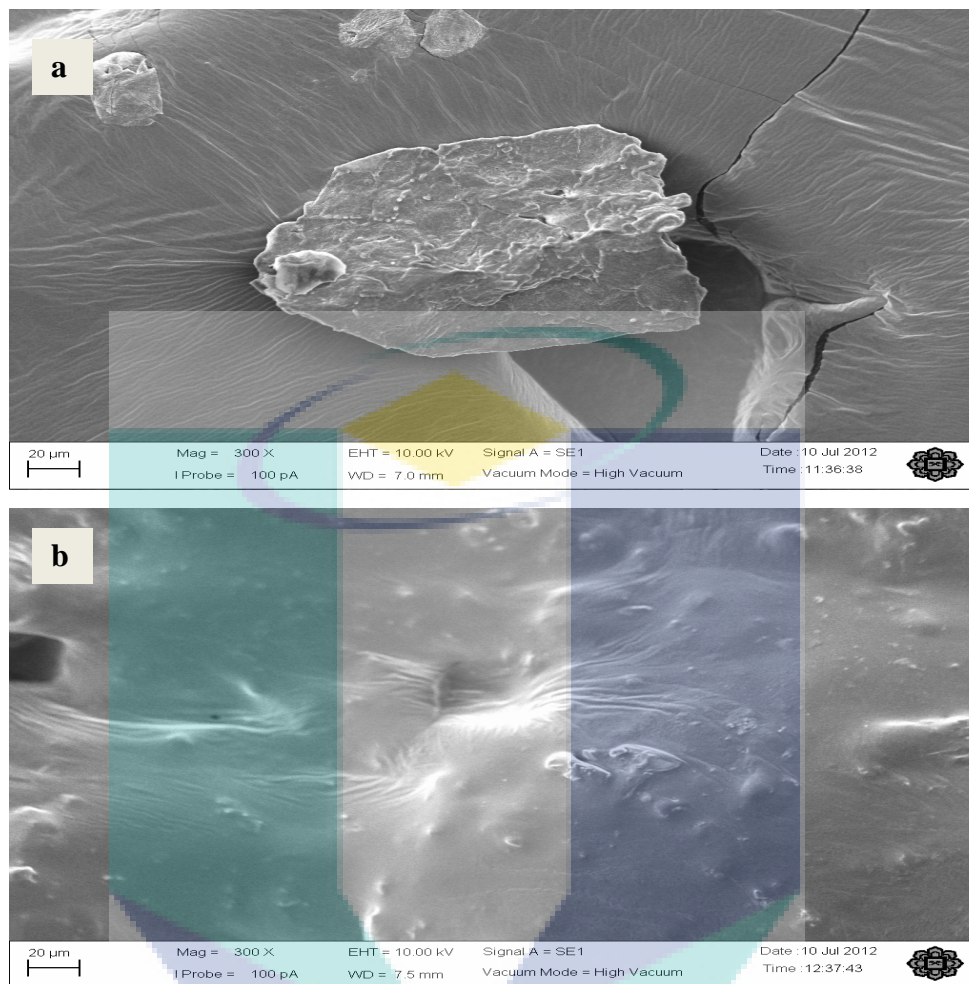
**Figure 4.30:** SEM micrographs of (a) Ni-HNRL (Aqueous) and (b) Pd-HNRL (Aqueous) at low magnification (300X)
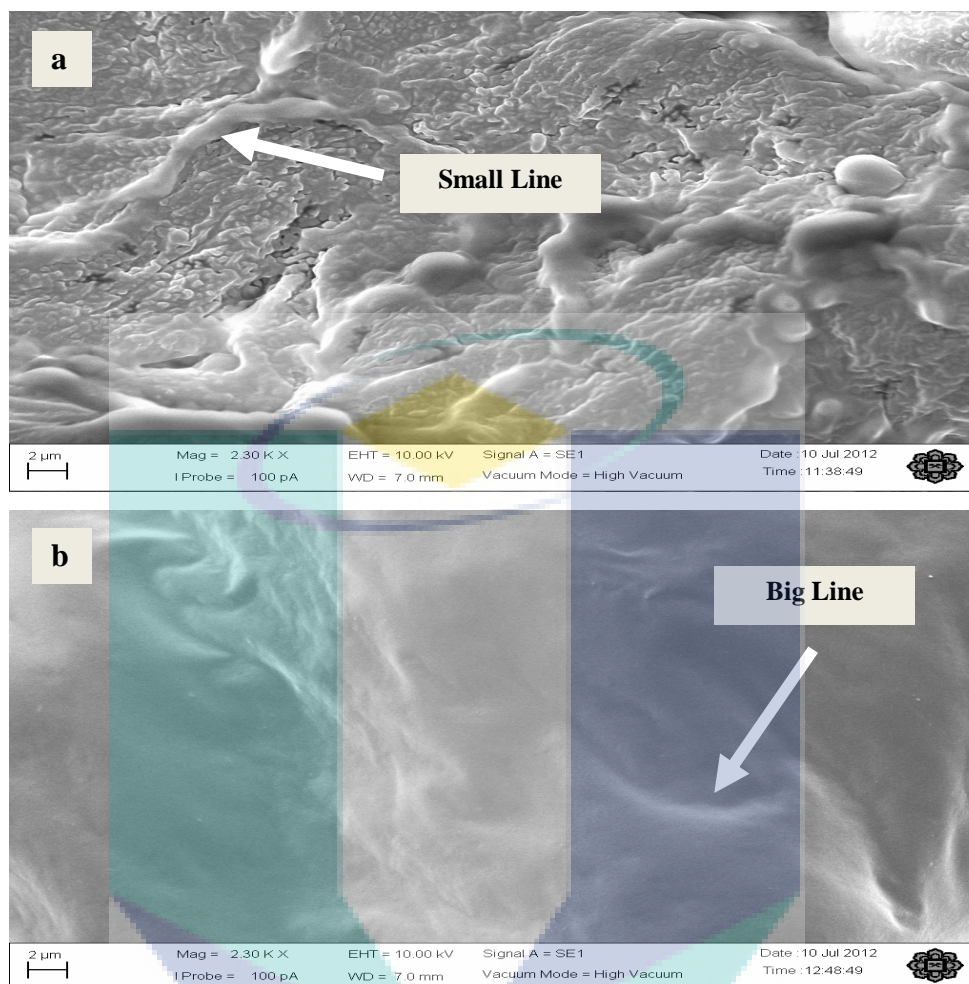
**Figure 4.31:** SEM micrographs of (a) Ni-HNRL (Aqueous) and (b) Pd-HNRL (Aqueous) at high magnification (2300X)

*Effect of catalyst amount*

The microstructures of the Ni-HNRL and Pd-HNRL in aqueous medium were determined using SEM and the effect of catalyst loading was studied. Figures 4.32 (a-d) and 4.33 (a-d) show the micrograph of Ni-HNRL and Pd-HNRL with $6.0 \times 10^{-6}$, $1.2 \times 10^{-5}$, $1.8 \times 10^{-5}$ and $2.4 \times 10^{-5}$ moles of catalyst loading at 2300X of magnification.

It is observed that, the presence of $6.0 \times 10^{-6}$ (Figures 4.32a and 4.33a) and $1.2 \times 10^{-5}$ (Figures 4.32b and 4.33b) moles of catalyst make the surface morphology of the Ni-HNRL and Pd-HNRL less ordered compared to surface morphology of NRL blank (4.18a and 4.19a). However, the morphology surface of the HNRLs becomes rougher with the increment of catalyst loading up to $2.4 \times 10^{-5}$ mole (Figures 4.33 (c-d) and 4.33 (c-d)). Thus, it could be concluded that, the morphological of the hydrogenated NRL was dependent on the type and amount of the catalyst.
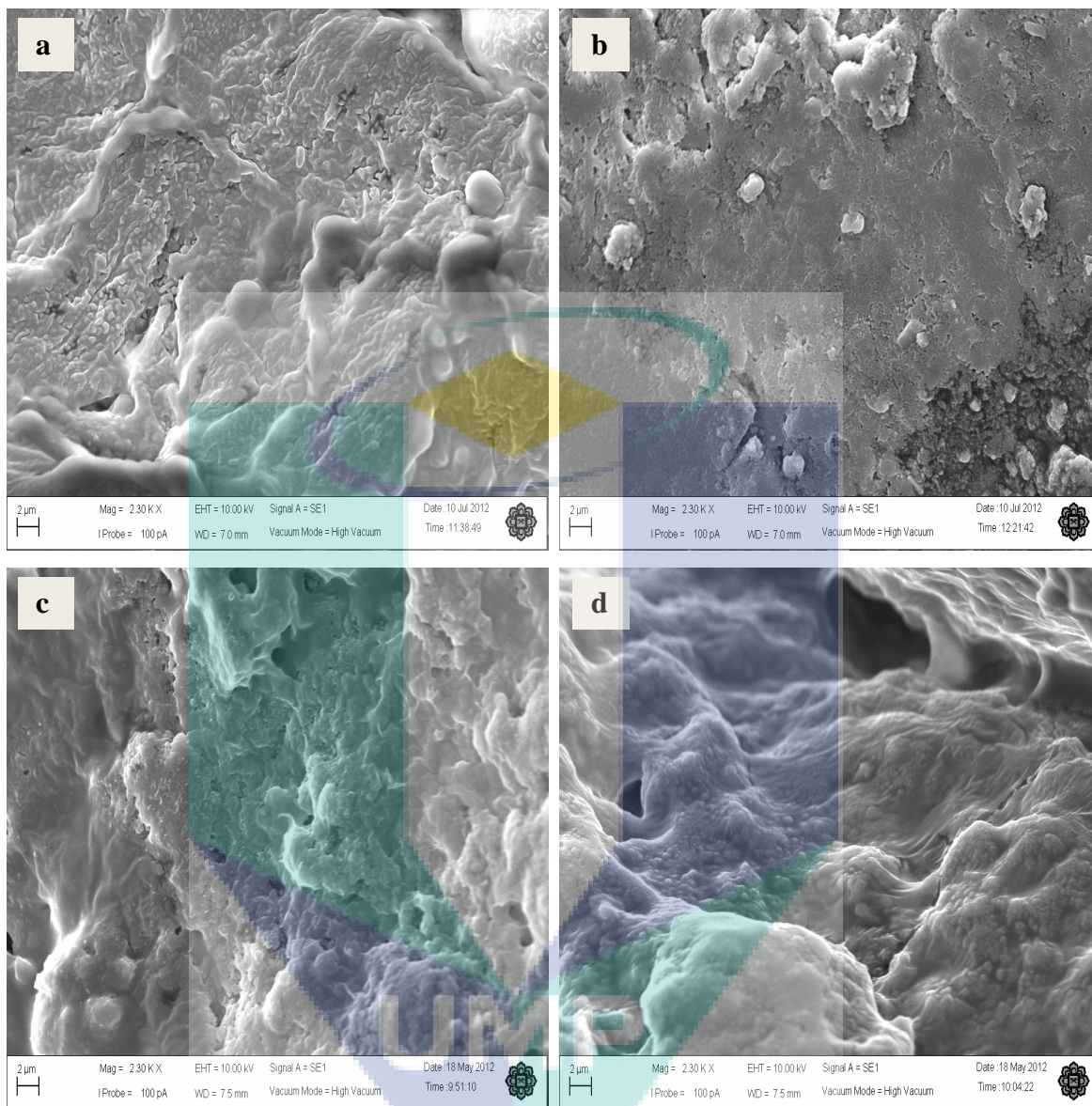
**Figure 4.32:** SEM micrographs of Ni-HNRL (Aqueous) at (a) $6.0 \times 10^{-6}$, (b) $1.2 \times 10^{-5}$, (c) $1.8 \times 10^{-5}$ and (d) $2.4 \times 10^{-5}$ mole catalyst loading
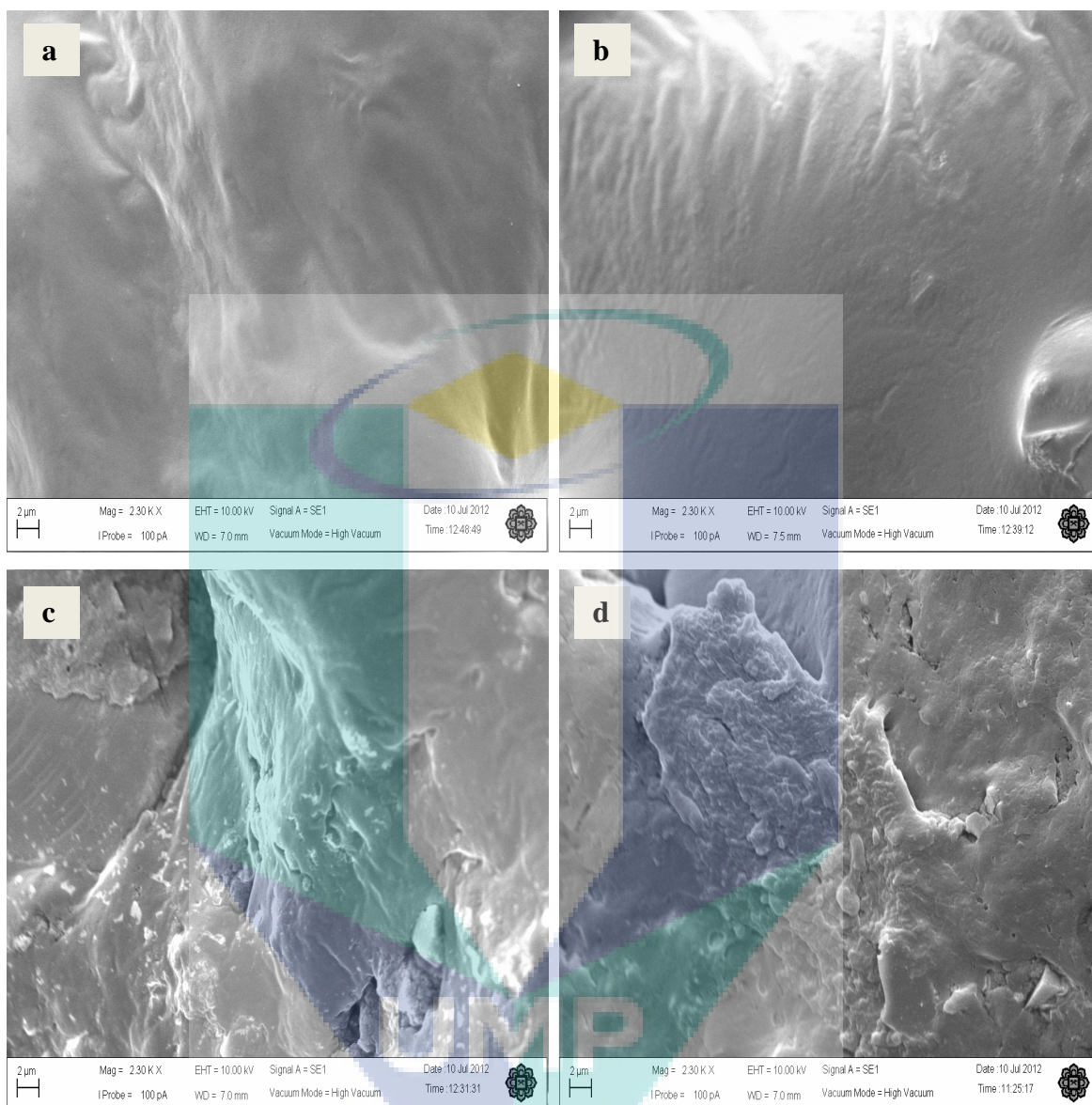
**Figure 4.33:** SEM micrographs of Pd-HNRL (Aqueous) at (a) $6.0 \times 10^{-5}$, (b) $1.2 \times 10^{-5}$, (c) $1.8 \times 10^{-5}$ and (d) $2.4 \times 10^{-5}$ mole catalyst loading

**4.6     Summary**

For the hydrogenation of NRL operated in monochlorobenzene, the extent of hydrogenation of NRL is dependent on the amount of catalyst and the nanoparticle sizes. When the amount of catalyst increases, the extent of hydrogenation increased. Nanoparticle sizes also influence the extent of hydrogenation. It can be seen that, with the increment of particles size of Ni-NRL and Pd-HNRL, the extent of hydrogenation increased. The extent of hydrogenation of Pd-HNRL is weakly dependent on the size of Pd-NRL nanoparticles. This observation can be attributed to the strong interaction of Pd-NRL within the NR matrix compared to Ni-NRL NPs. It can be confirmed with the intense signals of Pd-HNRL at 1739 cm$^{-1}$ and 1243 cm$^{-1}$ compared to that of Ni-HNRL which leads to the inhibition of it catalytic performance. FTIR analysis also showed that the characteristic signals of unsaturation of Ni-HNRL and Pd-HNRL reduced and confirmed by NMR analysis. Microstructure study revealed that the surface morphology of the hydrogenated products changed upon the hydrogenation reaction. The TGA analysis indicated that the hydrogenated latex have lesser chances to undergo polymerization reaction and hence are more volatile compound produced than NRL.

On the other hand, for the hydrogenation operated in aqueous medium, the extent of hydrogenation of NRL was also affected by the amount of catalyst. When the amount of catalyst was increased, the extent of hydrogenation increased. On the other hand, it can be concluded that monochlorobenzene led to higher conversion in the hydrogenation of NRL compared to water as a solvent. However, results also indicated the potential of green catalytic approached. NRL hydrogenation in aqueous medium requires a relatively high loading of catalyst compared to that in organic solvent medium to achieve similar conversion at the same reaction conditions. FTIR analysis showed that characteristic signals of unsaturation of Ni-HNRL and Pd-HNRL were reduced and had been confirmed by NMR analysis. On the other hand, microstructure study revealed that the surface morphology of the hydrogenated products changed upon the increment of catalyst amount.

For this work, the catalytic performances of Ni-NRL are comparable to that of Pd-NRL although Pd is known to be more active metal compared to Ni. Protein contents present in the NRLs moderate the catalytic performances of Pd-NRL for hydrogenation reaction of NRL compared to Ni-NRL. The stronger interaction between Pd with latex causes this phenomenon.
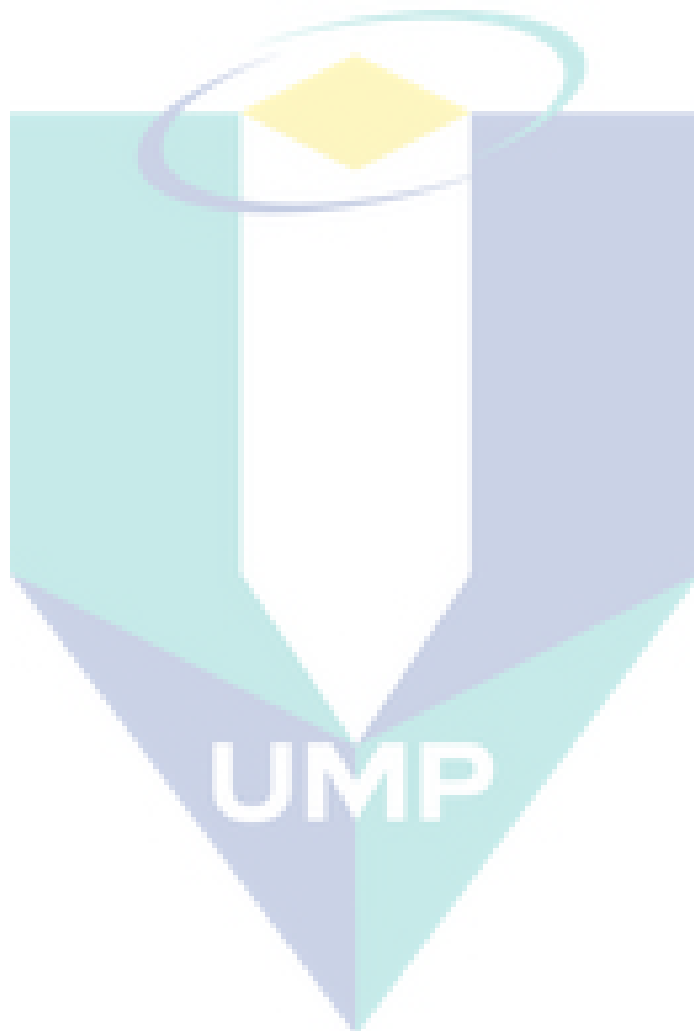
# CHAPTER 5

## CONCLUSION AND RECOMMENDATIONS FOR FUTURE RESEARCH

### 5.1    CONCLUSION

This research is divided into three parts. In the first part of this work, we found that latex can be used as stabilizer in the production of nanoparticles. Latex was able to stabilize Ni-NRL and Pd-NRL. Preparation involving the combination of ultrasonication and microwave irradiation upon the addition of $NaBH_4$ into latex and metal ion mixture resulted in the most well dispersed NPs. The particle sizes of the NPs decreased with increase in pH, sonication time, and stabilizer concentration. The particle size increased with the increased of metal ions precursor concentration. It was found that 10 ml of 0.003 M metal ions precursor concentration mixed with 30 ml of stabilizer at pH 11.50 and exposed to 15 minutes of sonication is a suitable condition to synthesize Ni-NRL and Pd-NRL. Under this preparation condition the mean size of Ni-NRL was found to be 10.8±0.3 nm while that for Pd-NRL was 30.6±2.9 nm.

Modifications of NRL via catalytic hydrogenation were done in the second part of this study. Hydrogenation of NRL using as-prepared NPs showed that the degree of hydrogenation increased with the increase of catalyst amount. The extent of hydrogenation was however weakly dependent on the particles sizes of the Pd-NRL but not for Ni-NRL. Under similar reaction condition, Pd-NRL caused higher conversion than that of Ni-NRL.

Aqueous phase catalytic hydrogenation of NRL by the Ni-NRL and Pd-NRL were also investigated and found to cause 30% conversion compared to 70% for that in monochlorobenzene. Monochlorobenzene was found to be a suitable solvent for the hydrogenation reaction. It was also found that the nanoparticles could also facilitate the hydrogenation reaction in aqueous medium indicating the possibility of green catalysis for hydrogenation of latex. Quadrupling the amount of nanocatalyst used to $2.4 \times 10^{-5}$ mole led to 90% conversion of latex. Hence, in this research it was found that not only the nanoparticles of Ni and Pd could be formed and stabilized in natural rubber latex but these nanoparticles could catalyze the hydrogenation reaction of latex.

Thermal analysis indicated that the hydrogenated NRL degraded at lower temperature. This could be due to the production of lower molecular rubber polymer because of the hydrogenation reaction. On the other hand, the solvents, catalyst used and catalyst loading affect the morphology of hydrogenated natural rubber latex.

Thus, based on observations made in this research, the catalytic activity of Ni for hydrogenation of NRL is comparable to that of Pd. Since Ni is cheaper than Pd while their catalytic performances are comparable, Ni has high potential to be used as catalyst for hydrogenating NRL.

## 5.2    RECOMMENDATION FOR FUTURE RESEARCH

Chemical modification of natural rubber via green catalytic hydrogenation could avoid negative consequences to the environment as it requires minimal rubber solvent and uses less energy.

This study involved batch reactor with hydrogen gas continuously flowed through the reaction mixture. Thus, it is recommended that future research be conducted in a high-pressure batch reactor to ensure efficient resource consumption and economical performance.

The system does not seem to work very well for hydrogenation of NRL as the nanocatalyst imbedded in the HNRL product and could be reuse and recycle. However, as Ni is cheap and has high potential for this hydrogenation system, it is recommended to further study the performance of Ni with higher loading of NRL amount.

The examination of the stability of the products as well as its mechanical strength and other properties including their glass transition temperatures, elasticity and abrasion resistance is also recommended. The findings of the proposed researches could extend the applications of NR for commercial usages.

# REFERENCES

Abbasi, A.R. and Morsali, A. 2010. Syntheses and characterization of Agl nano structures by ultrasonic method: Different morphologies under different conditions. *Ultrasonic Sonochemistry*. **17**: 572–578.

Abbasi, A.R. and Morsali, A. 2011. Synthesis and properties of silk yarn containing Ag nanoparticles under ultrasound irradiation. *Ultrasonics sonochemistry*. **18**(1): 82-7.

Abe, T., Tanizawa, M., Watanabe, K. and Taguchi, A. 2009. $CO_2$ methanation property of Ru nanoparticle-loaded $TiO_2$ prepared by a polygonal barrel-sputtering method. *Energy Environmental Science*. **2**: 315–321.

Abu Bakar, N.H.H., Ismail, J. and Abu Bakar, M. 2007. Synthesis and characterization of silver nanoparticles in natural rubber. *Materials Chemistry and Physics*. **104**(2-3): 276-283.

Adlim, M., Abu Bakar, M., Liew, K.Y. and Ismail, J. 2004. Synthesis of chitosan-stabilized platinum and palladium nanoparticles and their hydrogenation activity. *Journal of Molecular Catalysis A: Chemical*. **212**(1-2): 141-149.

Akamatsu, K., Takei, S., Mizuhata, M., Kajinami, A., Deki, S., Takeoka, S., Fujii, M., Hayashi, S. and Yamamoto, K. 2000. Preparation and characterization of polymer thin films containing silver and silver sulfide nanoparticles. *Thin Solid Films*. **359**(1): 55-60.

Anastas, P.T. and Warner, J.C. 1998. Green Chemistry: Theory and Practice. *Oxford University Press.*

Arayapranee, W., Prasassarakich, P. and Rempel, G.L. 2002. Synthesis of graft copolymers from natural rubber using cumene hydroperoxide redox initiator. *Journal of Applied Polymer Science*. **83**(14): 2993-3001.

Arayapranee, W., Prasassarakich, P. and Rempel, G.L. 2003. Process variables and their effects on grafting reactions of styrene and methyl methacrylate onto natural rubber. *Journal of Applied Polymer Science.* **8**(1): 63-74.

Arends, I. Sheldon, R. and Hanefeld, U. 2007. Green chemistry and catalysis. Weinheim: WILEY-VCH.

Bakar, N.H.H.A., Ismail, J. and Bakar, M.A. 2010. Silver nanoparticles in polyvinylpyrrolidone grafted natural rubber. *Reactive and Functional Polymers*. **70**(3): 168-174.

Bar, H., Bhui, D.K., Sahoo, G.P., Sarkar, P., De, S.P. and Misra, A. 2009. Green synthesis of silver nanoparticles using latex of Jatropha curcas. *Colloids and Surfaces A: Physicochemical and Engineering Aspects*. **339**(1-3): 134-139.

Beezhold, D.H., Kostyal, D.A. and Tomazic-Jezic, V.J. 2002. Measurement of latex proteins and assessment of latex protein exposure. *Methods*. **27**(1): 46-51.

Bennett, J.A., Fishwick, R.P., Spence, R., Wood, J., Winterbottom, J.M., Jackson, S.D. and Stitt, E.H. 2009. General hydrogenation of 2-pentyne over $Pd/Al_2O_3$ catalysts : Effect of operating variables and solvent selection. *Applied Catalysis A*. **364**: 57-64.

Bhattacharjee, S., Bhowmick, A.K., and Avasthit, B.N. 1993. Hydrogenation of epoxidized natural rubber in the presence of palladium acetate catalyst. *Polymer*. **34**(24): 5168-5173.

Binder, A., Seipenbusch, M., Muhler, M. and Kasper, G. 2009. Kinetics and particle size effects in ethene hydrogenation over supported palladium catalysts at atmospheric pressure. *Journal of Catalysis*. **268**(1): 150-155.

Boitiaux, J. P., Cosyns, J. and Vasudevan, S. 1983. Hydrogenation of highly unsaturated hydrocarbons over highly dispersed palladium catalyst: Part I: behaviour of small metal particles. *Applied Catalysis*. **6**(1), 41-51.

Campbell, P.S., Santini, C.C., Bayard, F., Chauvin, Y., Collière, V., Podgoršek, A. and Costa, M. F. 2010. Olefin hydrogenation by ruthenium nanoparticles in ionic liquid media : Does size matter ? *Journal of Catalysis*. **275**(1): 99-107.

Charmondusit, K., Prasassarakich P., McManus N.T. and Rempel G.L. 2003. Hydrogenation of *cis*-1,4-Poly(isoprene) catalyzed by $OsHCl(CO)(O_2)(PCy_3)_2$. *Journal Application Polymer Science*. **89**:142–52.

Chen, D.H, Yeh, J.J and Huang, T.C. 1999. Synthesis of platinum ultrafine particles in AOT reverse micelles. *Journal of Colloid and Interface Science*. **215**(1): 159–166.

Chen, Y., Liew, K.Y. and Li, J. 2008. Size-controlled synthesis of Ru nanoparticles by ethylene glycol reduction. *Materials Letters*. **62**(6-7): 1018-1021.

Choo, H., He, B., Liew, K.Y., Liu, H. and Li, J. 2006. Morphology and control of Pd nanoparticles. *Journal of Molecular Catalysis A: Chemical*. **244**(1-2): 217-228.

Clark, J.H. 2001. Catalysis for green chemistry. *Pure Application Chemistry* **73**(1): 103–111.

Couto, G.G., Klein, J.J., Schreiner, W.H., Mosca, D.H., de Oliveira, A. J. A. and Zarbin, A. J. G. 2007. Nickel nanoparticles obtained by a modified polyol process: synthesis, characterization, and magnetic properties. *Journal of Colloid and Interface Science*. **311**(2): 461-8.

Crabtree, R.H, Felkin, H. and Morris, G.E. 1977. Cationic iridium diolefin complexes as alkene hydrogenation catalysts and the isolation of some related hydrido complexes. *Journal of Organometallic Chemistry*. **141**(2): 205-215.

Dang, F., Kato, K., Imai, H., Wada, S., Haneda, H. and Kuwabara, M. 2011. Growth of BaTiO$_3$ nanoparticles in ethanol–water mixture solvent under an ultrasound-assisted synthesis. *Chemical Engineering Journal*. **170**(1): 333-337.

Darroudi, M., Khorsand, A., Muhamad, M.R., Huang, N.M. and Hakimi, M. 2012. Green synthesis of colloidal silver nanoparticles by sonochemical method. *Materials Letters*. **66**(1): 117-120.

Devarajan, S., Bera, P. and Sampath, S. 2005. Bimetallic nanoparticles: A single step synthesis, stabilization and characterization of Au-Ag, Au-Pd and Au-Pt in sol-gel derived silicates. *Journal Colloid and Interface Science* **290**(1): 117.

Department of Statistics, Malaysia. 2010. *Annual Rubber Statistics in Malaysia*.

Dubey, S.P., Lahtinen, M. and Sillanpää, M. 2010. Green synthesis and characterizations of silver and gold nanoparticles using leaf extract of *Rosa rugosa*. *Colloids and Surfaces A: Physicochemical and Engineering Aspects*. **364**(1-3): 34-41.

Dupont, J., Moreau, F., Lance, C. and Jacob, J.L. 1976. Phospholipid composition of membrane of lutoids  from *Hevea brasiliensis* latex. *Phytochemistry*. **15**: 1215–1217.

Dzikowicz, B. 2003. *Fundamental of Rubber Technology*. Norwalk: R.T. Vanderbilt Co, Inc.

Eluri, R. and Paul, B. 2012. Microwave assisted greener synthesis of nickel nanoparticles using sodium hypophosphite. *Materials Letters*. **76**: 36-39.

Escobar Barrios V.A., Herrera, R., Petit, A. and Pla, F. 2000. Selective hydrogenation of butadiene–styrene copolymers using a Ziegler–Natta type catalyst. Part 1. Kinetic study. *European Polymer Journal*. **36**:1 817–34.

Escobar Barrios, V.A., Petit, A., Pla, F. and Herrera Nájera, R. 2003. Selective hydrogenation of butadiene–styrene copolymers using a Ziegler–Natta type catalyst 2. Thermal properties. *European Polymer Journal*. **39**(6): 1151-1167.

Esmaeili-zare, M., Salavati-niasari, M. and Sobhani, A. 2012. Simple sonochemical synthesis and characterization of HgSe nanoparticles. *Ultrasonics Sonochemistry*, **19**(5): 1079-1086.

Filippo, E., Serra, A., Buccolieri, A. and Manno, D. 2010. Green synthesis of silver nanoparticles with sucrose and maltose: Morphological and structural characterization. *Journal of Non-Crystalline Solids*. **356**(6–8): 344-350.

Gilliom, L.R. 1989. Catalytic hydrogenation of polymers in the bulk. *Macromolecules*. 22: 662-665.

Gopalakrishnan, J. 1995. Chimie douce approaches to the synthesis of metastable oxide materials. *Chemistry of Materials.* **7**(7): 1265-1275.

Guidelli, J.E, Ramos, A.P., Zaniquelli, M.E.D. and Baffa, O. 2011. Green synthesis of colloidal silver nanoparticles using natural rubber latex extracted from *Hevea brasiliensis*. *Spectrochimica Acta Part A*. **82**: 140– 145.

Guo, X.Y and Rempel, G.L. 1998. Catalytic hydrogenation of nitrile–butadiene copolymer emulsion. *Journal of Applied Polymer Science*. **65**(4): 667–675.

Harpeness, R., Peng, Z., Liu, X., Pol, V.G., Koltypin, Y. and Gedanken, A. 2005. Controlling the agglomeration of anisotropic Ru nanoparticles by the microwave-polyol process. *Journal of Colloid and Interface Science*. **287**(2): 678-84.

Harraz, F. A., El-hout, S. E., Killa, H. M. and Ibrahim, I.A. 2012. Palladium nanoparticles stabilized by polyethylene glycol : Efficient, recyclable catalyst for hydrogenation of styrene and nitrobenzene. *Journal of Catalysis*. **286**: 184-192.

Hasma, H. and Subramaniam, A. 1986. Composition of lipids in latex of *Hevea brasiliensis* clone RRIM 501. *Journal Natural Rubber Research.* **1**: 30–40.

Hassanjani-Roshan, A., Vaezi, M.R., Shokuhfar, A. and Rajabali, Z. 2011. Synthesis of iron oxide nanoparticles via sonochemical method and their characterization. *Particuology*. **9**(1): 95-99.

He, B., Ha, Y., Liu, H., Wang, K. and Liew, K.Y. 2007. Size control synthesis of polymer-stabilized water-soluble platinum oxide nanoparticles. *Journal of Colloid and Interface Science*. **308**(1): 105-11.

He, B., Tan, J.J., Liew, K.Y. and Liu, H. 2004. Synthesis of size controlled Ag nanoparticles. *Journal of Molecular Catalysis A: Chemical*. **221**(1-2), 121-126.

Heilmann, A., Werner, J., Schwarzenberg, D., Henkel, S., Grosse, P. and Theiβ, W. 1995. Microstructure and optical properties of plasmapolymer thin films with embedded silver nanoparticles. *Thin Solid Films*. **270**(1–2): 103-108.

Heilmann, A., Werner, J., Stenzel, O. and Homilius, F. 1994. Changes of the optical and electrical properties of plasma polymer-metal composite films during thermal annealing. *Thin Solid Films*. **246**(1–2): 77-85.

Hinchiranan, N., Charmondusit, K., Prasassarakich, P. and Rempel, G.L. 2006. Hydrogenation of synthetic *cis*-1,4-poly(isoprene) and natural rubber catalyzed by [Ir(COD)py(PCy$_3$)]PF$_6$. *Journal Application Polymer Science*. **100**: 4219-4233.

Hinchiranan, N., Saelao, W., Chittapanyapong, O., Prasassarakich, P. and Rempel, G.L. 2008. Combination of hydrogenation and isomerization of NR using palladium catalyst. *KGK Kautschuk Gummi Kunststoffe*. **61**(5): 246-249.

Hirai, H., Nakaoa, Y. and Toshimaa, N. 1979. Preparation of colloidal transition metals in polymers by reduction with alcohols or ethers. *Journal of Macromolecular Science: Part A Chemistry*. **13**(6): 727-750.

Ho, C. C., Subramaniam, A. and Yong, W.M. 1976. Lipids associated with the particles in Hevea latex. *Proceeding International Rubber Conference Kuala Lumpur*. **2**: 441 – 445.

Hoxha, F., Vegten, N.V., Urakawa, A., Krumeich, F., Mallat, T. and Baiker, A. 2009. Remarkable particle size effect in Rh-catalyzed enantioselective hydrogenations. *Journal of Catalysis*. **261**(2): 224-231.

Hu, J., McManus, N.T. and Rempel, G.L. 2005. J.R. Sowa (Ed.). Catalysis of Organic Reactions. CRC Press, Taylor and Frances Group. Boca Raton. FL. 125–134.

Kappe, C.O., Dallinger, D. and Murphree, S. 2009. Practical Microwave Synthesis for Organic Chemists: Strategies, Instruments, and Protocols. Wiley-VCH.

Karelovic, A. and Ruiz, P. 2012. $CO_2$ hydrogenation at low temperature over Rh/γ-Al$_2$O$_3$ catalysts : Effect of the metal particle size on catalytic performances and reaction mechanism. *Applied Catalysis B, Environmental*. **113-114**: 237-249.

Kijima, N., Yoshinaga, M., Awaka, J. and Akimoto, J. 2011. Microwave synthesis, characterization, and electrochemical properties of α-Fe$_2$O$_3$ nanoparticles. *Solid State Ionics*. **192**(1): 293-297.

Kim, J., Park, J.-E., Momma, T. and Osaka, T. 2009. Synthesis of Pd–Sn nanoparticles by ultrasonic irradiation and their electrocatalytic activity for oxygen reduction. *Electrochimica Acta*. **54**(12): 3412-3418.

Kochthongrasamee, T., Prasassarakich, P. and Kiatkamjornwong, S. 2006. Effects of redox initiator on graft copolymerization of methyl methacrylate onto natural rubber. *Journal of Applied Polymer Science*. **101**(4): 2587-2601.

Kongparakul, S., Ng, F.T.T., and Rempel, G. L. 2011. Metathesis hydrogenation of natural rubber latex. *Applied Catalysis A: General*. **405**(1-2): 129-136.

Kongparakul, S., Prasassarakich, P. and Rempel, G.L. 2008. Catalytic hydrogenation of methyl methacrylate-g-natural rubber (MMA-g-NR) in the presence of $OsHCl(CO)(O_2)(PCy_3)_2$. *Applied Catalysis A: General*. **344**(1-2): 88-97.

Kongparakul, S., Prasassarakich, P., and Rempel, G.L. 2009. Catalytic hydrogenation of styrene-g-natural rubber (ST-g-NR) in the presence of $OsHCl(CO)(O2)(PCy_3)_2$. *European Polymer Journal*. **45**(8): 2358-2373.

Komarneni, S., Li, Q.H. and Roy, R. 1994. Microwave hydrothermal processing for layered and network phosphates. *Journal Material Chemistry*. **4**: 1903-906.

Lepore, S.D. and He, Y. 2003. Use of sonication for the coupling of sterically hindered substrates in the phenolic Mitsunobu reaction. *Journal of Organic Chemistry*. **68**(21): 8261-8263.

Li, D. and Komarneni, S. 2008. Nanoparticles of Pd: Synthesis by microwave-solvothermal method and optical properties. *Journal of Nanoscience and Nanotechnology*. **8**(8): 3930-3935.

Liu, D., Ren, S., Wang, G., Wen, L. and Yu, J. 2008. Rapid synthesis and morphology control of nickel powders via a microwave-assisted chemical reduction method. *Journal of Materials Science*. **44**(1): 108-113.

Lu, F., Liu, J. and Xu, J. 2008. Synthesis of chain-like Ru nanoparticle arrays and its catalytic activity for hydrogenation of phenol in aqueous media. *Materials Chemistry and Physics*. **108**: 369-374.

Lv, W., Qiu, Q., Wang, F., Wei, S., Liu, B. and Luo, Z. 2010. Sonochemical synthesis of cobalt aluminate nanoparticles under various preparation parameters. *Ultrasonics Sonochemistry*. **17**(5): 793-801.

Mahittikul, A., Prasassarakich, P. and Rempel, G. L. 2009. Hydrogenation of natural rubber latex in the presence of $[Ir(cod)(PCy_3)(py)]PF_6$. *Journal of Molecular Catalysis A: Chemical*. **297**(2): 135-141.

Mahittikul, A., Prasassarakich, P. and Rempel, G. L. 2006. Hydrogenation of natural rubber latex in the presence of $OsHCl(CO)(O_2)(PCy_3)_2$. *Journal of Applied Polymer Science*. **100**: 640-655.

Mao, T.-F. and Rempel, G. L. 2000. Catalytic hydrogenation of acrylonitrile – butadiene copolymers by a series of osmium complexes. *Journal of Molecular Catalysis A: Chemical*. **153**: 63–73.

Mao, T.-F. and Rempel, G.L. 1998. Catalytic hydrogenation of nitrile-butadiene copolymers by cationic rhodium complexes. *Journal of Molecular Catalysis A: Chemical*. **135**(2): 121-132.

Marzialetti, T., Oportus, M., Ruiz, D., Fierro, J.L.G. and Reyes, P. 2008. Enantioselective hydrogenation of 1-phenyl-1,2-propanedione, ethyl pyruvate and acetophenone on Ir/SiO$_2$ catalysts: Effect of iridium loading. *Catalysis Today*. **133–135**: 711-719.

Mayne, J.M., Dahlberg, K.A., Westrich, T.A., Tadd, A R. and Schwank, J. W. 2011. Effect of metal particle size on sulfur tolerance of Ni catalysts during autothermal reforming of isooctane. *Applied Catalysis A: General*. **400**(1-2): 203-214.

Medina-Ramirez, I., Bashir, S., Luo, Z. and Liu, L. J. 2009. Green synthesis and characterization of polymer-stabilized silver nanoparticles. *Colloids and Surfaces B: Biointerfaces*. **73**(2): 185-191.

Morris, M. and Lakin, B. 1995. Latex*: Educational Symposium*. Rubber Division, American Chemical Society Educational Symposium on Natural Rubber.

Musselwhite, N.E., Wagner, S. B., Manbeck, K.A., Carl, L.M., Gross, K.M. and Marsh, A. L. 2011. Activity and selectivity of colloidal platinum nanocatalysts for aqueous phase cyclohexenone hydrogenation. *Applied Catalysis A: General.* **402**(1-2): 104-109.

Nagao, D., Shimazaki, Y., Saeki, S., Kobayashi, Y. and Konno, M. 2007. Effect of ultrasonic irradiation on carbon-supported Pt–Ru nanoparticles prepared at high metal concentration. *Colloids and Surfaces A: Physicochemical and Engineering Aspects*. **302**(1-3): 623-627.

Nagaouda, M. N., Polshettiwav, V. and Varma, R.S. 2009. Self-assembly of palladium nanoparticles: Synthesis of nanobelts, nanoplates and nanotree using BI, and their application in carbon-carbon coupling reaction. *Journal of Materials Chemistry*. **19**(14): 2026-2031.

Nagaraju Rao, P. 2000. Nanocatalysis: Applications in the chemical industry. Network Spotlight. http://www.nanowerk.com/spotlight/spotid=18846.php#ixzz22AlmQ6ZT (online) (31 July 2012).

Narayanan, R. and El-Sayed, M. A. 2004. Changing catalytic activity during colloidal platinum nanocatalysis due to shape changes: Electron transfer reaction. *Journal of American Chemical Society*. **126**(23): 7194-7195.

Nawamawat, K., Sakdapipanich, J. T., Ho, C. C., Ma, Y., Song, J. and Vancso, J. G. 2011. Surface nanostructure of *Hevea brasiliensis* natural rubber latex particles. *Colloids and Surfaces A: Physicochemical and Engineering Aspects*. **390**(1-3): 157-166.

Nolte, P., Stierle, A., Jin-Phillipp, N. Y., Kasper, N., Schulli, T. U. and Dosch, H. 2008. Shape changes of supported Rh nanoparticles during oxidation and reduction cycles. *Science*. **321**(5896): 1654-1658.

Oliveira, M.M., Ugarte, D., Zanchet, D. and Zarbin A.J.G. 2005. Influence of synthetic parameters on the size, structure, and stability of dodecanethiol-stabilized silver nanoparticles. *Journal of Colloid and Interface Science*. **292**(2): 429-435.

Panapoy, M., Supattanapalapol, S. and Ksapabutr, B. 2008. Preparation and electrical conductivity of Ni/NiO composites using microwave radiation. *2$^{nd}$ IEEE International Nanoelectronics Conferences, INEC 2008*. 452-457.

Parent, J.S, McManus, N.T. and Rempel, G.L. 2001. Selectivity of the OsHCl(CO)(O$_2$)(PCy$_3$)$_2$ catalyzed hydrogenation of nitrile-butadiene rubber. *Journal of Application Polymer Science*. **79**: 1618–26.

Park, H.K., Han, Y.S., Kim, D.K. and Kim, C.H. 1998. Synthesis of LaCrO$_3$ powders by microwave induced combustion of metal nitrate-urea mixture solution. *Journal of Materials Science Letters*. **17**: 785-787.

Park, J.-E., Atobe, M. and Fuchigami, T. 2006. Synthesis of multiple shapes of gold nanoparticles with controlled sizes in aqueous solution using ultrasound. *Ultrasonics sonochemistry*. **13**(3): 237-41.

Parmar, D. U., Bhatt, S. D., Bajaj, H. C. and Jasra, R. V. 2003. Hydrogenation of alkenes and aromatic hydrocarbons using water-soluble RuCl$_2$(TPPTS)$_3$ in aqueous medium. *Journal of Molecular Catalysis A: Chemical*. **202**: 9-15.

Perrella, F.W. and Gaspari, A.A. 2002. Natural rubber latex protein reduction with an emphasis on enzyme treatment. *Methods*. **27**(1): 77-86.

Philip, D. 2010. Rapid green synthesis of spherical gold nanoparticles using *Mangifera indica* leaf. *Spectrochimica Acta Part A: Molecular and Biomolecular Spectroscopy*. **77**(4): 807-810.

Philip, D., Unni, C., Aromal, S.A. and Vidhu, V.K. 2011. *Murraya Koenigii* leaf-assisted rapid green synthesis of silver and gold nanoparticles. *Spectrochimica Acta Part A: Molecular and Biomolecular Spectroscopy*. **78**(2): 899-904.

Pinkas, J., Reichlova, V., Zboril, R., Moravec, Z., Bezdicka, P. and Matejkova, J. 2008. Sonochemical synthesis of amorphous nanoscopic iron(III)oxide from Fe(acac)$_3$. *Ultrasonics Sonochemistry*. **15**: 257–264.

Pradhan, A., Jones, R.C., Caruntu, D., O'Connor, C.J. and Tarr M.A. 2008. Gold–magnetite nanocomposite materials formed via sonochemical methods. *Ultrasonic Sonochemistry*. **15**: 891–897.

Prasassarakich, P., Sintoorahat, P. and Wongwisetsirikul, N. 2001. Enhanced graft copolymerization of styrene and acrolonitrile onto natural rubber. *Journal of Chemical Engineering of Japan.* **34**(2): 249-253.

Rashid, M.H. and Mandal, T.K. 2007. Synthesis and catalytic application of nanostructured silver dendrites. *Journal of Physical Chemistry.* **111**: 16750-16760.

Rippel, M.M., Leite, C.A., Lee, T. and Galembeck, F. 2005. Formation of calcium crystallites in dry natural rubber particles. *Journal Colloid Interface Science.* **288**(2): 449-56.

Rohani Bastami, T. and Entezari, M.H. 2012. A novel approach for the synthesis of superparamagnetic $Mn_3O_4$ nanocrystals by ultrasonic bath. *Ultrasonics Sonochemistry.* **19**(3): 560-9.

Salavati-Niasari, M., Hosseinzadeh, G. and Davar, F. 2011. Synthesis of lanthanum carbonate nanoparticles via sonochemical method for preparation of lanthanum hydroxide and lanthanum oxide nanoparticles. *Journal of Alloys and Compounds.* **509**(1): 134-140.

Sánchez-Delgado, R.A, Machalaba, N. and Ng-A-Qui, N. 2007. Hydrogenation of quinoline by ruthenium nanoparticles immobilized on poly(4-vinylpyridine). *Catalysis Communications.* **8**(12): 2115-2118.

Sansatsadeekul, J., Sakdapipanich, J. and Rojruthai, P. 2011. Characterization of associated proteins and phospholipids in natural rubber latex. *Journal of Bioscience and Bioengineering.* **111**(6): 628-634.

Saxena, V. K. and Chandra, U. 2010. Microwave Synthesis : A Physical Concept. 3-22.

Schrinner, M., Ballauff, M., Talmon, Y., Kauffmann, Y., Thun, J., Möller, M. and Breu, J. 2009. Single nanocrystals of platinum prepared by partial dissolution of Au-Pt nanoalloys. *Science.* **323**(5914): 617-20.

Silvestre-albero, J., Rupprechter, G. and Freund, H.-joachim. 2006. Atmospheric pressure studies of selective 1,3-butadiene hydrogenation on well-defined Pd /$Al_2O_3$/NiAl(110) model catalysts : Effect of Pd particle size. *Journal of Catalysis.* **240**: 58-65.

Siti Maznah, K., Baharin, A., Hanafi, I., Azhar, M. E., and Mas Rosemal Hakim, M. H. 2008. Effect of soaking in potassium hydroxide solution on the curing, tensile properties and extractable protein content of natural rubber latex films. *Polymer Testing.* **27**(8): 1013-1016.

Soloviev, M. and Gedanken, A. 2011. Coating a stainless steel plate with silver nanoparticles by the sonochemical method. *Ultrasonics Sonochemistry.* **18**(1). 356-62.

Southorn, W. A. and Yip, E. 1986. Latex flow studies: III. Electrostatic considerations in the colloidal stability of fresh Hevea latex. *Journal Rubber Research Institute Malaya*. **20**: 201 – 215.

Sreedhar, B., Devi, D. K. and Yada, D. 2011. Selective hydrogenation of nitroarenes using gum acacia supported Pt colloid an effective reusable catalyst in aqueous medium. *Catalyst Communications*. **12**(11): 1009-1014.

Suriyachi, P.A, Kiatkamjornwong, S.A. and Prasassarakich, P. 2004. Natural rubber-*g*-glycidyl methacrylate/styrene as a compatibilizer in natural rubber/PMMA blends. *Rubber Chemistry and Technology*. **77**(5): 914-930.

Tangpakdee, J. (1998) Ph.D. thesis, Tokyo University of Agriculture and Technology, Tokyo.

Tarachiwin, L., Sakdapipanich , J., Ute, K., Kitayama, T. and Tanaka, Y. 2005. Structural characterization of α-terminal group of natural rubber: 2. decomposition of branch-points by phospholipase and chemical treatments. *Biomacromolecules*. **6:** 1858–1863.

Telkar, M. M., Rode, C.V., Chaudhari, R.V., Joshi, S.S. and Nalawade, A.M. 2004. Shape-controlled preparation and catalytic activity of metal nanoparticles for hydrogenation of 2-butyne-1,4-diol and styrene oxide. *Applied Catalysis A: General*. **273**(1–2): 11-19.

Thakkar, K.N., Mhatre, S.S. and Parikh, R.Y. 2009. Biological synthesis of metallic nanoparticles. *Nanomedicine: Nanotechnology Biology and Medicine*. **6**: 257–262.

Thiraphattaraphun, L., Kiatkamjornwong, S., Prasassarakich, P. and Damronglerd, S. 2001. Natural rubber-*g*-methyl methacrylate/poly(methyl methacrylate) blends. *Journal of Applied Polymer Science*. **81**(2): 428-439.

Tian, N., Zhou, Z.Y., Sun, S.G., Ding, Y. and Wang, Z.L. 2007. Synthesis of tetrahexahedral platinum nanocrystals with high-index facets and high electro-oxidation activity. *Science*. **316**: 732-735.

Tong, X., Zhao, Y., Huang, T., Liu, H. and Liew, K. Y. 2009. Controlled synthesis of pompon-like self-assemblies of Pd nanoparticles under microwave irradiation. *Applied Surface Science*. **255**(23): 9463-9468.

Truscott, W. 1995. J.N. Fink (Ed.), Immunology and Allergy Clinics of North America, 89–121.

Turkevich, J. and Kim, G. 1970. Palladium: preparation and catalytic properties of particles of uniform size. *Science*. **169**(3948): 873-9.

Twu, Y.K., Chen, Y.W. and Shih, C.M. 2008. Preparation of silver nanoparticles using chitosan suspensions. *Powder Technology*. **185**(3): 1251-257.

UNCTAD secretariat. (undated). http://r0.unctad.org/infocomm/anglais/rubber/uses.htm (9 July 2012).

Vinod, V. T., Saravanan, P., Sreedhar, B., Keerthi Devi, D. and Sashidhar, R. B. 2011. A facile synthesis and characterization of Ag, Au and Pt nanoparticles using a natural hydrocolloid gum kondagogu (*Cochlospermum gossypium*). *Colloids and Surfaces B: Biointerfaces*. **83**(2): 91-298.

Wang, A., Yin, H., Lu, H., Xue, J., Ren, M. and Jiang, T. 2009. Catalytic activity of nickel nanoparticles in hydrogenation of *p*-nitrophenol to *p*-aminophenol. *Catalysis Communications*. **10**(15): 2060-2064.

Wang, Y., Ren, J., Deng, K., Gui, L. and Tang, Y. 2000. Preparation of tractable platinum, rhodium, and ruthenium nanoclusters with small particle size in organic media. *Chemistry Materials*. **12**: 1622.

Wang, Z. 2008. Green chemistry: Recent advances in developing catalytic processes in environmentally-benign solvent systems. Slide Wipf Group: Frontier of chemistry presentation.

Wehrli, J.T., Baiker, A., Monti, D.M. and Blaser, H.U. 1990. Enantioselective hydrogenation of α-ketoesters: Preparation and catalytic behavior of different alumina-supported platinum catalysts modified with cinchonidine. *Journal of Molecular Catalysis*. **6**(2): 207-226.

Wong, P. T. T. and Mantsch, H. H. 1988, High-pressure infrared spectroscopic evidence of water binding sites in 1,2-diacylphospholipids. *Chemistry and Physics of Lipids*. **46**: 213– 224.

Wu, Z., Chen, J., Di, Q. and Zhang, M. 2012. Size-controlled synthesis of a supported Ni nanoparticle catalyst for selective hydrogenation of *p*-nitrophenol to *p*-aminophenol. *Catalyst Communications*. **18**: 55-59.

Xu, W., Liew, K. Y., Liu, H., Huang, T., Sun, C. and Zhao, Y. 2008. Microwave-assisted synthesis of nickel nanoparticles. *Materials Letters*. **62**(17-18): 2571-2573.

Yang C., Hu, X., Wang, D., Dai, C., Zhang, L., Jin, H. and Agathopoulos, S. 2006. Ultrasonically treated multi-walled carbon nanotubes (MWCNTs) as PtRu catalyst supports for methanol electrooxidation. *Journal Power Sources*. 160: 187–193.

Yi, C. S., Lee, D.W. and He, Z. 2000. Acid-promoted homogeneous hydrogenation of alkenes catalyzed by the ruthenium-hydride complex (PCy$_3$)$_2$(CO)(Cl)RuH: Evidence for the formation of 14-electron species from the selective entrapment of the phosphine ligand. *Organometallics*. **19**(15): 2909-2915.

Yu, D. and Yam V.W. 2005. Hydrothermal-induced assembly of colloidal silver spheres into various nanoparticles on the basis of HTAB-modified silver mirror reaction. *Journal Physical Chemistry B*. **109**(12): 5497-503.

Yu, W.W. and Liu, H. 2006. Singular modification effects of metal cations and metal complex ions on the catalytic properties of metal colloidal nanocatalysts. *Journal of Molecular Catalysis A: Chemical*. **243**(1): 120-141.

Yu, W., Liu, M., Liu H. and Zheng, J. 1999. Preparation of polymer-stabilized noble metal colloids. *Journal of Colloid and Interface Science*. **210**: 218 –221.

Yu, Y., Zhao, Y, Huang, T., and Liu, H. 2010. Microwave-assisted synthesis of palladium nanocubes and nanobars. *Material Research Bulletin*. **45**(2): 159-164.

Zhang, W., Wang, Q., Qin, F., Zhou, H., Lu, Z. and Chen, R. 2011. Microwave-assisted facile synthesis of palladium nanoparticles in HEPES solution and their size-dependent catalytic activities to Suzuki reaction. *Journal of Nanoscience and Nanotechnology*. **11**(9). 7794-7801.

Zhang, Y., Yu, J., Niu, H. and Liu, H. 2007. Synthesis of PVP-stabilized ruthenium colloids with low boiling point alcohols. *Journal of Colloid and Interface Science*. **313**(2): 503-10.

Zheng, H.Y. and An, M.Z. 2008. Electrodeposition of Zn-Ni-Al$_2$O$_3$ nanocomposite coatings under ultrasound conditions. *Journal Alloys Compound*. **459**: 548-552.

Zhu, Y. and Chang, J. 2009. Microwave-assisted synthesis and processing of biomaterials. *NanoScience in Biomedicine*. 154-177
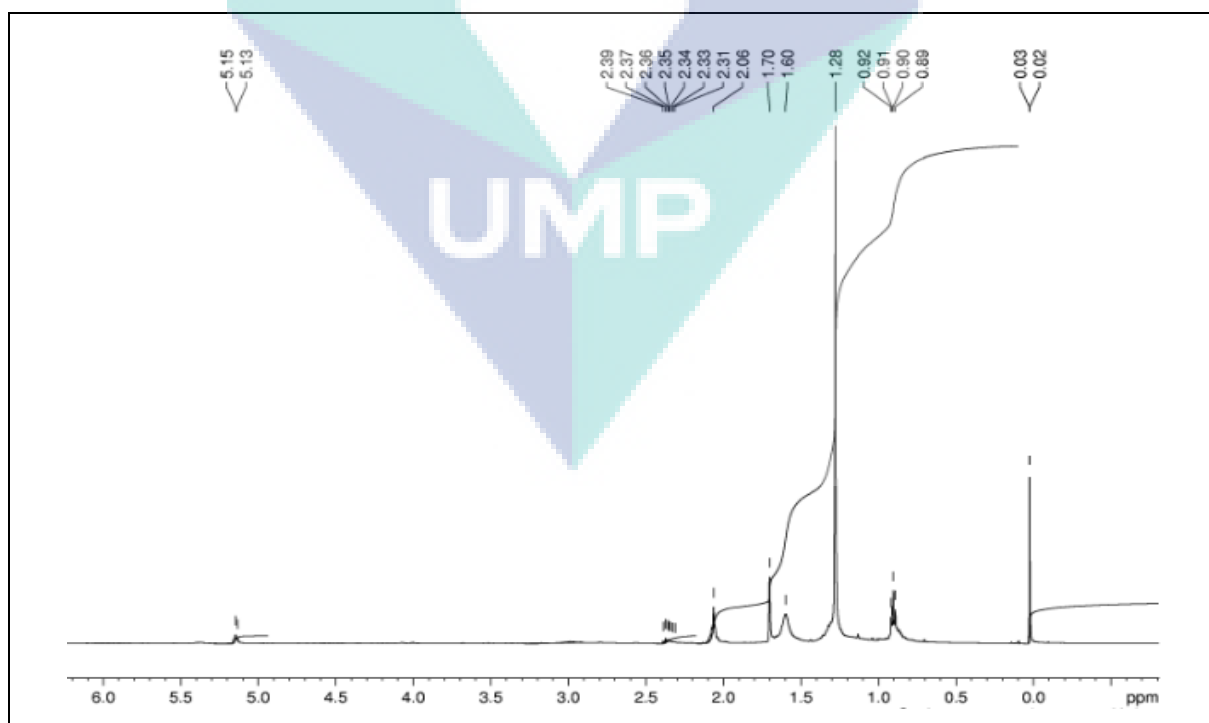
# APPENDIX A
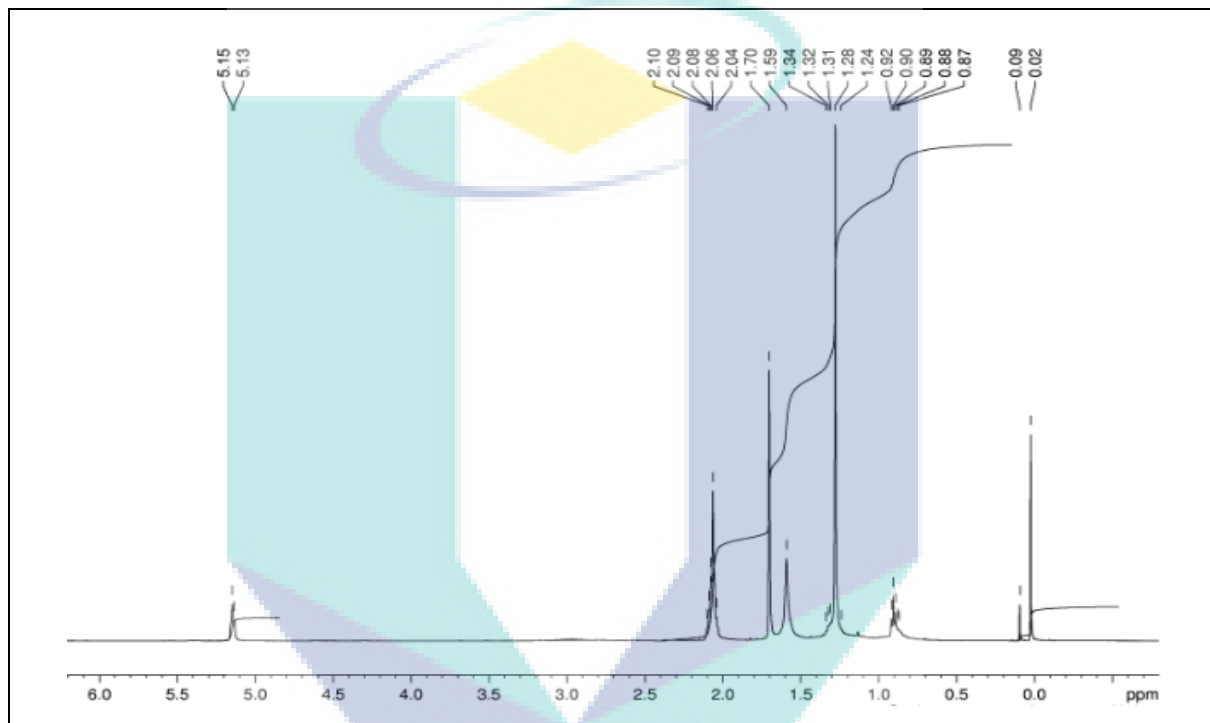


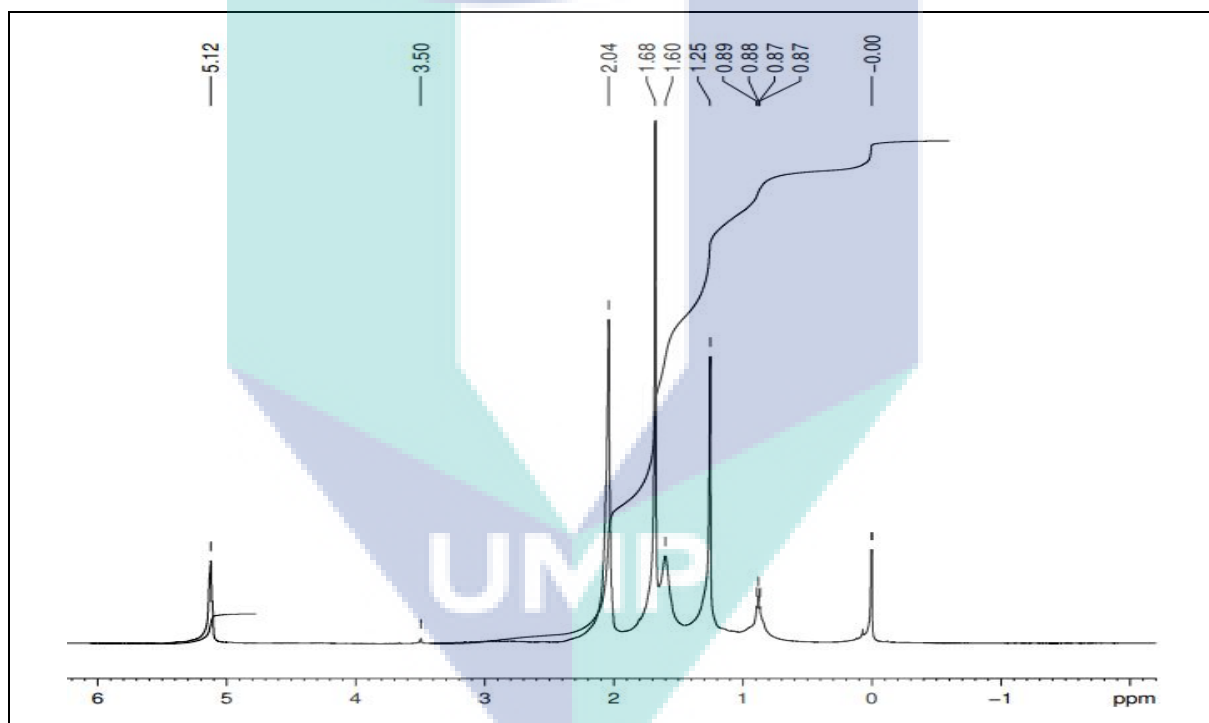**A1:** $^1$H NMR spectra of NRL (12 hour Treatment) in monochlorobenzene (Blank)
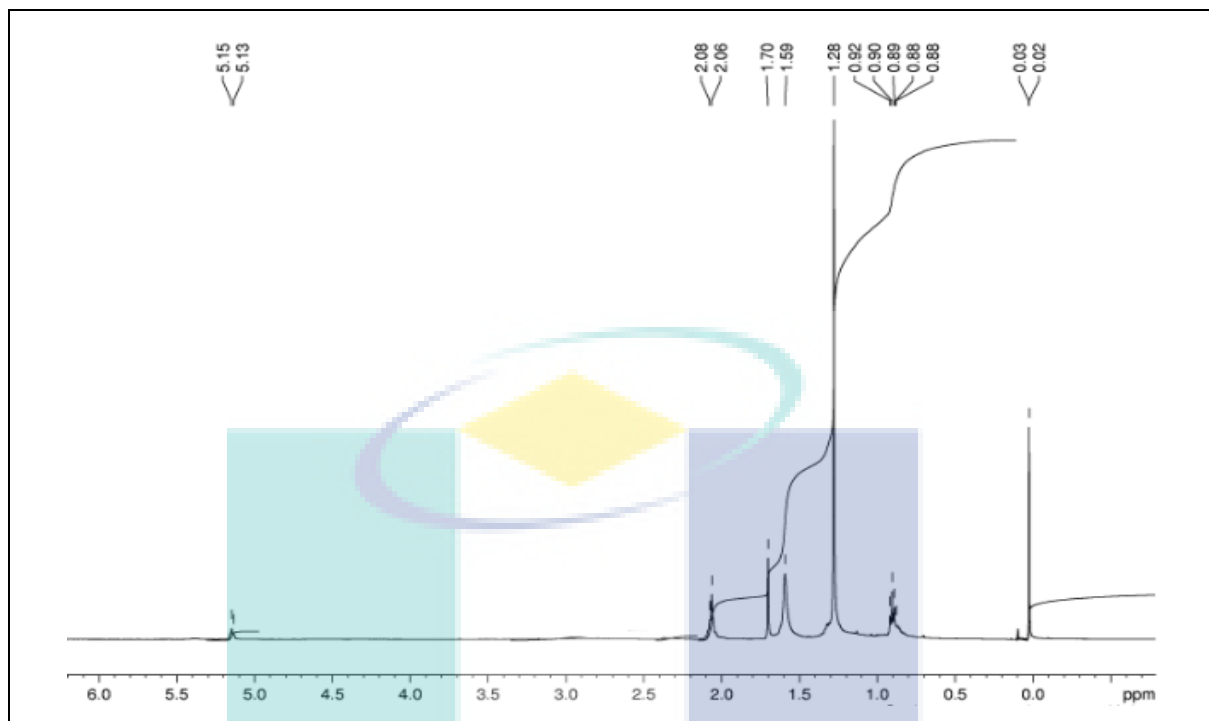
**A2:** $^1$H NMR spectra of Ni-HNRL (62% Conversion) in monochlorobenzene
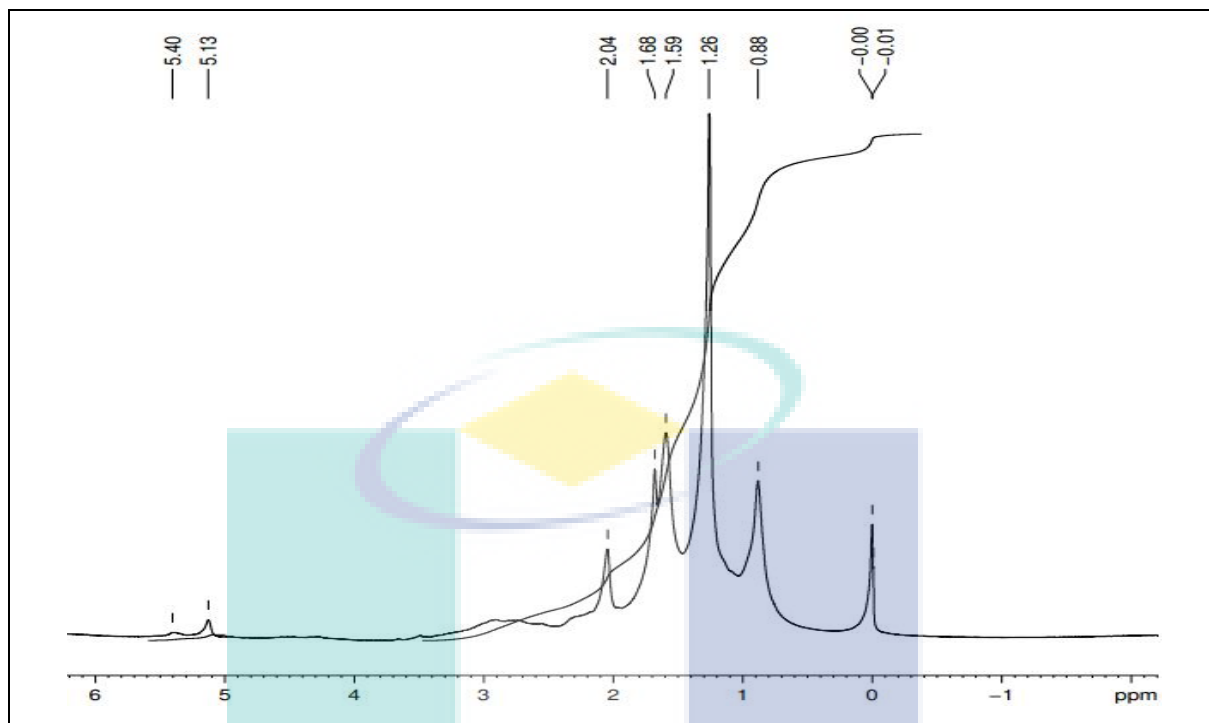


**A3:** $^1$H NMR spectra of Pd-HNRL (70% Conversion) in monochlorobenzene

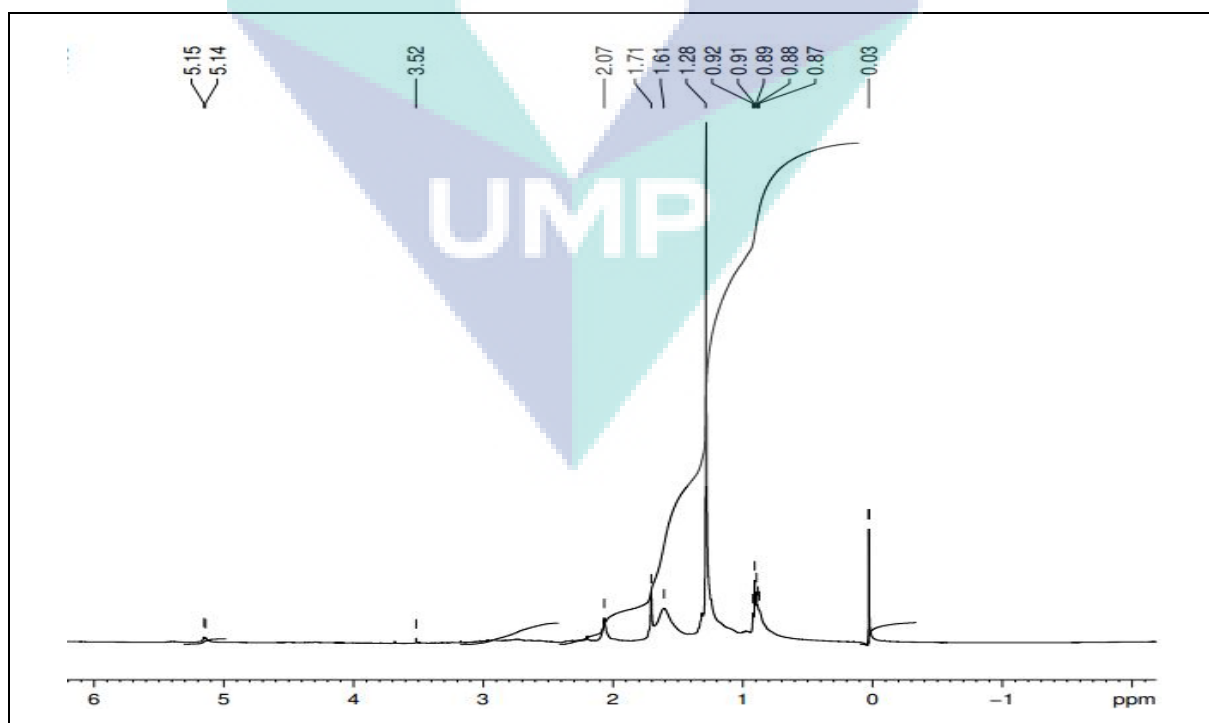**A4**: Degree of hydrogenation of NRL by Ni-NRL and Pd-NRL catalyst

| Sample Code | Region >5 ppm (cm) | Region >1.5 ppm (cm) | Region <1.5 ppm (cm) | Total (cm) | Total$_{>5.15\ ppm}$ / Total | % Conversion |
|---|---|---|---|---|---|---|
| NRL (Blank) | 0.50 = 4.61 % | 5.50 = 50.69 % | 4.85 = 44.70 % | 10.85 | 0.50/10.85 = 4.61 % | - |
| Ni-HNRL | 0.20 = 1.79 % | 3.80 = 33.93 % | 7.20 = 64.29 % | 11.20 | 0.20/11.20 = 1.79 % | 62 % |
| Pd-HNRL | 0.15 = 1.44 % | 3.30 = 31.58 % | 7.00 = 67.00 % | 10.45 | 0.15/10.45 = 1.44 % | 70 % |



**A5:** $^1$H NMR spectra of NRL (12 hour Treatment) in aqueous solution (Blank)

**A6:** $^1$H NMR spectra of Ni-HNRL (90.5% Conversion) in aqueous solution



**A7:** $^1$H NMR spectra of Pd-HNRL (92.3% Conversion) in aqueous solution

**A8**: Degree of hydrogenation of NRL in aqueous medium by Ni-NRL and Pd-NRL catalyst

| Sample Code | Region >5 ppm (cm) | Region >1.5 ppm (cm) | Region <1.5 ppm (cm) | Total (cm) | Total$_{>5.15\ ppm}$ / Total | % Conversion |
|---|---|---|---|---|---|---|
| NRL (Blank) | 0.60 = 6.12 % | 6.45 = 65.82 % | 2.70 = 27.55 % | 9.80 | 0.60/9.80 = 6.12 % | - |
| Ni-HNRL | 0.05 = 0.58 % | 3.50 = 40.46 % | 5.10 = 58.96 % | 8.65 | 0.05/8.65 = 0.58 % | 90.5% |
| Pd-HNRL | 0.05 = 0.47 % | 3.40 = 32.23 % | 7.10 = 67.30 % | 10.55 | 0.05/10.55 = 0.47 % | 92.3% |
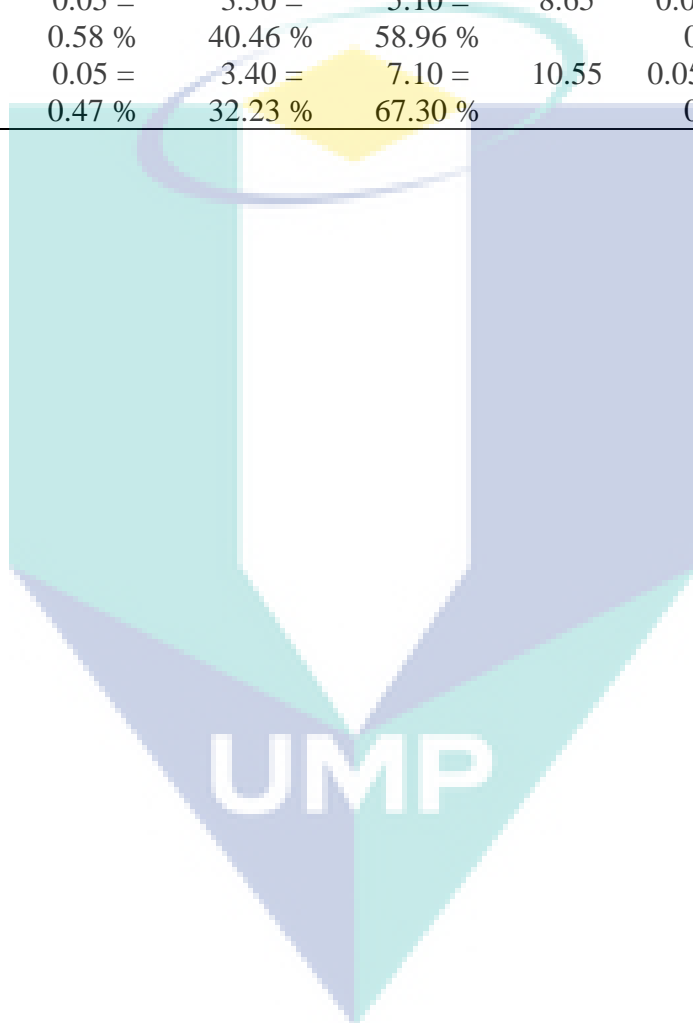
**APPENDIX B**

**LIST OF PUBLICATIONS/PRESENTATIONS**

1. Nurul Ain Ramli, Mohd Ridzuan Nordin, Siti Maznah Kabeb and Liew Kong Yong. 2011. Stability of Nickel Nanoparticles by Latex and Its Hydrogenation Activity. *Postgraduate Poster Competition 2011*. Universiti Malaysia Pahang, Malaysia. (Poster Presenter) - 2nd Runner Up Master Technical

2. Nurul Ain Ramli, Mohd Ridzuan Nordin, Siti Maznah Kabeb and Liew Kong Yong. 2012. Synthesis of Nickel and Palladium Nanoparticles in Natural Rubber Latex and Their Preliminary Catalytic Activity for Hydrogenation Reaction. *Asian International Conference on Materials, Minerals, and Polymer 2012 (MAMIP2012)*. Penang, Malaysia. (Oral Presenter)

3. Nurul Ain Ramli, Siti Maznah Kabeb and Mohd. Ridzuan Nordin. 2012. Green Catalytic Hydrogenation of Natural Rubber Latex (NRL) by Nanocatalyst. *Creation, Innovation, Technology & Research Exposition 2012 (CITREX2012)*. Universiti Malaysia Pahang, Malaysia. (Poster Presenter) – Bronze

4. Nurul Ain Ramli, Mohd Ridzuan Nordin, Siti Maznah Kabeb and Liew Kong Yong. 2012. Green Catalytic Hydrogenation of Natural Rubber Latex (NRL) by Nanocatalyst. *International Conference on Nanotechnology 2012 (ICONT12)*, Pahang, Malaysia. (Oral Presenter)